MIMO signal design, channel estimation, and symbol detection

Chienchun Cheng

université PARIS-SACLAY

NNT : 2016SACLC003

國立交通大學 National Chiao Tung University

CentraleSupélec

THESE DE DOCTORAT
DE
LA NATIONAL CHIAO TUNG UNIVERSITY
ET DE
L'UNIVERSITE PARIS-SACLAY
PREPAREE A CENTRALESUPELEC

ÉCOLE DOCTORALE N°580

Sciences et technologies de l'information et de la communication
Spécialité de doctorat : Réseaux, Information et Communications

Par

M. Chien-Chun CHENG

MIMO Signal Design, Channel Estimation, and Symbol Detection
(Systèmes MIMO: Conception, Estimation du Canal, et Détection)

Thèse présentée et soutenue à Gif-sur-Yvette, le 12 janvier 2016:

Composition du Jury :

M. Luc VANDENDORPE	Université Catholique de Louvain (UCL)	Rapporteur
M. Lajos HANZO	University of Southampton	Rapporteur
M. Pierre DUHAMEL	CentraleSupélec	Président du jury
M. Chung-Ju CHANG	National Chiao Tung University (NCTU)	Examinateur
M. Serdar SEZGINER	Sequans Communications	Examinateur
M. Dirk SLOCK	Eurecom	Examinateur
M. Hikmet SARI	CentraleSupélec	Directeur de thèse
M. Yu T. SU	National Chiao Tung University (NCTU)	Directeur de thèse

université PARIS-SACLAY
ÉCOLE DOCTORALE
Sciences et technologies de l'information et de la communication (STIC)

Titre : Systèmes MIMO: Conception, Estimation du Canal, et Détection

Mots clés : Systèmes MIMO, Traitement du Signal, Communications sans fil

Résumé: Cette thèse aborde plusieurs problèmes fondamentaux des systèmes de communications sans fil avec des antennes multiples, dites systèmes MIMO (multiple input, multiple output). Les contributions se situent aussi bien au niveau des algorithmes de réception qu'au niveau de la génération du signal à l'émission.
La plus grande partie de la thèse est dédiée à l'étude des algorithmes de réception. Les points abordés comprennent la modélisation et l'estimation du canal, la détection robuste des symboles, et la suppression des interférences. Un nouveau modèle de canal est proposé dans le chapitre 3 en exploitant les corrélations dans les domaines temporel, fréquentiel et spatial, et en réduisant l'espace des paramètres aux termes dominants. Ce modèle est utilisé pour proposer ensuite un estimateur de canal à faible complexité et aussi un sélecteur de mots de code pour envoyer vers l'émetteur les informations sur l'état du canal. Dans le chapitre 4, la réception robuste est étudiée pour les systèmes MIMO-OFDM sans une connaissance parfaite du canal. Des récepteurs robustes sont proposés pour les cas avec ou sans connaissance statistique du canal.
La conception de récepteurs pour les systèmes MIMO-OFDM en présence d'interférence est étudiée dans le chapitre 5 et des récepteurs robustes sont proposés prenant en compte séparément l'interférence causée par les ondes pilotes et celle causée par les symboles d'une part et l'asynchronisme entre le signal et l'interférence d'autre part.
Dans la deuxième partie de la thèse (chapitre 6), nous abordons les modulations spatiales qui sont particulièrement adaptées aux systèmes MIMO dans lesquels le nombre de chaines d'émission est inférieur aux nombre d'antennes. Remarquant que l'efficacité spectrale de ces systèmes reste très faible par rapport à la technique de multiplexage spatiale, nous avons développé des modulations spatiales améliorées (ESM, pour Enhanced Spatial Modulation) qui augmentent substantiellement l'efficacité spectrale. Ces modulations sont basées sur l'introduction de modulations secondaires, obtenues par interpolation. La technique ESM gagne plusieurs décibels en rapport signal à bruit lorsque les constellations du signal sont choisies de façon à avoir la même efficacité spectrale que dans les modulations spatiales conventionnelles.

Title : MIMO Signal Design, Channel Estimation, and Symbol Detection

Keywords : MIMO system, Signal processing, Wireless communication

Abstract: The aim of this thesis is to investigate multiple input multiple output (MIMO) techniques from the reception algorithms, i.e., channel estimation, symbol detection, and interference suppression, to the advanced spatial modulation (SM) transmission schemes.
In the reception algorithms, the proposed schemes are derived based on the detection theory and the statistical analysis, i.e., linear regression and Bayesian model comparison, in order to deal with the channel uncertainty, i.e., fading, correlations, thermal noise, multiple interference, and the impact of estimation errors.
In the transmission schemes, the signal constellations are targeted to find a good tradeoff between the average transmit energy and the minimum Euclidean distance in the signal space. The proposed schemes, denoted by enhanced spatial modulation (ESM), introduce novel modulation/antenna combinations and use them as the information bits for transmission.
The simulation results show that good system performance can be achieved with the advanced MIMO techniques. Several examples are presented in this thesis to provide some insights for the MIMO system designs.

Université Paris-Saclay
Espace Technologique / Immeuble Discovery
Route de l'Orme aux Merisiers RD 128 / 91190 Saint-Aubin, France

I would like to dedicate this thesis to my loving parents ...

Acknowledgements

I would like to express my deepest gratitude to both of my supervisors Prof. Yu T. SU and Prof. Hikmet SARI. Yu T. guided me especially at the beginning of my PhD with constructive feedback and careful reviews of my papers. Hikmet provided me with a constant flow of creative research ideas and gave me the freedom to work on the topics I liked. I am particularly thankful for the numerous opportunities both gave me to present my work, for their permanent availability for questions and discussions, for their encouragement and their invaluable support.

I would like to thank all jury members for their participation in my PhD defense and for their kind and motivating comments. Special thanks goes to Prof. Luc VANDENDORPE and Prof. Lajos HANZO for their careful reviews of the manuscript and for pointing out some research directions on which I hope to have an opportunity to work in the future.

I am also deeply indebted to many people without whom my PhD would not have been the same. In particular, I would like to thank:

- Serdar SEZGINER who made me familiar with the LTE system and stimulated my interest for the receiver design. I owe most of my knowledge in this area to him and to the related papers he recommended. I will always look back with pleasure on the countless hours of intensive work, fruitful discussions, and brainstorming on research problems we have spent together.
- Yen-Chih CHEN for his explanations and discussions on MIMO channel models and different algorithms to estimate them efficiently. This helped me a lot at the beginning of my PhD.
- All of the members of the NCTU TNTLab, the telecommunications department of Supélec, and the LANEAS group for making my PhD a very pleasant experience; among them in particular Tofar, Yen-Cheng, Stefano, Andres, Bakarime, Zheng, Matha, Salah, Ejder, Fei, Kenza, and my office mates Meryem, German, Chao, Victor, and Clement.

- Je voudrais remercier Jose FONSECA, Huu-Hung VUONG et Catherine MAGNET pour leur aide et soutien.

My last acknowledgments are for those who are closest to me: I would like to thank my family and my girl friend Chi-Ya HSU for supporting my decision to start a PhD in France.

Table of contents

List of figures

List of tables

Glossary

4G fourth-generation. 11

8APK 8-level amplitude-phase-keying. 88, 89

AoA angle of arrival. 27, 43

AoD angle of departure. 19–22, 24, 27, 31, 124

APEP average PEP. 92

AS angle spread. 27, 30, 43

AWGN additive white Gaussian noise. 18, 22, 26, 27, 34, 35, 39, 49, 51, 52, 55, 65–69, 73, 75, 76, 78, 81, 102, 123, 126

BER bit error rate. 44, 45, 47, 48, 50, 69–71, 73, 74, 76, 113, 114

BL block partitions. 73, 74

BMS Bayesian model selection. 33, 42, 124

bpcu bits per channel use. 79, 80, 82, 83, 85, 87, 88, 92, 97, 102, 104, 105, 108, 111, 112, 119, 120

BS base station. 19, 23, 27, 49

CCI co-channel interference. 49

CDI channel distribution information. 70, 71, 124

CDIR channel distribution information at receiver. 33, 39–41, 43, 45, 47, 48

CER codeword error rate. 120

CP cyclic prefix. 13, 14, 27, 43, 59, 64, 70

CS codeword selection. 18, 24, 25, 29–31

CSI channel state information. 4, 14, 17, 21, 23, 24, 29, 31, 33, 34, 36, 37, 39, 45–47, 49, 50, 53, 58, 65, 67, 68, 70, 76, 78, 91, 111, 113, 123, 124

DFT discrete Fourier transform. 4, 23, 25, 29, 31, 35, 36, 59, 61, 70, 124

eNB evolved node B. 51, 53, 57, 59, 65, 70, 125

EPA extended pedestrian A model. 41, 71

ESM enhanced spatial modulation. 6, 7, 80, 82, 83, 85–98, 100–102, 104, 105, 108, 110–113, 115–122, 125, 127

ETU extended typical urban model. 41, 73

EVA extended vehicular A model. 41

FDD frequency division duplexing. 43, 69

FFT fast Fourier transform. 14, 18, 27, 43

GSM generalized SM. 80, 90, 91

GSSK generalized SSK. 80

i.i.d. independent and identically distributed. 51, 73, 81

ICIC inter-cell interference coordination. 59

IRC interference rejection combining. 49, 50, 53, 57, 59, 64–71, 73, 76–78

IRC-DL IRC with diagonal loading. 54, 58, 60, 61, 69, 73, 78

ISI intersymbol interference. 3, 13, 14, 60, 61, 71, 73

LMMSE linear minimum mean square error. 36, 50, 54–57, 64, 69, 70, 73, 76–78, 124

LMMSE-C LMMSE with compensation. 57, 58, 60, 61, 69–71, 78

LS least squares. 18, 21, 22, 27, 36, 54, 55, 71

LS-C LS with compensation. 55, 56, 58, 60, 61, 69–71

LTE long-term evolution. 41, 43, 50–52, 69, 71, 73

MA moving average. 73, 74

MAE mean absolute error. 29, 30

MGF moment-generating function. 92

MIMO multiple-input multiple-output. 1, 3–6, 11, 12, 14, 15, 17–20, 23, 27, 30, 33–35, 37, 39, 40, 43, 47, 49, 50, 70, 77, 79–81, 92, 113–115, 123, 124

ML maximum likelihood. 5, 13, 33, 34, 38, 42, 47, 57, 91, 94, 95, 111–113, 121, 124

MMSE minimum mean square error. 71, 124

MS mobile station. 19, 27

MSE mean square error. 4, 5, 18, 26, 29, 30, 33, 63, 64, 73, 78

MSM multistream SM. 96–98, 104–106, 108, 110–112, 120, 122, 125

MSV-SC minimum singular value selection criterion. 23

OFDM orthogonal frequency division multiplexing. 3–5, 11–15, 18, 23, 27, 30, 34, 36, 39, 40, 43, 47, 50, 60, 70, 73, 77, 123, 124

OPT optimal receiver. 38–40, 42, 45, 48, 57, 58, 69

OSTBC orthogonal space time block code. 37, 39, 40, 43, 45, 48, 124

PEP pairwise error probability. 45, 48, 91–94

PSK phase-shift keying. 12

QAM quadrature amplitude modulation. 7, 12, 69, 93

QSM quadrature SM. 93, 115–118

RB resource block. 51, 69

RF radio frequency. 15, 79, 80, 93, 113, 116

RMLR robust ML receiver. 37, 38, 40, 45, 47

RX receive. xi, 19, 20, 34, 36, 50, 65, 76, 78, 119–121, 125, 126

SCM 3GPP spatial channel model. 27

SD sphere decoding. 112, 120

SER symbol error rate. 18, 29, 31

SIC successive interference cancellation. 50, 77, 78

SINR signal-to-interference-plus-noise ratio. 50, 62, 66–68, 70, 76–78, 126

SIR signal-to-interference ratio. 6, 53, 56–58, 64, 70, 71, 73–76, 78, 125

SM spatial modulation. 3, 6, 15, 79–83, 85–87, 89, 90, 92–95, 113, 115–119, 121, 125

SMX spatial multiplexing. 80–82, 92, 93, 113, 115–118

SNR signal-to-noise ratio. 6, 26, 27, 29, 30, 33, 44, 45, 53, 57, 59, 64, 69, 70, 73, 74, 76, 78, 81, 91, 92, 104, 108, 110, 111, 115, 124–126

SSK space-shift keying. 80

STC space–time code. 14, 15

SVER symbol vector error rate. 113, 115–117

TX transmit. 15, 19, 20, 34, 36, 65, 79–83, 85, 87, 88, 92, 94–97, 103, 104, 110, 121, 122, 124–126

UE user equipment. 51, 52, 54, 62, 70

VLSI very-large-scale integration. 1

WLANs wireless local area networks. 11

ZF zero-forcing. 23

Nomenclature

Roman Symbols

$\mathbf{X}$	upper case boldface letters denote the matrices
$\mathbf{x}$	lower case boldface letters denote the vectors
$\mathrm{card}(\cdot)$	the cardinality of a set that measures the number of elements of the set
$\det(\cdot)$	the determinant
$\mathrm{vec}(\cdot)$	the column vectorization
$\mathrm{diag}(\cdot)$	the diagonal matrix obtained from a components of the matrix
$\mathrm{var}(\cdot)$	the variance operation

Greek Symbols

$\mathscr{C}$	the complex-value set
$\mathcal{N}_c(\cdot)$	the distribution of a circularly symmetric complex Gaussian random variable
$\mathscr{R}$	the set of real values

Superscripts

$(\cdot)^*$	the complex conjugate
$(\cdot)^H$	the Hermitian conjugate
$(\cdot)^T$	the transpose

Subscripts

$[\cdot]_{ij}$ the (i,j)th entry of a matrix

Other Symbols

$\lfloor \cdot \rfloor$ the floor function that maps a real number to its integer part

$\mathbb{C}_k^n$ the number of k-combinations from a given n elements

$\mathbb{E}[\cdot]$ the expectation

$\otimes$ the Kronecker product

$\sim$ distributed as

$\|\cdot\|$ the Frobenius norm

$|\cdot|$ the absolute value

Chapter 1

Introduction

Multiple-input multiple-output (MIMO) communications currently represent one of the most dynamic areas of research. Over the past ten years, there has been a surge of research activities in this field. This is mainly due to an explosive demand for internet access, driven by wireless data applications on user equipment. Also, the significant progress in very-large-scale integration (VLSI) technology enabled the implementation of complex signal processing algorithms and resulted in a small area and low power consumption. This led to the development of various communications techniques and mathematical tools in the past decade and the research is still very vibrant in this field.

There are two fundamental issues of wireless MIMO communications that make the problem challenging. The first one is the effect of channel fading. Fading has a small-scale effect which is multipath propagation with time-varying channel strengths and large-scale effects such as path loss and shadowing due to obstacles. The second issue is that the existence of a large amount of users in cellular networks has driven communication channels from being noise-limited to interference-limited. Each transmitter–receiver pair cannot be viewed as an isolated point-to-point link, but wireless users communicate over the air and there is significant interference between them. The interference can be between transmitters communicating with a common receiver, between signals from a single transmitter to multiple receivers or between different transmitter–receiver pairs. How to deal with channel fading and with interference is central to the design of wireless communication systems. In particular, we focus on these issues for the single-user MIMO and the inter-cell interference network.

The single-user MIMO is the simplest MIMO channel model, where one pair of transmitter and receiver nodes are equipped with multiple antennas and communicate with each

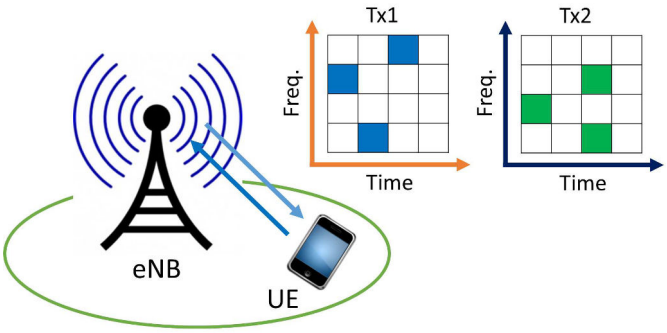

Fig. 1.1 The single-user MIMO system

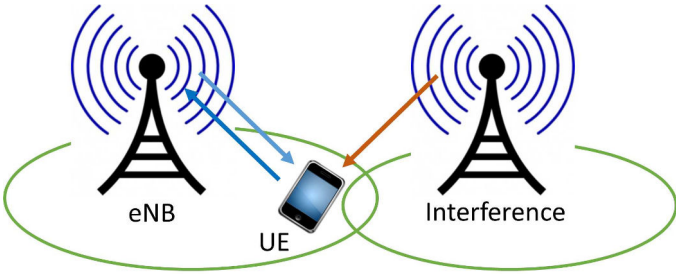

Fig. 1.2 The inter-cell interference network

other. In doing so, they have to deal with the wireless channel uncertainty. Variations of the channel strength over time, frequency, and space makes the issue more challenging. This system model consisting of multiple dimensions (time, frequency, and space) also implies a possible solution to improve network performance after the correlation in each dimension is modeled properly and well exploited.

The inter-cell interference network models the problem where interference appears from the neighbor cells. Two adjacent base stations have comparable signal strengths near their cell border, and the cell-edge user in one cell experiences a significant interference coming from the base station in the neighboring cell. The common approach to cope with interference is either to avoid it, by using different time and frequency channels, or to treat it as noise. However, these techniques may be detrimental for the spectrum efficiency of the network. Advanced design of interference-aware receivers potentially offer a practical way to deal with interference without sacrificing resources. In such receivers, the interference can be suppressed or partially canceled with some signal processing techniques.

1.1 Objective of the thesis

The traditional design of MIMO systems has focused on increasing the reliability of wireless transmission. In this context, channel fading and interference need to be properly handled. By using some signal processing techniques like channel equalization and interference suppression, advanced receivers in the network can boost the overall system performance. Recently the MIMO research has shifted more towards achieving an attractive compromise between area spectral efficiency and energy efficiency. Spectral efficiency and throughput versus energy efficiency and low complexity are rapidly changing the topology of operational cellular networks. This shift provides a new point of view that fading can be viewed as an opportunity to be exploited.

The main objective in this thesis is to provide a treatment of MIMO communications from both reliability and energy efficiency points of view. In addition to traditional topics such as channel estimation, symbol detection and interference suppression, a substantial part of the thesis is devoted to spatial modulation (SM), which is a signal design technique that aims at achieving low complexity together with energy efficiency. We address advanced theoretical concepts and their implementation issues. We try to develop an intuitive understanding of how these concepts are applied in actual wireless systems and show how they interact with some practical consideration such as channel estimation errors and different interference structures. Several examples are used in this thesis to provide insight in the design of efficient wireless MIMO systems.

1.2 Outline of the thesis and publications

The contents of the thesis are as follows:

Chapter 2: MIMO-OFDM wireless communication

In this chapter, we introduce the signal processing flow of MIMO-orthogonal frequency division multiplexing (OFDM) systems. We start the discussion by a brief overview on MIMO systems and their advantages in the spatial domain with respect to performance and system throughput. Then, we describe the basic principle of OFDM systems which provides the degrees of freedom in the time and frequency domains with low-complexity equalization and zero intersymbol interference (ISI) across adjacent frequency carriers.

We outline the benefits of combining the MIMO and OFDM schemes and we give a brief introduction to both of these techniques.

Chapter 3: Channel modeling and estimation

This chapter presents a novel channel model for wideband spatially-correlated MIMO systems. The key ideas in developing this model are exploiting the spatial, time and frequency correlations of the channel taps, and reducing the dimension of the parameter estimation space by retaining only the dominant terms. The proposed channel model is useful for many post-channel-estimation applications such as channel state information (CSI) feedback, precoder design, and channel selection. In particular, we show two examples based on this channel model: A low-complexity channel estimator and a low-complexity codeword selector for CSI feedback.

In the first example, we propose the channel estimator that offers the advantage of rendering both channel coefficients and the mean angle of departure (AoD) simultaneously. The proposed channel estimator not only offers fast and accurate estimates and gives mean square error (MSE) performance improvement, but also provides compact and useful CSI that leads to other potential post-processing complexity cutbacks.

In the second example, we show a codeword selection scheme that uses the common structures of the spatial channel model and the codebook used. Specifically, for a discrete Fourier transform (DFT)-based codebook with arbitrary size, implementation of the codeword selection can be dramatically simplified by only using a quantization operation instead of exhaustive search.

The results of this chapter can be found in:

- **C. C. Cheng**, Y. C. Chen, and Y. T. Su, "Modelling and Estimation of Correlated MIMO-OFDM Fading Channels," *In Proc. IEEE International Conference on Communications (ICC)*, 5-9 June 2011.

- **C. C. Cheng**, Y. C. Chen, Y. T. Su, and H. Sari, "Model-based channel estimation and codeword selection for correlated MIMO channels," *In Proc. IEEE Signal Processing Advances in Wireless Communications (SPAWC),* 17-20 June 2012.

Chapter 4: Robust symbol detection

In this chapter, a robust receiver for MIMO-OFDM systems is proposed. We are interested in the scenario when only a limited number of pilot symbols in both time and frequency domains are available. For this scenario, perfect channel state information is impossible to obtain and the receiver suffers from channel estimation errors.

To overcome this limitation, we first derive the optimal receiver in the sense of performing jointly channel and data estimation with the perfect channel statistical information. This scheme is statistically optimal and outperforms the conventional maximum likelihood (ML) symbol detection in some cases.

Then, we study the case without channel statistical information. In this case, the channel distribution is unknown and the receiver suffers from statistical information mismatch. To deal with that, we construct a finite set of covariance matrices and derive an efficient selection scheme based on Bayesian inference. The proposed detector simply compares a few models to obtain sufficient information instead of estimating the covariance matrices.

The results of this chapter can be found in:

- **C. C. Cheng**, S. Sezginer, H. Sari, and Y. T. Su, "Robust MIMO-OFDM detection with channel estimation errors," *in Proc. International Conference on Telecommunications (ICT)*, 6-8 May 2013
- **C. C. Cheng**, S. Sezginer, H. Sari, and Y. T. Su, "Robust MIMO Detection Under Imperfect CSI Based on Bayesian Model Selection,"*IEEE Trans. Wireless Commun. Lett.*, vol.2, no.4, pp.375-378, Aug. 2013

Chapter 5: Interference suppression

This chapter examines receiver design for multi-user systems with co-channel interference. We first focus on the design of an interference suppression strategy, which is robust to channel estimation errors, co-variance estimation errors, and a timing delay between desired signal and interfering signal, in particular to handle a mixture of interference in which pilot symbols and data symbols appear simultaneously.

Then we consider a mechanism to deal with interference in the presence of frequency-selective fading, where the covariance matrices of the interference can be regarded as a continuous function across subcarriers. The moving average technique with an adaptive window length is proposed based on an analysis focusing on the MSE of the covariance

estimate. These results only require information of the signal-to-noise ratio (SNR) and signal-to-interference ratio (SIR) and are robust against variations of the power delay profile of the interfering channel.

Finally, the scalability of a MIMO receiver to handle a growing amount of receive antennas is considered. In general, more receive antennas result in better interference-suppression capability. However, as the number of receive antennas increases, the receiver becomes more complex and loses its scalability. Therefore, a baseband algorithm is proposed which involves a minimum modification of the existing receiver structure when additional receive antennas become available.

The results in this chapter can be found in:

- **C. C. Cheng**, S. Sezginer, H. Sari, and Y. T. Su, "Linear interference suppression with covariance mismatches in MIMO-OFDM downlink," *in Proc. IEEE International Conference on Communications (ICC)*, 10-14 June 2014
- **C. C. Cheng**, S. Sezginer, H. Sari, and Y. T. Su, "Linear Interference Suppression with Covariance Mismatches in MIMO-OFDM Systems," *IEEE Trans. Wireless Commun.*, vol.13, no.12, pp.7086-7097, Dec. 2014
- **C. C. Cheng**, S. Sezginer, H. Sari, and Y. T. Su, "Moving-Average Based Interference Suppression on Frequency Selective SIMO Channels," *in Proc. IEEE Vehicular Technology Conference (VTC Spring)*, 18-21 May 2014
- **C. C. Cheng**, S. Sezginer, H. Sari, and Y. T. Su, "SINR Enhancement of Interference Rejection Combining for the MIMO Interference Channel," *in Proc. IEEE Vehicular Technology Conference (VTC Spring)*, 18-21 May 2014

Chapter 6: Spatial modulation design

In this chapter, we introduce a new SM technique using one or two active antennas and multiple signal constellations. The proposed technique, which we refer to as enhanced spatial modulation (ESM), conveys information bits not only by the index(es) of the active antenna(s), but also by the constellations transmitted from each of them. The main feature of ESM is that it uses a primary signal constellation during the single active antenna periods and some other secondary constellations during the periods with two active transmit antennas. The secondary signal constellations are derived from the primary constellation by means of geometric interpolation in the signal space.

Then we go one step further in the interpolation process and derive additional modulations, which leads to a significant increase of the number of active antenna and modulation combinations used. Other variants of the proposed ESM scheme are also provided, in which the primary modulation is partitioned into two or more subsets, and these lower-energy subsets are used in a larger number of combinations. We give design examples using two and four transmit antennas and different levels of quadrature amplitude modulation (QAM) as the primary modulation, in order to achieve different spectral efficiencies.

The results of this chapter can be found in:

- **C. C. Cheng**, H. Sari, S. Sezginer, and Y. T. Su, "Enhanced spatial modulation with multiple constellations," *in Proc. IEEE Black Sea Conference on Communications and Networking (BlackSeaCom)*, 27-30 May 2014
- **C. C. Cheng**, H. Sari, S. Sezginer, and Y. T. Su, "Enhanced spatial modulation with multiple constellations and two active antennas," *in Proc. IEEE Latin-America Conference on Communications (LATINCOM)*, 5-7 Nov. 2014
- **C. C. Cheng**, H. Sari, S. Sezginer, and Y. T. Su, "Enhanced Spatial Modulation with Multiple Signal Constellations," *IEEE Trans. Commun.*, vol.63, no.6, pp.2237-2248, June 2015
- **C. C. Cheng**, H. Sari, S. Sezginer, and Y. T. Su, "New Signal Design for Enhanced Spatial Modulation with Multiple Constellations," *in Proc. IEEE Personal Indoor and Mobile Radio Communications (PIMRC)*, Sep. 2015

Chapter 7: General conclusions and perspectives

In the last chapter, our general conclusions are presented. We revisit the motivation behind our work, summarize the contributions made, and point out future directions.

1.3 List of publications

The following publications have been produced in the course of this thesis:

Journal articles

[1] C. C. Cheng, H. Sari, S. Sezginer, and Y. T. Su, "Enhanced Spatial Modulation with Multiple Signal Constellations," *IEEE Trans. Commun.*, vol.63, no.6, pp.2237-2248, June 2015

[2] C. C. Cheng, S. Sezginer, H. Sari, and Y. T. Su, "Linear Interference Suppression with Covariance Mismatches in MIMO-OFDM Systems," *IEEE Trans. Wireless Commun.*, vol.13, no.12, pp.7086-7097, Dec. 2014

[3] C. C. Cheng, S. Sezginer, H. Sari, and Y. T. Su, "Robust MIMO Detection under Imperfect CSI Based on Bayesian Model Selection," *IEEE Wireless Commun. Lett.*, vol.2, no.4, pp.375-378, Aug. 2013

Conference papers

[1] C. C. Cheng, H. Sari, S. Sezginer, and Y. T. Su, "New Signal Design for Enhanced Spatial Modulation with Multiple Constellations," *in Proc. IEEE Personal Indoor and Mobile Radio Communications (PIMRC)*, Sep. 2015

[2] C. C. Cheng, H. Sari, S. Sezginer, and Y. T. Su, "Enhanced Spatial Modulation with Multiple Constellations," *in Proc. IEEE Black Sea Conference on Communications and Networking (BlackSeaCom)*, May 2014

[3] C. C. Cheng, H. Sari, S. Sezginer, and Y. T. Su, "Enhanced Spatial Modulation with Multiple Constellations and Two Active Antennas," *in Proc. IEEE Latin-America Conference on Communications (LATINCOM)*, Nov. 2014

[4] C. C. Cheng, S. Sezginer, H. Sari, and Y. T. Su, "Linear Interference Suppression with Covariance Mismatches in MIMO-OFDM downlink,"*in Proc. IEEE International Conference on Communications (ICC)*, June 2014

[5] C. C. Cheng, S. Sezginer, H. Sari, and Y. T. Su, "SINR Enhancement of Interference Rejection Combining for the MIMO Interference Channel," *in Proc. IEEE Vehicular Technology Conference (VTC Spring)*, May 2014

[6] C. C. Cheng, S. Sezginer, H. Sari, and Y. T. Su, "Moving-Average Based Interference Suppression on Frequency Selective SIMO Channels," *in Proc. IEEE Vehicular Technology Conference (VTC Spring)*, May 2014

[7] C. C. Cheng, S. Sezginer, H. Sari, and Y. T. Su, "Robust MIMO-OFDM Detection with Channel Estimation Errors," *in Proc. IEEE International Conference on Telecommunications (ICT)*, May 2013

[8] C. C. Cheng, Y. C. Chen, Y. T. Su, and H. Sari, "Model-based Channel Estimation and Codeword Selection for Correlated MIMO Channels," *in Proc. IEEE Signal Processing Advances in Wireless Communications (SPAWC)*, June 2012

[9] C. C. Cheng, Y. C. Chen, and Y. T. Su, "Modelling and Estimation of Correlated MIMO-OFDM Fading Channels," *in Proc. IEEE International Conference on Communications (ICC)*, June 2011

[10] C. C. Cheng, D. C. Chang, and Y. F. Chen, "Modified Decision Feedback Method for Mobile OFDM Channel Estimation," *in Proc. IEEE Personal Indoor and Mobile Radio Communications (PIMRC)*, Sept. 2010

[11] S. H. Lee, C. C. Cheng, and D. C. Chang, "Modified Decision Feedback Methods for OFDM Channel Tracking," *in Proc. IEEE International Conference on Communications, Circuits and Systems*, May 2008

Chapter 2

MIMO-OFDM wireless communications

MIMO-OFDM is the leading air interface for wireless local area networks (WLANs), and fourth-generation (4G) mobile cellular wireless systems. This technique combines MIMO technology, which multiplies capacity by transmitting different signals over multiple antennas, and OFDM, which divides a wireless channel into many subchannels to provide more reliable communications at high speeds.

2.1 MIMO systems

MIMO indicates the presence of multiple transmit antennas (multiple input) and multiple receive antennas (multiple output). While multiple transmit antennas can be used for beamforming and multiple receive antennas can be used for diversity, the term MIMO, the use of multiple antennas at both sides, often refers to the simultaneous transmission of multiple signals (spatial multiplexing) to multiply spectral efficiency (capacity).

Traditionally, researchers treated multipath propagation as an impairment to be mitigated. MIMO is the first technology that treats multipath propagation as a phenomenon to be exploited. MIMO technology realizes a diversity gain and an array gain by coherent combining, and achieves an additional fundamental gain, spatial multiplexing gain, by transmitting multiple signals over multiple, co-located antennas [1]. This is accomplished without the need for additional power or bandwidth.

- **Spatial multiplexing** yields a linear (in the minimum of the number of transmit and receive antennas) capacity increase without additional power or bandwidth. The corresponding gain is available if the scattering environment is rich enough to

allow the receive antennas to separate out the signals from the different transmit antennas. Under suitable channel fading conditions, the MIMO channel provides an additional spatial dimension for communication and yields a degree-of-freedom gain. These additional degrees of freedom can be exploited by spatially multiplexing several data streams onto the MIMO channel, and they lead to an increase in the capacity.

- **Diversity gain** leads to improved link reliability by making the channel more robust to fading and by increasing the robustness to co-channel interference. Spatial diversity can be obtained by placing multiple antennas at the transmitter (transmit diversity) and/or the receiver (receive diversity). If the antennas are placed sufficiently far apart, the channel gains between different antenna pairs fade more or less independently, and independent signal paths are created. By averaging over multiple independent signal paths, the error probability of the transmission is decreased and a diversity gain is obtained. More diversity gains can be provided by space-time codes without the need of channel knowledge at the transmitter.

- **Array gain** also called array power gain can be achieved simply by having multiple receive antennas and coherent combining at the receiver. The effective total received signal power increases linearly and this improves cellular system capacity. In general, the array gain can be realized both at the transmitter and the receiver and it requires channel knowledge for coherent combining.

Due to many advantages both from a theoretical perspective and a hardware implementation perspective, MIMO has become an essential element of wireless communication standards and will be one of the main concepts for the next-generation of mobile telecommunications standards beyond the current standards.

2.2 OFDM modulation

OFDM is a method of encoding digital data on multiple carrier frequencies. It is a frequency-division multiplexing scheme with a large number of closely spaced orthogonal sub-carrier signals which are used to carry parallel data streams. Each sub-carrier is modulated with a conventional modulation scheme such as QAM or phase-shift keying (PSK) at a low symbol rate, maintaining total data rates similar to conventional single-carrier modulation schemes in the same bandwidth.

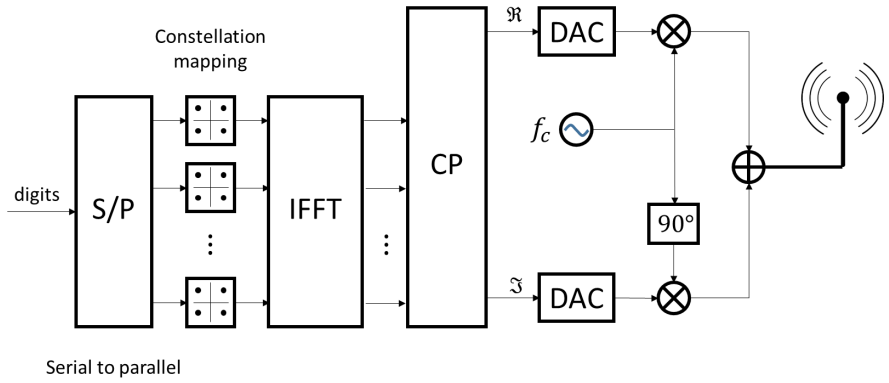

Fig. 2.1 The OFDM transmission scheme

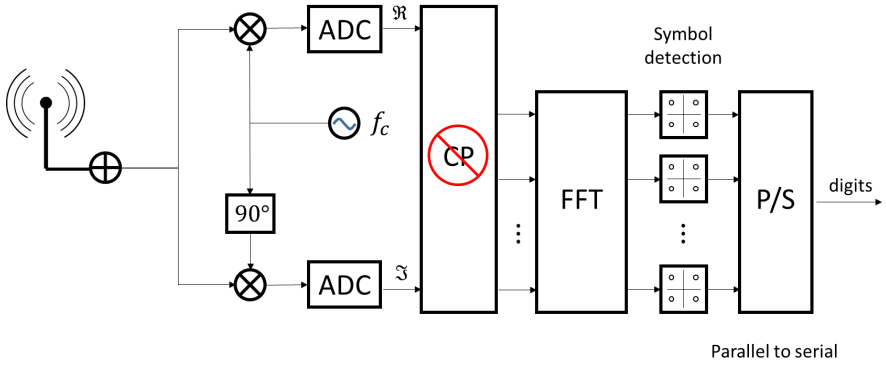

Fig. 2.2 The OFDM reception scheme

Traditionally, the biggest obstacle to reliable broadband communications is to deal with ISI: the delayed replicas of previous symbols interfere with the current symbol. The common approach for single-carrier systems is using channel-equalization at the receiver, mitigating ISI to some extent. However, the complexity of the optimal process, ML detection of transmitted symbols, grows exponentially with the number of channel taps, and it is typically used only when the number of significant taps is small [2].

- **The primary advantage** of OFDM over single-carrier schemes is its ability to deal with ISI without complex equalization filters. Indeed, OFDM being a set of slowly modulated narrowband signals, it makes the use of a guard interval between symbols affordable and eliminates ISI efficiently. The insertion of a guard interval, called cyclic prefix (CP), which is a copy of the last part of the OFDM symbol with a duration to accommodate the delay spread of the channel, eliminates the overlap between adjacent symbols and reduces channel equalization to a complex multiplication per sub-carrier.

- **Another key feature** of OFDM is that all the carrier signals are orthogonal to each other. The orthogonality allows for efficient modulator and demodulator implementation using the fast Fourier transform (FFT) algorithm on the receiver side, and inverse FFT on the sender side. This greatly simplifies the design of both the transmitter and the receiver. Unlike conventional frequency-division multiplexing, a separate filter for each sub-channel is not required. In OFDM, the equalizer only has to multiply each detected sub-carrier (Fourier coefficient) in each OFDM symbol by a complex number.

In fact, OFDM has developed into a popular scheme for wideband digital communication due to many of its advantages: high spectral efficiency, low-complexity equalization, robustness against ISI, robustness against co-channel interference, efficient implementation using FFT, and low sensitivity to time synchronization errors. This scheme will be also one of the main concepts for the next generation standards of wireless communications.

2.3 MIMO-OFDM systems

MIMO-OFDM is a particularly powerful combination because MIMO does not attempt to mitigate multipath propagation and OFDM avoids the need for signal equalization. The signaling schemes used in OFDM-based MIMO systems can be sub-divided into two main categories, spatial multiplexing and space-time coding.

- **In spatial multiplexing of MIMO-OFDM**, multiple data streams are transmitted simultaneously from different transmit antennas in each frequency sub-carrier. Since all the carrier signals are orthogonal to each other and a CP is inserted between OFDM blocks, the spatial multiplexing signals have no ISI in both time and frequency domains. Thus, if these signals arrive at the receiver antenna array with sufficiently different spatial signatures and the receiver has accurate CSI, it can separate these streams into parallel channels and decode the transmitted signal. This scheme boosts the system throughput since that different information can be transmitted simultaneously over multiple antennas.

- **A space–time code (STC)** is a method employed to improve the reliability of data transmission using redundancy across space and time. STCs rely on transmitting multiple, redundant copies of a data stream across a number of antennas with the objective that at least some of them survive the physical channel path between transmission and reception in a good enough state to allow reliable decoding. In

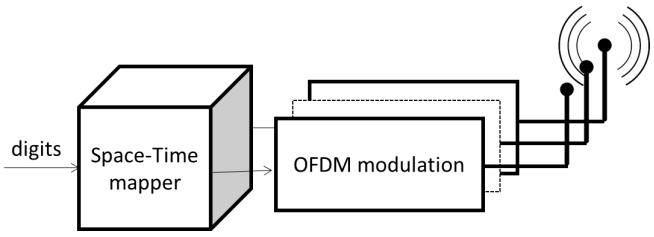

Fig. 2.3 The MIMO-OFDM transmission scheme

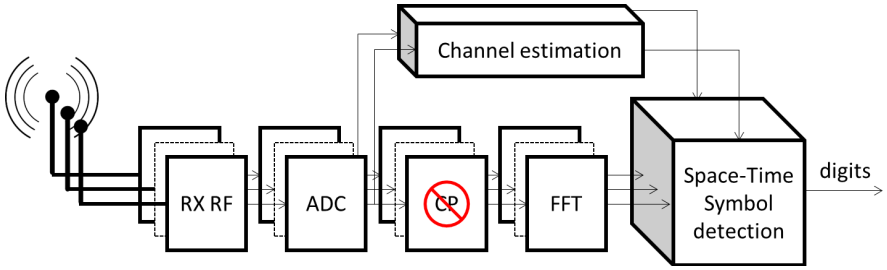

Fig. 2.4 The MIMO-OFDM reception scheme

MIMO-OFDM, STCs can consist of coding across antennas and OFDM time slots, and there also can be coding across antennas and OFDM frequency sub-carriers in order to achieve a space diversity gain.

MIMO-OFDM supports high data rates and improves reliability using multiple data streams and joint coding over the space, time, and frequency domains. It achieves a great spectral efficiency and, therefore, delivers a high capacity and data throughput.

In the first part of this thesis, from Chapter 3 to Chapter 5, we will place special attention on the main elements of MIMO-OFDM reception, particularly focusing on two key functions in the receiver: channel estimation and symbol detection. Our goal in this part is to improve system performance at the receiver side. In Chapter 6, we study MIMO transmission, mainly investigating SM, a radio frequency (RF) limited system, in which the number of active transmit (TX) antennas is limited to one or two. The reason is that multiple analog RF chains are bulky, expensive and power consuming. New signal modulations are presented in this part in order to achieve better system throughput and reduced hardware complexity.

Chapter 3

Channel modeling and estimation

In this chapter, we present a MIMO channel model on the basis of the spatial correlation between different pairs of TX and RX antennas. When the spatial correlation exists, this channel model can use fewer parameters to obtain CSI compared to the conventional channel models. This property of parameter reduction is useful for the post-channel-estimation applications. We will develop two examples of these applications given in the following; A low-complexity channel estimator and a low-complexity codeword selector for CSI feedback.

We start with a short introduction of different MIMO channel models. The ideal MIMO channel model assumes that the environment has rich scatterers and the channels are statistically independent. In this case, the channel model requires parameters for each independent channel. Practically, the MIMO channel has spatial correlations [3], which depend on physical parameters such as antenna spacing, antenna arrangement, and distributions of scatterers. Antenna correlations reduce the number of equivalent orthogonal subchannels [4], but unfortunately they do not reduce the number of parameters for channel modeling. In contrast, the stochastic MIMO channel models proposed in [5–8] need more parameters than the ideal MIMO channel model. These models add extra parameters to represent the impact of different physical parameters on channel statistics.

The motivation of the proposed channel model is to have a compact representation for CSI with only a few and important parameters. We found that channel statistics require many parameters to identify precisely. Therefore, the proposed MIMO channel model requires no information about second-order channel statistics. Spatial, frequency, and time covariance (or correlation) functions are identified by non-parametric regression. This representation has fewer parameters than the ideal channel model when the spatial

correlation exists. This model enables us to develop effective algorithms to identify the realistic channel responses. The first example is the channel estimation schemes, which can improve the conventional least squares (LS) scheme and provide a 10-dB gain in the MSE performance. Then, we present the other example that is to simplify a codeword selector for closed-loop MIMO systems. The proposed codeword selection (CS) schemes perform efficiently in terms of computational complexity, because they only need a quantization operation instead of exhaustive search. The numerical results show that the proposed CS scheme only degrades around 1-dB the symbol error rate (SER) performance when a 64-codeword codebook is used.

3.1 System model

We consider an N-subcarrier MIMO-OFDM system with linear arrays of N_T transmit and N_R receive antennas ($N_T \leq N_R$), respectively. The channel is a block fading channel in which the channel gain matrix remains unchanged within a block of B symbol intervals. The received signals at the kth subcarrier can be written as

$$\mathbf{Y}_{t,k} = \mathbf{H}_{t,k}\mathbf{X}_{t,k} + \mathbf{N}_{t,k}, \tag{3.1}$$

where $\mathbf{Y}_{t,k}$ is the $N_R \times B$ receive vector with time index t, $\mathbf{X}_{t,k}$ is the $N_T \times B$ transmit block, $\mathbf{N}_{t,k}$ is a zero mean additive white Gaussian noise (AWGN) vector, and $\mathbf{H}_{t,k}$ is the $N_R \times N_T$ matrix.

3.1.1 Spatial channel model

The channel matrix represents the frequency domain channel response of the kth subcarrier, which can be rewritten by its time-domain impulses as

$$\mathbf{H}_{t,k} = \left[\mathbf{I}_{N_T} \otimes \mathbf{w}_k^T\right] \begin{bmatrix} \mathbf{h}_t^{11} & \cdots & \mathbf{h}_t^{1N_T} \\ \vdots & \ddots & \vdots \\ \mathbf{h}_t^{N_R 1} & \cdots & \mathbf{h}_t^{N_R N_T} \end{bmatrix} \triangleq \left[\mathbf{I} \otimes \mathbf{w}_k^T\right] \bar{\mathbf{H}}_t \tag{3.2}$$

where $\mathbf{w}_k = \left[1, e^{-j2\pi k/N}, \cdots, e^{-j2(D-1)\pi k/N}\right]^T$ is the kth row of a FFT matrix, $\otimes$ denotes the Kronecker product, and $\mathbf{h}_t^{p,q} = \left[h_{t,(0)}^{p,q}, h_{t,(1)}^{p,q}, \cdots, h_{t,(D-1)}^{p,q}\right]^T$ is a discrete-time MIMO

channel impulse response with D multi-paths between the pth base station (BS) antenna and qth mobile station (MS) antenna.

In order to see the spatial correlation in the channel matrix, we further rewrite $\bar{\mathbf{H}}_t$ by its vector form as

$$vec(\bar{\mathbf{H}}_t) = vec\left(\left[vec(\bar{\mathbf{H}}_t^{(0)}), vec(\bar{\mathbf{H}}_t^{(1)}) \cdots, vec(\bar{\mathbf{H}}_t^{(D-1)})\right]^T\right)$$

where $\bar{\mathbf{H}}_t^{(d)}$ is an $N_R \times N_T$ time-domain MIMO channel matrix at the dth multi-path, and each element can be seen as a single-tap frequency non-selective channel. Therefore, the correlation between the elements of $\bar{\mathbf{H}}_t^{(d)}$ is the spatial correlation between the TX and the RX antennas.

Now, we can apply the spatial-correlated channel model [9]. This model shows that a correlated MIMO channel matrix at the dth multi-path can be expressed as:

$$\bar{\mathbf{H}}_t^{(d)} = \begin{bmatrix} h_{t,(d)}^{11} & \cdots & h_{t,(d)}^{1M} \\ \vdots & \ddots & \vdots \\ h_{t,(d)}^{N_R 1} & \cdots & h_{t,(d)}^{N_R N_T} \end{bmatrix} = \mathbf{Q}_R \mathbf{C}_t^{(d)} \mathbf{Q}_T^T \tag{3.3}$$

where $\mathbf{C}_t$ is a complex random coefficient matrix, $\mathbf{Q}_R$ and $\mathbf{Q}_T$ are predefined unitary matrices. Also, [9] suggested that the average angle of departure (AoD) can be embedded in the channel model by the alternative representation

$$\bar{\mathbf{H}}_t^{(d)} = \mathbf{Q}_R \mathbf{C}_t^{(d)} \bar{\mathbf{Q}}_T^T \mathbf{W} \tag{3.4}$$

where $\bar{\mathbf{Q}}_T \mathbf{W} = \mathbf{Q}_T^T$ and $\mathbf{W}$ is a diagonal matrix with unit modulus entries given as

$$\mathbf{W} = diag(w_1, w_2, \ldots, w_M) \tag{3.5}$$

where $w_i = \exp\left(-j2\pi \frac{(i-1)\xi}{\lambda} sin\phi\right)$, and ξ is the distance between neighboring elements at the base station linear array, λ denotes the wavelength, and ϕ is AoD information. Note that the only parameters in this model are $\mathbf{C}_t^{(d)}$ and ϕ.

In order to have a compact formulation, the time-domain correlation also needs to be modeled. We first arrange the received signals at all subcarriers into a matrix. The stacked received vector from the 0th subcarrier to the $(N-1)$th subcarrier can be expressed as

$$\mathbf{Y}_{N,t} = \left[\mathbf{Y}_{t,0}, \mathbf{Y}_{t,1}, \cdots, \mathbf{Y}_{t,(N-1)}\right]. \tag{3.6}$$

For the time indexes with an observation window of size L, the received sample vector from time t to time $(t+L-1)$ can be expressed as:

$$\mathbf{Y}_L = \left[\mathbf{Y}_{N,t}, \mathbf{Y}_{N,t+1}, \cdots, \mathbf{Y}_{N,t+L-1}\right]. \tag{3.7}$$

To arrange the pilot signal matrices, we assume that the same transmit matrix $\mathbf{X}_{t,k} = \mathbf{X}_p$ is used for all subcarrier indexes $k = 1, \cdots N$ and all time indexes $t = 1, \cdots, L$. Therefore, applying vectorization to the stacked version, we have a compact form of the relation between the TX signal and the RX signal as follows

$$vec(\mathbf{Y}_L) = \mathbf{X} \cdot vec(\mathbf{H}_L) + \mathbf{N}_L, \tag{3.8}$$

where $\mathbf{X}$ and $\mathbf{H}_L$ are defined as

$$\begin{aligned} vec(\mathbf{H}_L) &= \left[vec(\bar{\mathbf{H}}_t)^T, vec(\bar{\mathbf{H}}_{t+1})^T, \cdots, vec(\bar{\mathbf{H}}_{t+L-1})^T\right]^T \\ \mathbf{X} &= (\mathbf{I}_L \otimes \mathbf{A})(\mathbf{I}_L \otimes \mathbf{X}_p^T \otimes \mathbf{I}_{N_R D}) \\ \mathbf{A} &= \left[\mathbf{I}_{BN_R} \otimes \mathbf{w}_0^T, \cdots, \mathbf{I}_{BN_R} \otimes \mathbf{w}_{N-1}^T\right]^T. \end{aligned}$$

With this representation, we can model the time-domain correlation in the channel matrix $\mathbf{H}_L$ by the orthogonal transform with the unitary matrix $\mathbf{Q}_L$. Recalling the spatial model with the unitary matrices $\mathbf{Q}_T$ and $\mathbf{Q}_R$, we have

$$\begin{aligned} vec(\mathbf{H}_L) &= [(\mathbf{I}_L \otimes \mathbf{Q}_T \otimes \mathbf{Q}_R)(\mathbf{Q}_L \otimes \mathbf{I}_{N_R N_T}) \otimes \mathbf{I}_D]\bar{\mathbf{c}}_{coef} \\ &\approx [(\mathbf{I}_L \otimes \mathbf{W}^T \mathbf{Q}_{T,K_T} \otimes \mathbf{Q}_{R,K_R})(\mathbf{Q}_{L,K_L} \otimes \mathbf{I}_{N_R N_T}) \otimes \mathbf{I}_D]\mathbf{c}_{coef}, \end{aligned} \tag{3.9}$$

where we use the unitary matrices $\mathbf{Q}_{T,K_T}$, $\mathbf{Q}_{R,K_R}$ and $\mathbf{Q}_{L,K_L}$ with ranks $K_T (\leq N_T)$, $K_R (\leq N_R)$ and $K_L (\leq L)$ for $\mathbf{Q}_T$, $\bar{\mathbf{Q}}_R$ and $\mathbf{Q}_L$ in order to find the more compact coefficients of $vec(\mathbf{H}_L)$. Then, by using the approximation, we decouple the signal part into the product of two modeling domains - space and time domains

$$\begin{aligned} vec(\mathbf{Y}_L) &\approx \mathbf{X}(\mathbf{Q}_{L,K_L} \otimes \mathbf{W}^T \mathbf{Q}_{T,K_T} \otimes \mathbf{Q}_{R,K_R} \otimes \mathbf{I}_D)\mathbf{c}_{coef} + \mathbf{N}_L \\ &= \mathbf{X}(\mathbf{I}_L \mathbf{Q}_{L,K_L} \otimes \mathbf{W}^T \mathbf{Q}_{T,K_T} \otimes \mathbf{Q}_{R,K_R} \otimes \mathbf{I}_D)\mathbf{c}_{coef} + \mathbf{N}_L \\ &= \mathbf{A}_L \left[(\mathbf{W}_L \mathbf{X}_L)^T \tilde{\mathbf{Q}}_{T,K_T} \otimes \tilde{\mathbf{Q}}_{R,K_R}\right] \mathbf{c}_{coef} + \mathbf{N}_L \end{aligned} \tag{3.10}$$

where $\mathbf{A}_L = \mathbf{I}_L \otimes \mathbf{A}$, $\mathbf{X}_L = \mathbf{I}_L \otimes \mathbf{X}_p$, $\mathbf{W}_L = \mathbf{I}_L \otimes \mathbf{W}$, $\tilde{\mathbf{Q}}_{T,K_T} = \mathbf{Q}_{L,K_L} \otimes \mathbf{Q}_{T,K_T}$ and $\tilde{\mathbf{Q}}_{R,K_R} = \mathbf{Q}_{R,K_R} \otimes \mathbf{I}_D$. Note that this model has fewer parameters than the conventional MIMO channel model. The only unknown parameters are the term $\mathbf{c}_{coef}$ and the AoD information in $\mathbf{W}_L$.

3.2 Channel estimation

With the proposed channel model, the CSI matrix $\mathbf{H}_L$ can be obtained by only estimating $\mathbf{c}_{coef}$ and $\mathbf{W}_L$. The estimation problem is formulated by a LS minimization as follows

$$\arg \min_{\mathbf{W}_L, \mathbf{c}_{coef}} \| vec(\mathbf{Y}_L) - \mathbf{X} \cdot vec(\mathbf{H}_L) \|^2. \tag{3.11}$$

To solve this problem efficiently, we derive an iterative algorithm for obtaining the solution. For each iteration, we express the corresponding LS channel estimate from the previous iteration in terms of $\mathbf{W}_{L,opt}$ and $\mathbf{c}_{coef,opt}$.

3.2.1 Phase I: coefficient estimation

The first step is the coefficient estimation. We assume that the AoD matrix in this step is optimum, i.e., $\mathbf{W}_L = \mathbf{W}_{L,opt}$. Then, the LS estimate of $\mathbf{c}_{coef}$ is given by

$$\hat{\mathbf{c}}_{coef} = (\mathbf{Z}^H \mathbf{Z})^{-1} \mathbf{Z}^H vec(\mathbf{Y}_L) = F(\mathbf{W}_{L,opt}), \tag{3.12}$$

where $\mathbf{Z} = \mathbf{A}_L \left[(\mathbf{W}_L \mathbf{X}_L)^T \tilde{\mathbf{Q}}_{T,K_T} \otimes \tilde{\mathbf{Q}}_{R,K_R} \right]$. This result is a function of the optimal directional matrix $\mathbf{W}_{L,opt}$. At the ith iteration, since the optimal directional matrix is not available, the tentative estimation, $\hat{\mathbf{W}}_{L,i-1}$, replaces $\mathbf{W}_{L,opt}$.

3.2.2 Phase II: direction estimation

The second step is the direction estimation. Similar to the first step, we begin with the assumption that the optimal coefficient vector is available, i.e., $\mathbf{c}_{coef} = \mathbf{c}_{coef,opt}$. Define a new matrix $\mathbf{G} = \tilde{\mathbf{Q}}_{R,K_R} \mathbf{C}_{coef,opt} \tilde{\mathbf{Q}}_{T,K_T}^T$, where $\mathbf{C}_{coef,opt}$ is a $K_R D \times K_L K_T$ matrix derived by

$$\begin{cases} \mathbf{C}_{coef,opt}(i,j) = \mathbf{c}_{coef,opt}(K_R D(j-1) + i) \\ \text{where } 1 \le i \le K_R D, 1 \le j \le K_L K_T \end{cases} \tag{3.13}$$

We rewrite the received matrix in a vector form

$$vec(\mathbf{Y}_L) = \mathbf{A}_L vec(\mathbf{G} \mathbf{W}_L \mathbf{X}_L) + \bar{\Upsilon}_L \tag{3.14}$$

where $\bar{\Upsilon}_L$ represents the sum of the modeling error associated with $\mathbf{G}$ and AWGN term $\mathbf{N}_L$. As previously, since the optimal matrix is not available, the tentative estimation, $\hat{\mathbf{G}}_{i-1}$, replaces $\mathbf{G}_{opt}$ at the ith iteration.

3.2.3 Algorithm: root-finding method

Since we assume that $\mathbf{W}$ is constrained to be a diagonal matrix, i.e., $\mathbf{W} = diag(\mathbf{w})$, then $\mathbf{I}_L \otimes \mathbf{W} = diag(\mathbf{1}_L \otimes \mathbf{w})$ and therefore

$$\begin{aligned} vec(\mathbf{Y}_L) &= \mathbf{A}_L vec(\mathbf{G} \cdot diag(\mathbf{1}_L \otimes \mathbf{w}) \cdot \mathbf{X}_L) + \bar{\Upsilon}_L \\ &= \mathbf{A}_L[(\mathbf{1}_{BL} \otimes \mathbf{G}) \odot (\mathbf{X}_L^T \otimes \mathbf{1}_{ND})](\mathbf{1}_L \otimes \mathbf{I}_{N_T})\mathbf{w} + \bar{\Upsilon}_L \\ &= \mathbf{T}\mathbf{w} + \bar{\Upsilon}_L \end{aligned} \tag{3.15}$$

The LS estimate of $\mathbf{w}_{opt}$ is given by $\hat{\mathbf{w}}_{LS} = \mathbf{T}^{\dagger} vec(\mathbf{Y}_L)$, where † denotes pseudo-inverse operation. To improve the estimate and reconstruct a steering vector $\hat{\mathbf{w}}$, we analogously define a steering vector

$$\mathbf{v}(\theta) = [1, v(\theta), \ldots, v^{M-1}(\theta)]^T \tag{3.16}$$

where $\mathbf{v}(\theta) = \exp(-j2\pi \frac{d}{\lambda} sin(\theta))$. The AoD information $\hat{\phi}$ can be retrieved as

$$\hat{\phi} = \arg \max_{-\pi \le \theta \le \pi} \Re\{\angle(\hat{\mathbf{w}}_{LS})^H \mathbf{v}(\theta)\} \tag{3.17}$$

where $\angle$ denotes the phase extraction operator defined by

$$\angle([a_0 e^{jb_0}, a_1 e^{jb_1}, \ldots, a_k e^{jb_k}]) = [1, e^{(b_1 - b_0)}, \ldots, e^{(b_k - b_0)}]$$

for $a_i{}_{i=0}^{N} \in \Re^{N+1}$ and $b_i{}_{i=0}^{N} \in [0, 2\pi)$. Having obtained $\hat{\phi}$, we then convert (3.17) into a root finding problem. It searches for the root of the correlation polynomial $P(z)$ which is the closest to the unit circle, i.e.,

$$\begin{cases} \hat{z} = \arg \min_{z} ||z| - 1|, \\ \text{s.t. } P(z) = \angle(\hat{\mathbf{w}}_{LS})^H \mathbf{z} - M = 0 \end{cases} \tag{3.18}$$

and then retrieves the AoD information from $\hat{z} = \exp[-j2\pi \frac{d}{\lambda} sin(\hat{\phi})]$. Finally, the directional matrix is to be reconstructed by $\hat{\mathbf{W}}_L = \mathbf{I}_L \otimes diag(\hat{\mathbf{z}})$, where $\hat{\mathbf{z}} = [1, \hat{z}, \ldots, \hat{z}^{M-1}]$.

3.3 Precoding codeword selection

The proposed channel model can be applied to simplify the codeword selection process. The procedure for codeword selection is that after channel estimation, the receiver selects a beamforming vector from a given codebook based on the estimated CSI. The selected vector will be fed back to the BS with the purpose of improving the link quality.

To make it simpler, we only use one OFDM symbol at the time and frequency index (t,k) and omit their index. The received symbol vector can be written as

$$\mathbf{y} = \mathbf{H}\mathbf{F}_v\mathbf{x} + \mathbf{n}, \tag{3.19}$$

where $\mathbf{y}$ is a $N_R \times 1$ vector, $\mathbf{H}$ is a $N_R \times N_T$ channel matrix, $\mathbf{F}_v$ is $N_T \times K$ precoding matrix, and $\mathbf{x}$ is a $K \times 1$ transmitted vector with K independent data streams.

3.3.1 Codebook structure

In order to design an efficient codeword selection algorithm, the codebook structure plays a key role. It is well known that the DFT-based codebook is suitable for use in the correlated MIMO channel, due to its perfect-matching to the linear array antenna [10]. As shown in [11], we generate the codebook set by

$$\mathbf{F}_v = \Gamma^{v-1}\mathbf{F}_1, \ v = 2, \cdots, V \tag{3.20}$$

where $\mathbf{F}_1$ is an $N_T \times K$ matrix consisting of K columns of the N_T-point DFT matrix and $\Gamma = \text{diag}(1, e^{j2\pi/V}, \cdots, e^{j2\pi(N_T-1)/V})$ is an $N_T \times N_T$ diagonal matrix. Geometrically, the construction can be interpreted as rotating an initial vector through the N_T-dimensional complex space by using a diagonal matrix whose elements are the Vth roots of unity.

3.3.2 Codeword selection

In order to choose an optimal codeword index v, we follow the minimum singular value selection criterion (MSV-SC) [12]. That is, when a zero-forcing (ZF) receiver is used, the optimal codeword $\mathbf{F}_v$ can be found using:

$$\hat{v} = \arg\max_{v} \lambda_{min}\{\hat{\mathbf{H}}\mathbf{F}_v\} \tag{3.21}$$

where $\hat{\mathbf{H}}$ is the estimated CSI and λ_{min} denotes the minimum eigenvalue. Recall the spatial-correlated channel model $\mathbf{H} = \mathbf{Q}_R \mathbf{C} \bar{\mathbf{Q}}_T^T \mathbf{W}$. The estimated CSI can be written as

$$\hat{\mathbf{H}} = \mathbf{Q}_{K_R} \hat{\mathbf{C}} \mathbf{Q}_{K_T}^H \hat{\mathbf{W}}, \tag{3.22}$$

where $\hat{\mathbf{C}}$ and $\hat{\mathbf{W}}$ are the estimated coefficient matrix and the AoD information matrix. The estimation process can be done by the proposed iterative algorithm.

Replace the estimated CSI in (3.21) by the proposed channel estimation in (3.22). An upper bound of the minimum singular value is derived as follows:

$$\begin{aligned}
\lambda_{min}\{\hat{\mathbf{H}}\mathbf{F}_v\} &\overset{(a)}{=} \lambda_K\{\hat{\mathbf{H}}\mathbf{F}_v\} = \lambda_K\{\mathbf{Q}_{K_R} \hat{\mathbf{C}} \mathbf{Q}_{K_T}^H \hat{\mathbf{W}} \Gamma^{v-1} \mathbf{F}_1\} \\
&\overset{(b)}{\leq} \lambda_K\{\hat{\mathbf{C}} \mathbf{Q}_{K_T}^H \hat{\mathbf{W}} \Gamma^{v-1}\} \\
&\overset{(c)}{=} \lambda_K\{\hat{\mathbf{C}} \mathbf{Q}_{K_T}^H\} \\
&\overset{(d)}{\leq} \lambda_K\{\hat{\mathbf{C}}\}
\end{aligned} \tag{3.23}$$

where in (a) we use the assumption that the dimension of $\mathbf{F}_v$ is $N_R \times K$, (b) and (d) are obtained by invoking *Lemma 3.31* of [13], (c) follows as both $\hat{\mathbf{W}}$ and Γ^{v-1} are unitary. This upper bound can be achieved if $\mathbf{Q}_{K_R}$ is a unitary matrix, the model order is the same as the stream number such as $K_T = K$, and

$$\mathbf{Q}_{K_T}^H \hat{\mathbf{W}} \Gamma^{v-1} \mathbf{F}_1 = \mathbf{I}. \tag{3.24}$$

Note that finding the optimum index v which achieves (3.24) is much simpler than the exhaustive search in (3.21). We choose the orthogonal basis $\mathbf{Q}_{K_T} = \mathbf{F}_1$ and recall that both $\hat{\mathbf{W}}$ and Γ^{v-1} are diagonal matrices

$$\begin{aligned}
\hat{\mathbf{W}} &= \text{diag}[1, e^{-j2\pi\hat{\theta}}, \cdots, e^{-j2\pi(N_T-1)\hat{\theta}}] \\
\Gamma^{v-1} &= \text{diag}[1, e^{j2\pi\frac{(v-1)}{V}}, \cdots, e^{\frac{-j2\pi(N_T-1)(v-1)}{V}}].
\end{aligned}$$

The identity of (3.24) implies $\hat{\mathbf{W}}\Gamma^{v-1} = \mathbf{I}$, and therefore we have $v = \hat{\theta}L + 1$ that achieves the upper bound in (3.23). Due to the finite size of the codebook, the quantization $\hat{v} = \lfloor \hat{\theta} V + 1 \rceil$, where $\lfloor \cdot \rceil$ denotes the rounding operation, is necessary to use in the procedure.

In short, CS can be simplified if the channel estimator and the codebook are well structured. The main idea behind this design is that both the channel estimation and the CS try to find the same singular vector of CSI. Therefore, if we can properly choose the right

model for them, some duplicated efforts can be avoided. That is, when the codebook $\mathbf{F}_v = \Gamma^{v-1}\mathbf{F}_1$ is used and the channel estimate $\hat{\mathbf{H}} = \mathbf{Q}_{K_R}\hat{\mathbf{C}}\mathbf{Q}_{K_T}^H\hat{\mathbf{W}}$ is obtained, then CS is accomplished by the simple operation $\hat{i} = \lfloor \hat{\theta} V + 1 \rceil$.

3.3.3 Non-DFT codebook and model calibration

Finally, it is worth mentioning that, for non-DFT-based codebook systems, $\mathbf{Q}_{K_T} \neq \mathbf{F}_1$, our scheme can be also applied. We first introduce the chordal distance, dist$(\cdot)$, defined by

$$\text{dist}(\mathbf{F}_a, \mathbf{F}_b) \stackrel{def}{=} \sqrt{K - \sum_{p=1}^{K} \lambda_p^2\{\mathbf{F}_a^H\mathbf{F}_b\}}. \tag{3.25}$$

When $\mathbf{Q}_{K_T} \neq \mathbf{F}_1$, the upper bound (3.23) can be achieved by minimizing the chordal distance between the subspaces generated by both sides of (3.24)

$$\begin{aligned}
\hat{v} &= \arg \min_{v\in 1,\cdots,V} \text{dist}(\mathbf{Q}_{K_T}^H\hat{\mathbf{W}}\Gamma^{v-1}\mathbf{F}_1, \mathbf{I}) \\
&= \arg \max_{v\in 1,\cdots,V} \sum_{p=1}^{K} \lambda_p^2\{\mathbf{Q}_{K_T}^H\hat{\mathbf{W}}\Gamma^{v-1}\mathbf{F}_1\} \\
&\approx \arg \max_{v\in 1,\cdots,V} \sum_{p=1}^{K} \lambda_p^2\{\mathbf{F}_1^H\Gamma^{v_c-1}\hat{\mathbf{W}}\Gamma^{v-1}\mathbf{F}_1\} \qquad (3.26) \\
&\leq \arg \max_{v\in 1,\cdots,V} \sum_{p=1}^{K} \lambda_p^2\{\Gamma^{v_c-1}\hat{\mathbf{W}}\Gamma^{v-1}\} \\
&= \left\lfloor \hat{\theta} V + \frac{(\hat{v}_c - 1)V}{L_c} + 1 \right\rceil \qquad (3.27)
\end{aligned}$$

which indicates that even if $\mathbf{Q}_{K_T} \neq \mathbf{F}_1$, the simplicity of our CS scheme can still be preserved by using an approximation in (3.26) where the estimator basis $\mathbf{Q}_{K_T}$ is approximated by

$$\mathbf{Q}_{K_T} \approx \Gamma^{\hat{v}_c-1}\mathbf{F}_1 \tag{3.28}$$

The required function $\Gamma^{\hat{v}_c-1}$ can be found using an off-line calibration process to minimize the distance between the spaces spanned by the two bases as

$$\hat{v}_c = \arg \min_{v_c\in 1,\cdots,L_c} \text{dist}(\mathbf{Q}_{K_T}, \Gamma^{v_c-1}\mathbf{F}_1) \tag{3.29}$$

where L_c should be chosen as large as possible in order to improve the approximation (calibration) accuracy. As it can be operated off-line, it does not involve extra real-time computational complexity.

3.4 Performance analysis

We now describe the MSE analysis of the proposed channel estimator. In analyzing the MSE performance, we optimistically assume that the orthogonal pilot matrix is used and the directional matrix $\mathbf{W}$ is perfect. Therefore

$$\begin{aligned}\epsilon &= E\{\|\mathbf{H}_L - \hat{\mathbf{H}}_L\|_F^2\} \\ &= E\{\|\, vec(\mathbf{H}_L) - \Psi\Omega vec(\mathbf{H}_L\mathbf{X}_L + \mathbf{N}_L\|_2^2\}\end{aligned} \tag{3.30}$$

where $\Psi = \mathbf{A}_L(\mathbf{W}_{L,opt}\mathbf{X}_L)^T\tilde{\mathbf{Q}}_{T,K_T} \otimes \tilde{\mathbf{Q}}_{R,K_R}$ and $\Omega = (\mathbf{Z}^H\mathbf{Z})^{-1}\mathbf{Z}^H$. As $\mathbf{H}_L\mathbf{X}_L$ and $\mathbf{N}_L$ are statistically independent, the MSE can be separated into two terms which are contributed by the modeling error (reduced-rank basis matrices) and AWGN, respectively.

$$\begin{aligned}\epsilon &= \epsilon_h + \epsilon_n \\ &= E\{\|\, vec(\mathbf{H}_L) - \Psi\Omega vec(\mathbf{H}_L\mathbf{X}_L)\|_2^2\} + E\{\|\Psi\Omega vec(\mathbf{N}_L)\|_2^2\} \\ &= tr\{(\mathbf{I} - \mathbf{P}_w^H)(\mathbf{I} - \mathbf{P}_w)\mathbf{R}_h\} + tr\{\frac{N_0}{B}\mathbf{P}_w\} \\ &= \sum_{k=1}^{\chi} \lambda_k \|(\mathbf{I} - \mathbf{P}_w\mathbf{f}_k)\|_2^2 + \frac{N_0}{B}K_s\end{aligned} \tag{3.31}$$

where

$$\mathbf{P}_w = [\mathbf{W}_{L,opt}^T\tilde{\mathbf{Q}}_{T,K_T}(\tilde{\mathbf{Q}}_{T,K_T}^T\tilde{\mathbf{Q}}_{T,K_T})^{-1}\tilde{\mathbf{Q}}_{T,K_T}^T\mathbf{W}_{L,opt}^*] \otimes \tilde{\mathbf{Q}}_{R,K_R}\tilde{\mathbf{Q}}_{R,K_R}^T, \tag{3.32}$$

$\mathbf{R}_h = E\{vec(\mathbf{H}_L)\, vec(\mathbf{H}_L)^H\}$ is the channel correlation matrix, $\mathbf{f}_k$ is $\mathbf{R}_h$'s eigenvector associated with the eigenvalue λ_k, and $\chi = N_R N_T LD$ is the degree of freedom of $\mathbf{H}_L$.

Let M be the rank of the dominant signal subspace of the channel covariance matrix $\mathbf{R}_h$, where $1 < M < \chi$. We define $K_s = K_T K_R K_L D$ is the compound modeling order. If K_s is chosen to be smaller than M, there is an under-modeling error contributed by $\sum_{k=1}^{\chi} \lambda_k \|(\mathbf{I} - \mathbf{P}_w\mathbf{f}_k)\|_2^2$. This error dominates the mean squared error when the AWGN is small (high SNR region). On the other hand, the thermal noise can be reduced by using a

small model order of K_s. This noise-reduction effect dominates the mean squared error when the AWGN is large (low SNR region).

3.5 Numerical results

The simulation results reported here use an 8×8 MIMO-OFDM system with FFT-size $N = 128$ and angle spread (AS) = $2°$. The channel model is based on the 3GPP spatial channel model (SCM) which generates the channel coefficients according to a set of selected parameters (e.g., AS, AoD, angle of arrival (AoA), etc.). It is a popular parametric stochastic model whose spatial cross correlations are functions of the joint distribution of the AoD at the transmit side and the AoA at the receive side.

We assume that the environment surrounding the MS is rich in scattering with negligible spatial correlations. Hence, a full rank basis matrix is used to characterize the spatial correlation at the receive side. Other assumptions and conditions used in our simulation are: (i) the antenna spacing at transmit and receive arrays are both 0.5λ, (ii) an orthogonal training matrix is used, (iii) 10 iterations are used for all simulations (although in most cases, convergence occurs in less than 3 iterations), and (iv) SNR is defined as (E_b/N_0) at the input of each receive antenna, (v) orthonormal polynomial basis matrices [9] are used for $\mathbf{Q_T}$, $\mathbf{Q_R}$, and $\mathbf{Q_L}$.

3.5.1 Channel estimation results

The algorithm computes the frequency domain channel response $\hat{\mathbf{H}}_L$ by substituting the final result of the estimated coefficient matrix $\hat{\mathbf{c}}_{coef}$ and that of $\hat{\mathbf{W}}_L$ into $vec(\hat{\mathbf{H}}_L) = \mathbf{A}_L vec(\hat{\mathbf{G}}\hat{\mathbf{W}}_L)$ to compare with the conventional LS solution. The channel is a block fading channel with an approximated rank of two. Since the BS spatial correlations are high, the corresponding correlation function lies in a low-dimension subspace so that a small K_T is sufficient to describe the channel.

In Fig. 3.1, we compare the performance of our proposed algorithm for long (ratio= 16/128) and short (ratio= 8/128) CP length systems. Assume the modeling order of channel taps D is perfectly equal to the CP length. Since a longer channel delay (long CP case) needs a higher model order D, that degrades noise-reduction ability. Therefore, the short CP cases (three top lines) have better performance than the one with the long CP (three bottom lines), but both of them are superior to the conventional LS solution.

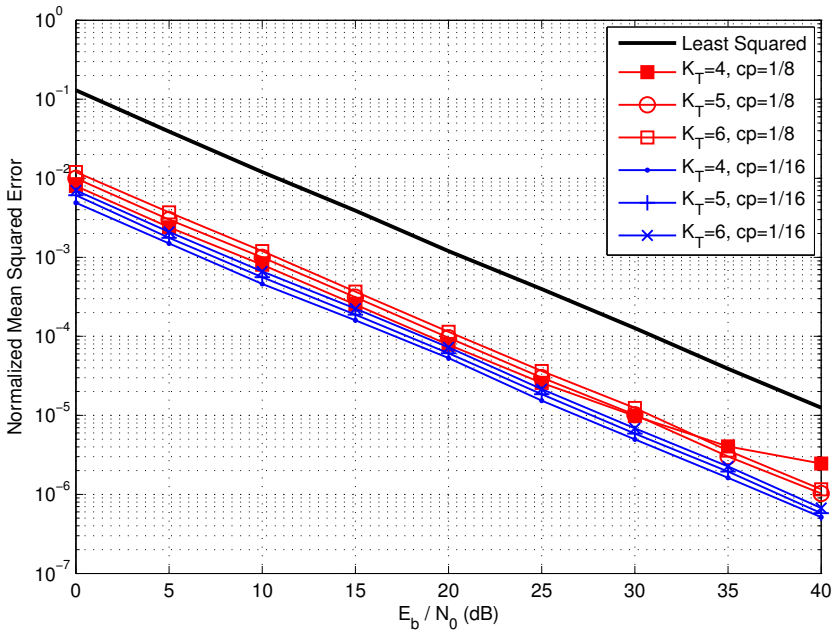

Fig. 3.1 The effect of CP length on the MSE performance in a SCM channel; $AS = 2^\circ$ and $f_d T_s = 0.02844$

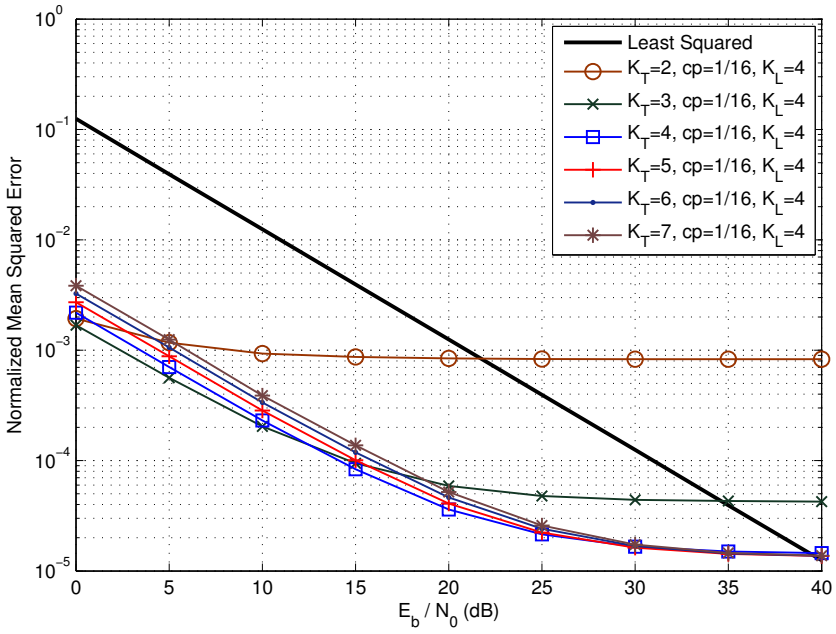

Fig. 3.2 The effect of the model order (K_T) on the MSE performance in a SCM channel; $AS = 2^\circ$ and $f_d T_s = 0.02844$

In Fig. 3.2, considering a time correlated fading environment with an observation window $L = 7$, the processing dimension can be drastically reduced when the spatial or time domain correlation is high enough. We find that an optimal K_T exists for any given SNR. Increasing the model order does not necessarily improve the performance. In contrast, performance degradation occurs when the modeling order is not large enough to capture the channel characteristic. Such behavior is consistent with what the performance analysis has predicted and is similar to those observed in other model-based approaches [7, 8].

Besides, considering a certain level of an acceptable MSE, we can reduce the processing dimension (K_T, K_L, D). For example, in a case of $K_T = 4$, $K_L = 4$, and cp=1/16 with $MSE = 10^{-3}$, the compression rate is $\frac{4}{8} \times \frac{4}{7} \times \frac{1}{16} \approx 0.018$, which means that only 2% of the coefficients are needed to properly represent the channel response.

3.5.2 Codeword selection results

The performance of the proposed CS algorithm is evaluated by using the SER and the mean absolute error (MAE). The SER is defined based on [14] as follows

$$\text{SER} \overset{def}{=} 1 - \prod_{k=1}^{K} (1 - P_k) \tag{3.33}$$

where $P_k = N_e Q\left(\sqrt{(\text{SNR}_k d_{min}^2)/2}\right)$ is the error probability, d_{min} is the minimum distance of the constellation used, N_e represents the average number of nearest neighbors, and SNR_k denotes the SNR value on the kth data stream. Then, we define the distance of the error event by MAE. The MAE denotes the average Euclidean distance between the estimated index and the perfect index defined by

$$MAE \overset{def}{=} E\left\{|I_{perf} - I_{est}|\right\} \tag{3.34}$$

where I_{perf} is the optimal codeword index that is chosen by perfect CSI, and I_{est} is the estimated index by using the proposed CS scheme or exhaustive search with the estimated CSI.

In Fig. 3.3, we show the SER and MAE performance of our CS algorithm and the conventional one using exhaustive search with a 64-codeword DFT-based codebook. Due to the high spatial correlations and the use of a linear receiver, the system only provides a limited number of data streams K. In the SER (left-hand side figure), the two bottom curves ($K = 1$) show a very small SER gap (within 1 dB) between the conventional and

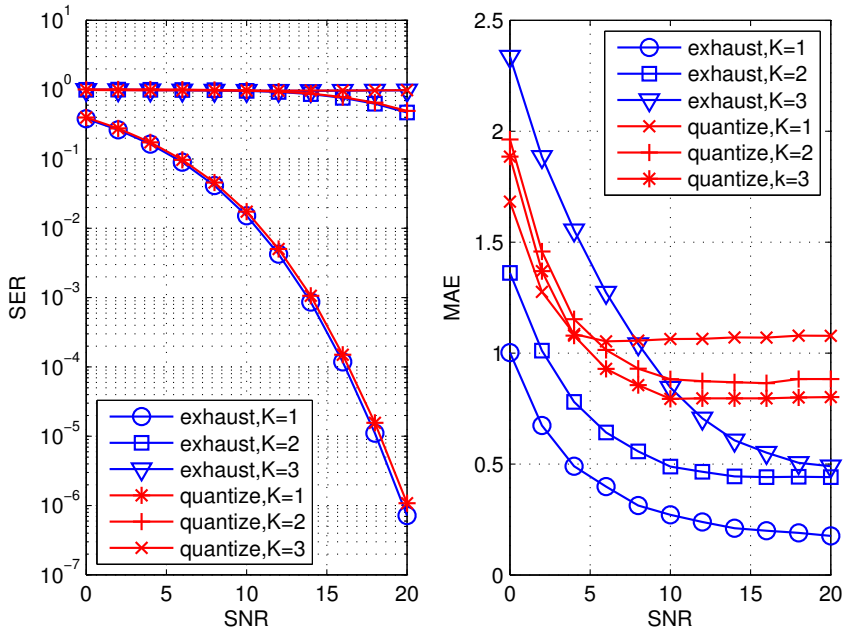

Fig. 3.3 SER and MAE performance of the proposed CS (quantize) and the exhaustive search (exhaust) algorithms with $V = 64$.

the proposed scheme. We notice, in the right figure, the MAE of the proposed CS scheme is less than 1 when the SNR is high. This means that the proposed scheme selects the codeword index that is almost identical to the perfect codeword index.

3.6 Conclusion

Channel correlation degrades the capacity of MIMO systems, reducing the number of independent data streams that can be sent. However, we show the fact that exploiting the correlation can simplify the signal processing and improve the receiver performance. Two examples are introduced, i.e., the channel estimator and the codeword selector, for a correlated MIMO-OFDM channel.

The key ideas in developing the proposed channel estimator are exploiting the spatial, time and frequency correlations of the channel taps, and reducing the dimensionality of the parameter estimation space by retaining only the dominant terms. Numerical results show that the proposed algorithms give 10 to 15 dB MSE gain and are most effective when the AS is small, i.e., when the dimension of the dominant subspace is much smaller than full channel correlation rank. Not only they offer fast and accurate estimates, give MSE

performance improvement due to the noise reduction effect, but more importantly, they also provide compact and useful CSI that leads to feedback channel bandwidth reduction and other potential post-processing complexity cutbacks.

The proposed CS is one of the examples to show how this compact CSI works. If the DFT-based codebook is used, the selection process can be simply performed by a rounding operation on the estimated AoD as the part of the channel estimate. As a result, the use of the compact CSI reduces computational complexity from an exhaustive search to a simple rounding operation. Also, the system performance is maintained. The SER loss presented in the numerical results is less than 1 dB when the 64-codeword DFT-based codebook is used. Finally, we demonstrate how to generalize this CS scheme to the non-DFT based codebook. The mismatch between different codebooks can be compensated by a linear transform (calibration) without the need of extra real-time computational complexity.

Chapter 4

Robust symbol detection

In Chapter 3, different channel estimation schemes were investigated. We found that the resulting MSE can have a very small value, but it never goes to zero as the SNR increases. This means that the channel estimation always has some errors, known as the imperfect CSI, which is not avoidable due to the nature of wireless channel, e.g., fading, thermal noise, and channel modeling errors.

The impact of imperfect CSI on MIMO symbol detection is the main concern in this chapter. The first part of our study focuses on the case that the receiver has channel estimation errors, but the channel distribution information at receiver (CDIR) is perfectly known. In this case, the statistically optimal solution can be found by the ML criterion with the given CDIR. Then we further consider the case when the receiver has both channel estimation errors and imperfect CDIR. In this case, we can guarantee the system performance by using Bayesian model selection (BMS).

Efforts to enhance MIMO detection against imperfect CSI come from two main fronts: 1) those using space-time coding or channel coding and 2) those proposing improved sub-optimum detectors.

- Among the former, it is worth citing [15], where a space-time trellis coded optimum receiver for Rayleigh fading was proposed. This work was later extended to deal with frequency and spatially selective Rician fading [16]. In both cases, the CSI uncertainty models, which are channel estimates dependent, are used to modify the ML criterion. In another approach, Sadough *et al.* [17] applied a soft-input soft-output decoder for bit interleaved coded modulation. They suggested a modified

iterative decoding scheme to reduce the imperfect CSI impact. Unfortunately, their solutions are suitable for time-flat or slow fading only.

- Among those in search of improved detection algorithms are the modified sphere decoder [18] and an improved successive interference cancelation scheme [19]. The statistic information of channel estimation errors is used to devise better early stopping, ordering, regularizing and pre-whitening strategies. Nevertheless, none of them is designed for use in a time and/or frequency selective environment.

According to the literature survey, we found the need to study the imperfect CSI on a channel model, including spatial, time, and frequency fading effects. In this case, CSI is obtained by reference signal assisted estimation for which pilot symbols are periodically inserted in the data frame. This information is never perfect and estimation errors can significantly degrade the MIMO receiver performance even if a ML symbol detector is in place.

4.1 System model

Recall a single-user MIMO-OFDM system with N_T TX and N_R RX antennas. The received symbol vector at the t-th time slot and the k-th subcarrier can be written as

$$\begin{aligned}\mathbf{y}_{tk} &= \mathbf{H}_{tk}\mathbf{x}_{tk} + \mathbf{n}_{tk} \\ &= \mathbf{X}_{tk}\mathbf{h}_{tk} + \mathbf{n}_{tk},\end{aligned} \tag{4.1}$$

where $\mathbf{y}_{tk}$ is a $N_R \times 1$ symbol vector, $\mathbf{H}_{tk}$ is a $N_R \times N_T$ channel matrix, $\mathbf{n}_{tk}$ is a $N_R \times 1$ AWGN vector, $\mathbf{X}_{tk} = \mathbf{x}_{tk}^T \otimes \mathbf{I}_{N_R}$, and $\mathbf{h}_{tk} = vec(\mathbf{H}_{tk})$. We assume that $\mathbf{n}_{tk} \sim \mathcal{N}_c(\mathbf{0}, \Sigma_\mathbf{n})$ and $\mathbf{h}_{tk} \sim \mathcal{N}_c(\mathbf{0}, \Sigma_\mathbf{h})$.

4.1.1 Pilot symbols

The pilot symbols are represented by $\mathbf{X}_{t'k'}$, where t' and k' are the pilot locations shown in Fig. 4.1. Denoting the set of pilot positions by $\mathscr{P}$ and considering only the received samples $\mathbf{y}_p$ in the $|\mathscr{P}| = N_p$ pilot positions, the received pilot symbols are given by

$$\mathbf{y}_p = \mathbf{X}_p\mathbf{h}_p + \mathbf{n}_p,\ p \in \mathscr{P}, \tag{4.2}$$

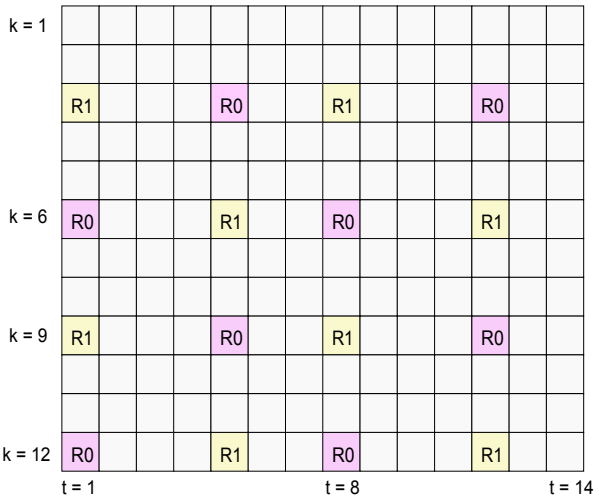

Fig. 4.1 Mapping of the pilot symbols, where $R0$ and $R1$ denote the pilot positions.

where $\mathbf{y}_p = [\mathbf{y}^T_{t'_1 k'_1}, \cdots, \mathbf{y}^T_{t'_p k'_p}]^T$ is a $N_R N_p \times 1$ symbol vector, $\mathbf{h}_p = [\mathbf{h}^T_{t'_1 k'_1}, \cdots, \mathbf{h}^T_{t'_p k'_p}]^T$, and $\mathbf{X}_p = diag(\mathbf{X}_{t'_1 k'_1}, \cdots, \mathbf{X}_{t'_p k'_p})$ with $diag(\cdot)$ as the block diagonalization. We assume the orthogonality of pilots as $\mathbf{X}^H_p \mathbf{X}_p = \mathbf{I}_{N_T N_p}$, the distribution of the channel vector as $\mathbf{h}_p \sim \mathcal{N}_c(\mathbf{0}, \Sigma_{\mathbf{h}_p})$, and the AWGN vector as $\mathbf{n}_p \sim \mathcal{N}_c(\mathbf{0}, \Sigma_{\mathbf{n}_p})$.

4.1.2 Channel model

The correlated channel model including space, time, and frequency domain correlations, known as the triply selective channel, can be found in [20]. However, the model of [20] is only in the time domain and a DFT process is necessary to simplify our analysis. For this purpose, we express the MIMO channel impulse response with an effective memory of L taps as

$$\bar{\mathbf{h}}_t = [\tilde{\mathbf{h}}^{(1,1)}_t, \cdots, \tilde{\mathbf{h}}^{(1,N_T)}_t, \cdots, \tilde{\mathbf{h}}^{(N_R,1)}_t, \cdots, \tilde{\mathbf{h}}^{(N_R,N_T)}_t]^T,$$

where $\tilde{\mathbf{h}}^{(m,n)}_t = [\tilde{h}_t(1)^{(m,n)}, \cdots, \tilde{h}_t(L)^{(m,n)}]$ denotes the coefficients of the (m,n)th subchannel between the nth transmit and the mth receive antennas at the time index t. The frequency domain correlation matrices of the above channel can be computed by

$$\begin{aligned} \Sigma_{\mathbf{h}_{t_1,k_1}\mathbf{h}_{t_2,k_2}} &= E[vec(\mathbf{H}_{t_1,k_1})\, vec(\mathbf{H}_{t_2,k_2})^H] \\ &= E[\Omega_{k_1} \bar{\mathbf{h}}_{t_1} \bar{\mathbf{h}}^H_{t_2} \Omega^H_{k_2}] = \Omega_{k_1} \mathbf{F}(\mathscr{S}) \Omega^H_{k_2}, \end{aligned} \tag{4.3}$$

where $\Omega_{k_i} = \mathbf{I}_{N_T N_R} \otimes [\omega^{(k_i-1)0}, \cdots, \omega^{(k_i-1)(L-1)}]$ is the k_ith row of the N_F-point DFT matrix, and the correlation function $\mathbf{F}(\mathscr{I})$ is given by

$$\mathbf{F}(\mathscr{I}) = \Psi_{Rx} \otimes \Psi_{Tx} \otimes \mathbf{C}_{ISI} \cdot J_0\left(2\pi f_d (t_1 - t_2) T_s\right) \tag{4.4}$$

where $J_0(\cdot)$ is the zero-order Bessel function of the first kind, f_d is the maximum Doppler frequency, $\Delta t = t_1 - t_2$ is the difference of two time indexes, T_s is the duration of one OFDM symbol, and $\mathbf{C}_{ISI}$ is the covariance matrix of the intersymbol interference. The matrices Ψ_{Rx} and Ψ_{Tx} are the RX and TX correlation matrices, respectively.

4.1.3 Channel estimation errors

To model channel estimation errors, we start with the classical channel estimator for the correlated fading channels. This approach is called 2D-MMSE channel estimator, which follows the linear minimum mean square error (LMMSE) criterion given as follows

$$\begin{aligned} \hat{\mathbf{h}}_{tk} &= \hat{\mathbf{W}}_{tk} \hat{\mathbf{h}}_p \\ &= \Sigma_{\mathbf{h}_{tk}\hat{\mathbf{h}}_p} \Sigma_{\hat{\mathbf{h}}_p}^{-1} \hat{\mathbf{h}}_p \end{aligned} \tag{4.5}$$

The channel estimation on the pilot positions $\hat{\mathbf{h}}_p$ is obtained by the LS criterion as $\hat{\mathbf{h}}_p = \mathbf{X}_p^{\dagger}\mathbf{y}_p$ with Moore-Penrose pseudoinverse denoted by $\dagger$. The interpolation matrix $\hat{\mathbf{W}}_{tk}$ is obtained by the orthogonality principle. That is, $E[(\mathbf{h}_{tk} - \hat{\mathbf{W}}_{tk}\hat{\mathbf{h}}_p)\hat{\mathbf{h}}_p^H] = \mathbf{0}$.

For the 2D-MMSE estimator, the channel estimation errors can be modeled as:

$$\mathbf{e}_{tk} = \mathbf{h}_{tk} - \hat{\mathbf{h}}_{tk}. \tag{4.6}$$

The error vector comes from the estimated CSI of the pilot symbols $\hat{\mathbf{h}}_p$ and also from the interpolation matrix $\hat{\mathbf{W}}_{tk}$. Now, we can briefly evaluate its impact on the symbol detection. The received signal can be reformulated as follows:

$$\begin{aligned} \mathbf{y}_{tk} &= \mathbf{X}_{tk}(\hat{\mathbf{h}}_{tk} + \mathbf{e}_{tk}) + \mathbf{n}_{tk} \\ &= \mathbf{X}_{tk}\hat{\mathbf{W}}_{tk}\hat{\mathbf{h}}_p + (\mathbf{X}_{tk}\mathbf{e}_{tk} + \mathbf{n}_{tk}). \end{aligned} \tag{4.7}$$

To decode the transmit symbol $\mathbf{X}_{tk}$, the noise term, including both $\mathbf{X}_{tk}\mathbf{e}_{tk}$ and $\mathbf{n}_{tk}$, needs to be taken into account. Obviously $\mathbf{X}_{tk}\mathbf{e}_{tk}$ is more harmful than $\mathbf{n}_{tk}$ because it is related to the transmitted symbol $\mathbf{X}_{tk}$. This problem would be more serious when the orthogonal

space time block code (orthogonal space time block code (OSTBC)) is used. A simple example of $N_T \times 2$ OSTBC is given by

$$\begin{aligned}[\mathbf{y}_{11}, \mathbf{y}_{21}] =& [\mathbf{X}_{11}\hat{\mathbf{W}}_{11}, \mathbf{X}_{21}\hat{\mathbf{W}}_{21}]\hat{\mathbf{h}}_p \\ &+ [\mathbf{X}_{11}\mathbf{e}_{11}, \mathbf{X}_{21}\mathbf{e}_{21}] + [\mathbf{n}_{11}, \mathbf{n}_{21}] \end{aligned} \tag{4.8}$$

In this case, the channel estimation errors result in a strong and correlated noise term $[\mathbf{X}_{11}\mathbf{e}_{11}, \mathbf{X}_{21}\mathbf{e}_{21}]$, which will degrade the performance of a MIMO symbol detector.

4.2 Symbol detection with perfect CDIR

For comparison purposes, we first review the conventional approach without considering imperfect CSI, referred to as the mismatched receiver. Omitting the time and frequency index (t, k), the resulting outputs of the mismatched receiver are given by

$$\hat{\mathbf{X}}_{MR} = \arg\min_{\mathbf{X}\in\mathbb{X}} \|\mathbf{y} - \mathbf{X}\hat{\mathbf{h}}\|^2. \tag{4.9}$$

The mismatched receiver decodes symbols by using the channel estimate in the perfect CSI decision metric. We treat this receiver as the performance benchmark.

4.2.1 Robust ML receiver

The main idea of the robust ML receiver (RMLR) is to model the uncertainty of the channel estimation results. Assume $\mathbf{h}_p$ and $\mathbf{n}_p$ are independent of each other, the channel estimation on the pilots, $\hat{\mathbf{h}}_p$, is computed as:

$$\begin{aligned}\hat{\mathbf{h}}_p &= \mathbf{X}_p^{\dagger}\mathbf{y}_p = \mathbf{h}_p + \mathbf{X}_p^H\mathbf{n}_p \\ &\sim \mathcal{N}_c(\mathbf{0}, \Sigma_{\mathbf{h}_p} + \Sigma_{\mathbf{n}_p}). \end{aligned} \tag{4.10}$$

Using (4.5), the channel estimation errors $\mathbf{e}_{tk}$ in (4.7) are shown as follows:

$$\begin{aligned}\mathbf{e} &= \mathbf{h} - \hat{\mathbf{h}} = \mathbf{h} - \Sigma_{\mathbf{h}\hat{\mathbf{h}}_p}^H \Sigma_{\hat{\mathbf{h}}_p}^{-1}\hat{\mathbf{h}}_p \\ &\sim \mathcal{N}_c(\mathbf{0}, \Sigma_{\mathbf{h}} - \Sigma_{\mathbf{h}\hat{\mathbf{h}}_p}^H \Sigma_{\hat{\mathbf{h}}_p}^{-1}\Sigma_{\mathbf{h}\hat{\mathbf{h}}_p}), \end{aligned} \tag{4.11}$$

where $\Sigma_{\hat{\mathbf{h}}_p} = E[\hat{\mathbf{h}}_p \hat{\mathbf{h}}_p^H]$ is given in (4.10), and $\Sigma_{\mathbf{h}\hat{\mathbf{h}}_p} = E[\mathbf{h}(\mathbf{h}_p + \mathbf{X}_p^H \mathbf{n}_p)^H] = \Sigma_{\mathbf{h}\mathbf{h}_p}$. Thus, we have the conditional probability of the received signal in (4.7) as follows:

$$P(\mathbf{y}|\mathbf{X}, \hat{\mathbf{h}}_p) \sim \mathcal{N}_c(\mathbf{X}\hat{\mathbf{W}}\hat{\mathbf{h}}_p, \Sigma_{\mathbf{n}} + \mathbf{X}\Sigma_{\mathbf{e}}\mathbf{X}^H), \tag{4.12}$$

where $\Sigma_{\mathbf{e}} = E[\mathbf{e}\mathbf{e}^H]$ is defined in (4.11). The RMLR decodes the transmitted codeword $\mathbf{X}$ by maximizing the conditional probability (4.12) with the channel estimation results $\hat{\mathbf{h}}_p$. The resulting output of the RMLR can be defined as

$$\begin{aligned}
\hat{\mathbf{X}}_{RML} &= \arg\max_{\mathbf{X}\in\mathbb{X}} \ln P(\mathbf{X}|\mathbf{y}, \hat{\mathbf{h}}_p) \\
&= \arg\max_{\mathbf{X}\in\mathbb{X}} \ln P(\mathbf{y}|\mathbf{X}, \hat{\mathbf{h}}_p) \\
&= \arg\min_{\mathbf{X}\in\mathbb{X}} (\|\mathbf{y} - \mathbf{X}\hat{\mathbf{h}}\|^2_{\Sigma_{\mathbf{y}}} + \ln det(\Sigma_{\mathbf{y}})),
\end{aligned} \tag{4.13}$$

where the notation is defined as $\|\Phi\|^2_\Psi = \Phi^H \Psi^{-1} \Phi$. The correlation function $\Sigma_{\mathbf{y}} = \Sigma_{\mathbf{n}} + \mathbf{X}\Sigma^H_{\mathbf{h}\mathbf{h}_p}(\Sigma_{\mathbf{h}_p} + \Sigma_{\mathbf{n}_p}/N_p)^{-1}\Sigma_{\mathbf{h}\mathbf{h}_p}\mathbf{X}^H$ is based on (4.10), (4.11) and (4.12). Note that the RMLR is a modified version of the mismatched receiver with a weighting matrix $\Sigma_{\mathbf{y}}$, which provides more freedom to change the decoding metric according to the uncertainty of the channel estimation results.

4.2.2 Optimal receiver

The optimal receiver (OPT) decodes the transmitted codeword $\mathbf{X}_{tk}$ by jointly processing the received signal $\mathbf{y}_{tk}$ and the received pilots $\mathbf{y}_p$. This scheme performs symbol detection directly without the channel estimation process. The OPT is optimal if there is no modelling errors from the interpolation matrix $\mathbf{W}_{tk}$.

Assume that the perfect channel response at the (t,k)th positions $\mathbf{h}_{tk}$ can be constructed by linear interpolation of those at the pilot positions $\mathbf{h}_p$ with negligible error

$$\mathbf{h}_{tk} = \mathbf{W}_{tk}\mathbf{h}_p, \tag{4.14}$$

where the interpolation matrix $\mathbf{W}_{tk}$ is obtained by applying the orthogonality principle, $E[(\mathbf{h}_{tk} - \mathbf{W}_{tk}\mathbf{h}_p)\mathbf{h}_p^H] = \mathbf{0}$, i.e., $\mathbf{W}_{tk} = \Sigma_{\mathbf{h}_{tk}\mathbf{h}_p}\Sigma^{-1}_{\mathbf{h}_p}$.

The OPT performs ML detection that maximizes the conditional probability on the transmit matrix $\mathbf{X}$ given the following matrices: the received signal $\mathbf{y}$, the received pilot signal

$\mathbf{y}_p$, and the pilot signal $\mathbf{X}_p$. The resulting output of OPT can be written as

$$\begin{aligned}\hat{\mathbf{X}}_{OPT} &= \arg\max_{\mathbf{X}\in\mathbb{X}} \ln P(\mathbf{X}|\mathbf{X}_p,\mathbf{y}_p,\mathbf{y}) \\ &= \arg\max_{\mathbf{X}\in\mathbb{X}} \ln E_{\mathbf{h}_p}[P(\mathbf{y}|\mathbf{X},\mathbf{h}_p)P(\mathbf{y}_p|\mathbf{X}_p,\mathbf{h}_p)] \\ &= \arg\min_{\mathbf{X}\in\mathbb{X}} (-\mathbf{B}^H\mathbf{A}^{-1}\mathbf{B} + \ln det(\mathbf{A})), \end{aligned} \tag{4.15}$$

where the matrices $\mathbf{A}$ and $\mathbf{B}$ are defined as:

$$\begin{aligned}\mathbf{B} &= \mathbf{W}^H\mathbf{X}^H\Sigma_{\mathbf{n}}^{-1}\mathbf{y} + \mathbf{X}_p^H\Sigma_{\mathbf{n}_p}^{-1}\mathbf{y}_p, \\ \mathbf{A} &= \mathbf{W}^H\mathbf{X}^H\Sigma_{\mathbf{n}}^{-1}\mathbf{X}\mathbf{W} + \mathbf{X}_p^H\Sigma_{\mathbf{n}_p}^{-1}\mathbf{X}_p + \Sigma_{\mathbf{h}_p}^{-1}.\end{aligned}$$

The result in (4.15) can be obtained when the required CDIR is given. That includes the interpolation matrix $\mathbf{W}$, the correlation matrices of AWGN $\Sigma_{\mathbf{n}}$ (also $\Sigma_{\mathbf{n}_p}$), and the correlation matrix of CSI on the pilot positions $\Sigma_{\mathbf{h}_p}$. In other words, the OPT scheme exploits all information related to CSI and the transmitted symbol in order to directly perform the symbol detection without the procedures of channel estimation and imperfect CSI modeling.

4.2.3 OSTBC-MIMO systems

For a MIMO-OFDM system with OSTBC, the $N_T \times N_d$ encoded codeword $\bar{\mathbf{X}}_{d,k}$ at the kth sub-carrier can be written as $\bar{\mathbf{X}}_{d,k} = (\mathbf{x}_{1k}, \cdots, \mathbf{x}_{N_d k})$, and the received codeword $\mathbf{y}_{d,k}$ at the kth sub-carrier is obtained as

$$\begin{bmatrix} \mathbf{y}_{1k} \\ \vdots \\ \mathbf{y}_{N_d k} \end{bmatrix} = \begin{bmatrix} \mathbf{H}_{1k} & & \mathbf{0} \\ & \ddots & \\ \mathbf{0} & & \mathbf{H}_{N_d k} \end{bmatrix} \bar{\mathbf{X}}_{d,k} + \begin{bmatrix} \mathbf{n}_{1k} \\ \vdots \\ \mathbf{n}_{N_d k} \end{bmatrix}.$$

In the derivation of the decoding metric, we rearrange the matrices and obtain the following equivalent equation:

$$\mathbf{y}_{d,k} = \mathbf{X}_{d,k}\mathbf{h}_{d,k} + \mathbf{n}_{d,k}, \tag{4.16}$$

where we define that $\mathbf{y}_{d,k} = vec(\mathbf{y}_{1k}, \cdots, \mathbf{y}_{Ndk})$, $\mathbf{n}_{d,k} = vec(\mathbf{n}_{1k}, \cdots, \mathbf{n}_{Ndk})$, $\mathbf{X}_{d,k} = diag(\mathbf{x}_{1k}^T \otimes \mathbf{I}_{N_R}, \cdots, \mathbf{x}_{N_d k}^T \otimes \mathbf{I}_{N_R})$, and $\mathbf{h}_{d,k} = vec(\mathbf{h}_{1k}, \cdots, \mathbf{h}_{N_d k})$. According to the previous definition and omitting the frequency index k, we can write the mismatched receiver output by the

following expression:

$$\hat{\mathbf{X}}_{d,MM} = \underset{\mathbf{X}_d \in \mathbb{X}_d}{\arg\min} \|\mathbf{y}_d - \mathbf{X}_d \hat{\mathbf{h}}_d\|^2. \tag{4.17}$$

where $\hat{\mathbf{h}}_d = vec(\hat{\mathbf{W}}_1 \hat{\mathbf{h}}_p, \cdots, \hat{\mathbf{W}}_{N_d} \hat{\mathbf{h}}_p)$ is the cascade of the channel estimation vectors. Next, we have the resulting output of the RMLR as

$$\begin{aligned} \hat{\mathbf{X}}_{d,RML} &= \underset{\mathbf{X}_d \in \mathbb{X}_d}{\arg\max} \ln P(\mathbf{X}_d | \mathbf{y}_d, \hat{\mathbf{h}}_p) \\ &= \underset{\mathbf{X}_d \in \mathbb{X}_d}{\arg\min} (\|\mathbf{y}_d - \mathbf{X}_d \hat{\mathbf{h}}_d\|^2_{\Sigma_{\mathbf{y}_d}} + \ln det(\Sigma_{\mathbf{y}_d})). \end{aligned} \tag{4.18}$$

where $\Sigma_{\mathbf{y}_d} = \Sigma_{\mathbf{n}_d} + \mathbf{X}_d \Sigma_{\mathbf{e}_d} \mathbf{X}_d^H$, $\Sigma_{\mathbf{e}_d} = E[\mathbf{e}_d \mathbf{e}_d^H] = \Sigma_{\mathbf{h}_d} - \Sigma^H_{\mathbf{h}_d \mathbf{h}_p} \Sigma^{-1}_{\hat{\mathbf{h}}_p} \Sigma_{\mathbf{h}_d \mathbf{h}_p}$, and $\mathbf{e}_d = vec(\mathbf{e}_1, \cdots, \mathbf{e}_{N_d})$. Finally, the OPT output is obtained by

$$\begin{aligned} \hat{\mathbf{X}}_{d,OPT} &= \underset{\mathbf{X}_d \in \mathbb{X}_d}{\arg\max} \ln P(\mathbf{X}_d | \mathbf{X}_p, \mathbf{y}_p, \mathbf{y}_d) \\ &= \underset{\mathbf{X}_d \in \mathbb{X}_d}{\arg\min} (-\mathbf{B}_d^H \mathbf{A}_d^{-1} \mathbf{B}_d + \ln det(\mathbf{A}_d)), \end{aligned} \tag{4.19}$$

where the details are shown as follows:

$$\begin{aligned} \mathbf{W}_d &= \Sigma^H_{\mathbf{h}_d \mathbf{h}_p} \Sigma^{-1}_{\hat{\mathbf{h}}_p}, \\ \mathbf{B}_d &= \mathbf{W}_d^H \mathbf{X}_d^H \Sigma^{-1}_{\mathbf{n}_d} \mathbf{y}_d + \mathbf{X}_p^H \Sigma^{-1}_{\mathbf{n}_p} \mathbf{y}_p, \\ \mathbf{A}_d &= \mathbf{W}_d^H \mathbf{X}_d^H \Sigma^{-1}_{\mathbf{n}_d} \mathbf{X}_d \mathbf{W}_d + \mathbf{X}_p^H \Sigma^{-1}_{\mathbf{n}_p} \mathbf{X}_p + \Sigma^{-1}_{\mathbf{h}_p}. \end{aligned}$$

The presented equations show that the proposed schemes can be applied to OSTBC MIMO-OFDM systems by simply replacing the symbol notations by their cascaded forms.

4.3 Symbol detection with imperfect CDIR

The main focus of this section is to deal with the imperfect covariance matrices used in the proposed receiver. Recall that the OPT scheme is as follows

$$\hat{\mathbf{X}}_{OPT} = \underset{\mathbf{X} \in \mathbb{X}}{\arg\min} (-\mathbf{B}^H \mathbf{A}^{-1} \mathbf{B} + \ln det(\mathbf{A})). \tag{4.20}$$

This scheme is optimum over an arbitrarily correlated Rayleigh fading MIMO channel when the perfect CDIR is available. In practice, it is difficult for a receiver to reliably estimate the correlation matrices, $\Sigma_{\mathbf{hh_p}}$, $\Sigma_{\mathbf{h_p}}$, and N_0 with only limited observations.

4.3.1 Correlation model set

In order to obtain CDIR, the sample covariance matrix is the most commonly used estimator of a covariance matrix. However, it is highly unstable for large covariance matrices with a limited number of observations. Instead of using the sample mean and the sample variance [16], we apply the triply selective channel model to generate the correlation matrices $\Sigma_{\mathbf{h_p}}$ and $\Sigma_{\mathbf{hh}_p}$. For simplicity, we assume that N_0 can be accurately estimated. The ranges of the parameters are known as $f_d \in [0, f_{max}]$ and $n_L \in [1, n_{cp}]$. Then we discretize these ranges into K_M levels and define the model set as:

$$\mathbf{M}_i = \left\{ \Sigma^{(i)}_{\mathbf{h}_p}, \Sigma^{(i)}_{\mathbf{hh}_p} \right\}, \, i = 1, \cdots, K_M,$$

where i denotes the index of different covariance matrices. However, finding a good model set $\mathbf{M}_i$ for triply selective channels is not obvious.

One alternative for designing a model set is to use different propagation channel models defined in the long-term evolution (LTE) specification [21]. Three different delay profiles are representative of low, medium, and high delay spread environment. These are: (i) extended pedestrian A model (EPA), (ii) extended vehicular A model (EVA) and (iii) extended typical urban model (ETU). A brief description of our proposed model set is as follows: The receiver makes no attempt to estimate the parameters such as f_d and n_L, and assumes the model set is

$$\begin{aligned}
\mathbf{M}_i &\triangleq \mathscr{F}\{\text{delay spread, spatial correlation, speed}\} \\
\mathbf{M}_1 &= \mathscr{F}\{ETU, \text{High}, 300 \text{ km/hr}\} \\
\mathbf{M}_2 &= \mathscr{F}\{EVA, \text{Medium}, 150 \text{ km/hr}\} \\
\mathbf{M}_3 &= \mathscr{F}\{EPA, \text{Low}, 10 \text{ km/hr}\},
\end{aligned}$$

where $\mathscr{F}$ is the function to generate the correlation matrices. For instance, given the sampling time, $\Delta t = 0.065\,\mu s$ and carrier frequency 2 GHz, the model $\mathbf{M}_2$ can be obtained according to the triply selective model shown in eqn. (4.4), where

$$\Psi_{Rx} = \begin{bmatrix} 1 & 0.9 \\ 0.9 & 1 \end{bmatrix}, \Psi_{Tx} = \begin{bmatrix} 1 & 0.3 \\ 0.3 & 1 \end{bmatrix},$$

$\mathbf{C}_{ISI} = diag([1, 0.712, \cdots, 0.024])_{39\times 39}$, and $f_d = 278\,Hz$ based on 150 km/hr speed and 2 GHz carrier frequency.

4.3.2 Bayesian model selection

An efficient model selection can be derived by invoking the BMS approach [22]. This approach maximizes the conditional probability $P(\mathbf{M}_i|\mathbf{y})$, which is equivalent to picking up the model with the highest evidence. The BMS is derived as follows

$$\begin{aligned}\hat{\mathbf{M}}_i &= \underset{i=1,\cdots,K_M}{\arg\max} \ln P(\mathbf{y}|\mathbf{M}_i) \\ &= \underset{i=1,\cdots,K_M}{\arg\max} \ln \sum_{\mathbf{X}\in\mathbb{X}} P(\mathbf{y}|\mathbf{X},\mathbf{M}_i) \\ &\approx \underset{i=1,\cdots,K_M}{\arg\max} \ln P(\mathbf{y}|\hat{\mathbf{X}}_i,\mathbf{M}_i) \qquad (4.21) \\ &= \underset{i=1,\cdots,K_M,\mathbf{X_i}\in\mathbb{X}}{\arg\min\min} \left(-\mathbf{B}_i^H\mathbf{A}_i^{-1}\mathbf{B}_i + \ln\det(\mathbf{A}_i)\right),\end{aligned}$$

where (4.21) is obtained by using the Laplace approximation $P(\mathbf{y}|\mathbf{X},\mathbf{M}_i) = \delta(\mathbf{y}|\mathbf{X}-\hat{\mathbf{X}}_i,\mathbf{M_i})$. $\delta(\cdot)$ denotes the Dirac delta function. $\hat{\mathbf{X}}_\mathbf{i}$ is the conditional ML estimate by given $\mathbf{M_i}$. The rest of the notations are defined as:

$$\mathbf{A}_i = \mathbf{W_i}^H\mathbf{X_i}^H\mathbf{X_i}\mathbf{W_i}/N_0 + \mathbf{X}_p^H\mathbf{X}_p/N_0 + \left(\Sigma^{(i)}_{\mathbf{h}_p}\right)^{-1}, \qquad (4.22)$$

$$\mathbf{B}_i = \mathbf{W_i}^H\mathbf{X_i}^H\mathbf{y}/N_0 + \mathbf{X}_p^H\mathbf{y}_p/N_0, \qquad (4.23)$$

and $\mathbf{W_i} = \Sigma^{(i)}_{\mathbf{hh_p}}\left(\Sigma^{(i)}_{\mathbf{h}_p}\right)^{-1}$. This scheme actually runs K_M times of the OPT scheme to find the best covariance matrices from the K_M candidates.

Finally, in the case we have more samples either in the frequency domain or in the time domain, the model selection results can be improved without complicated computation. Assuming that we have n_w independent observations, the BMS can be rewritten as

$$\hat{\mathbf{M}}_\mathbf{i} = \underset{\mathbf{X}_i\in\mathbb{X},i=1,\cdots,K_M}{\arg\max} \sum_{j=1}^{n_w} \ln P(\mathbf{y}_{tk}^{(j)}|\mathbf{X}_i^{(j)},\mathbf{M}_i), \qquad (4.24)$$

where $\mathbf{y}_{tk}^{(j)}$ is a $N_R\times 1$ complex vector that denotes the jth observation, i.e, the jth received symbol at the (t,k)th time-frequency slot.

Obviously, if we assume the channel characteristics are stable, then n_w should be as large as possible. In contrast, when considering mobility and practical implementation, a moving average design would be more appropriate. In this case, n_w should be chosen according to the coherent time information.

4.4 Numerical results

Consider the MIMO-OFDM system with $N_T = 2$ transmit and $N_R = 2$ receive antennas with the configuration parameters from LTE specifications [21]. The system parameters are given by the frequency division duplexing (FDD) radio frame with normal CP, FFT-size of $N_F = 128$, and 2 GHz center frequency. The detection and channel estimation algorithms are performed in one subframe defined by 14 time slots and 12 subcarriers, which is also shown in Fig. 4.1. The discrete-time MIMO fading channel is generated according to [20] as follows:

$$\bar{\mathbf{h}}_t(k) = (\Psi_{Rx}^{1/2} \otimes \Psi_{Tx}^{1/2} \otimes \mathbf{C}_{ISI}^{1/2}) \cdot \Phi(k), \tag{4.25}$$

where $(\cdot)^{1/2}$ is the square root of the matrix. We also define that $\Phi(k)$ is an $(N_T N_R L) \times 1$ vector, whose elements are zero-mean and uncorrelated flat Rayleigh fading, and

$$E\left[\Phi(k_1) \cdot \Phi^H(k_2)\right] = J_0\left(2\pi f_d (k_1 - k_2) T_s\right) \cdot \mathbf{I}_{N_T N_R L}. \tag{4.26}$$

The correlation coefficient matrices can be calculated by the formulas in [20] under certain parameters. For example, if the transmit and receive antennas are spaced by 12λ and 0.5λ, where λ is the wavelength, the AoA is 90°, and the AS is 10°, then we get $\alpha = 0.215$ and $\beta = -0.304$ such that the spatial correlations are given by

$$\Psi_{Tx} = \begin{bmatrix} 1.000 & 0.215 \\ 0.215 & 1.000 \end{bmatrix}, \quad \Psi_{Rx} = \begin{bmatrix} 1.0000 & -0.304 \\ -0.304 & 1.0000 \end{bmatrix}.$$

The power delay profile is exponentially decaying, and the elements $c(l_1, l_2)$ of the matrix $\mathbf{C}_{ISI}$ are obtained from [20]. Having the above matrices, we can now compare the different receivers under the following assumptions: 1) without OSTBC, 2) with OSTBC, and 3) with imperfect CDIR.

4.4.1 Without OSTBC

We present some numerical examples to illustrate the performance of the proposed algorithms without OSTBC. The covariance matrix of the noise term is defined as

$$\Sigma_{\mathbf{n}} = \frac{N_0}{1+\rho} \begin{bmatrix} 1 & \rho \\ \rho & 1 \end{bmatrix}. \tag{4.27}$$

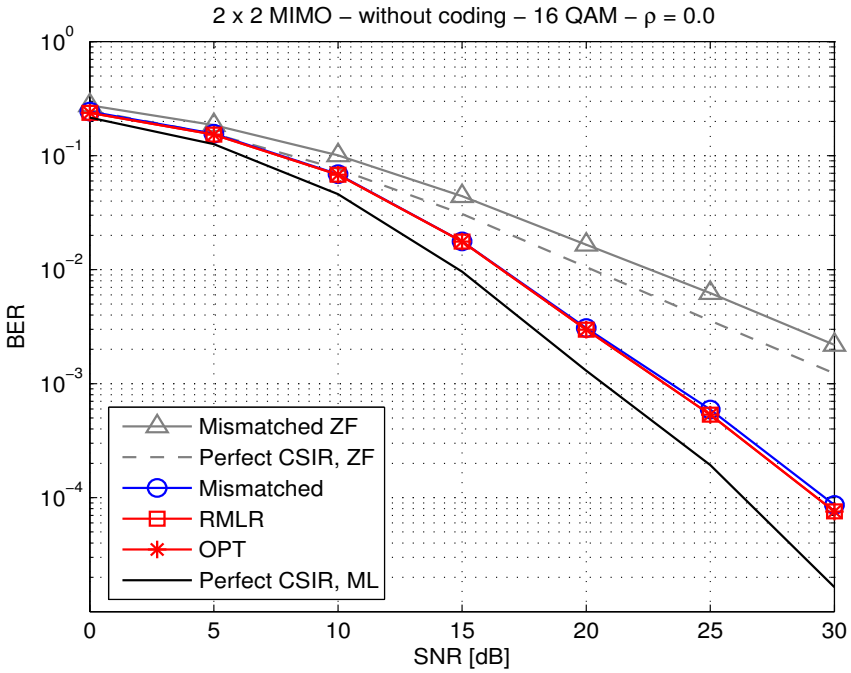

Fig. 4.2 BER vs. SNR for different detection algorithms with $\rho = 0$.

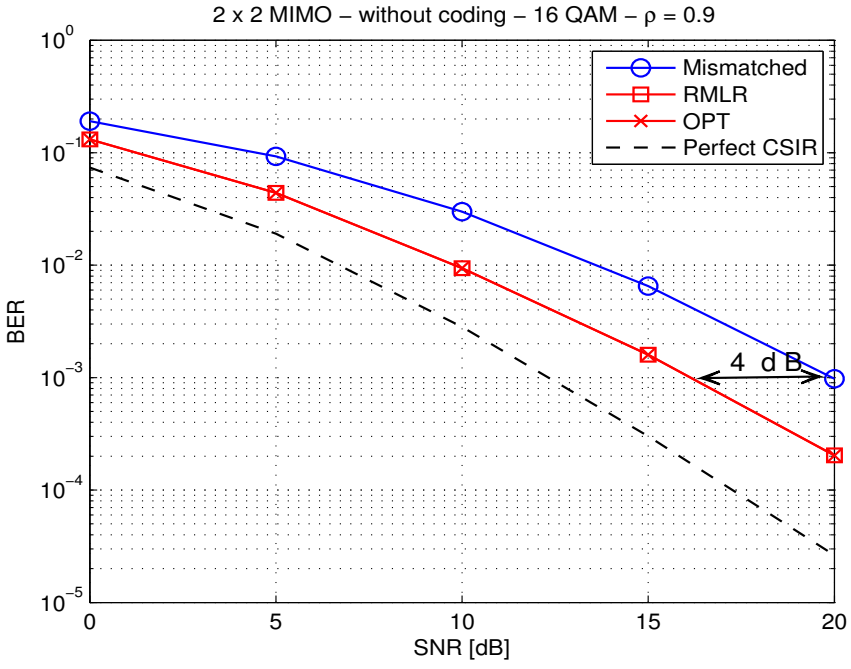

Fig. 4.3 BER vs. SNR for different detection algorithms with $\rho = 0.9$.

In Fig. 4.2, we consider $\rho = 0$ and compare different algorithms in terms of bit error rate (BER) for different SNR levels. The results show that there is only a slight improvement by

using the RMLR and the OPT compared to the mismatched receiver. Since the OPT can be seen as the optimum approach given full CDIR and pilot information, these results imply that there is almost no performance loss by using the mismatched receiver under imperfect CSI.

Fig. 4.3 shows the BER performance of different schemes when $\rho = 0.9$. The resulting curves show that there is a 4 dB gain by using the RMLR and the OPT compared to the mismatched receiver at $BER = 10^{-3}$. The improvement mainly comes from considering the correlation matrix $\Sigma_{\mathbf{n}}$ and its impact on both channel estimation and symbol detection. Besides, we found that the RMLR and the OPT come to the same BER performance even though they are derived from different criteria. Indeed, it can be proved that both decision metrics tend to be equivalent in the high SNR region.

4.4.2 With OSTBC

Consider an OSTBC proposed by [23] with $\rho = 0$. We study the pairwise error probability (PEP) performance corresponding to a pair of codewords given as follows:

$$\begin{aligned} \bar{\mathbf{X}}_1 &= STC(2,1,3,1,0,1,3,1,0,1,1,0,1,3) \\ \bar{\mathbf{X}}_2 &= STC(2,1,3,3,3,3,3,1,0,1,1,0,1,3), \end{aligned} \tag{4.28}$$

where we define the inner space-time encoding function

$$STC(m_1,\cdots,m_{N_d}) = \begin{pmatrix} s_1 & -s_2^* & \cdots & s_{N_d-1} & -s_{N_d}^* \\ s_2 & s_1^* & \cdots & s_{N_d} & s_{N_d-1}^* \end{pmatrix}$$

and $s_k = exp(j(2m_k+1)\pi/4)$. Here $(\cdot)^*$ denotes the conjugate operator. These two codewords represent a worst-case minimum distance error event [23].

Figs. 4.4 and 4.5 illustrate the PEP performance for different number of pilots ($N_p = 12$ and $N_p = 8$). The curves show that RMLR and OPT gain from 1 dB to 2 dB as the N_p ranges from 12 to 8. This means RMLR and OPT can improve more when the CSI quality is decreased, i.e., decreasing the number of pilots.

To show the impact of the CSI quality on the error performance, Fig. 4.6 shows the PEP performance when we reduce the power of pilots by half. It can be noticed that the curves show a 4 dB improvement with respect to the mismatched receiver when the PEP is 10^{-3}.

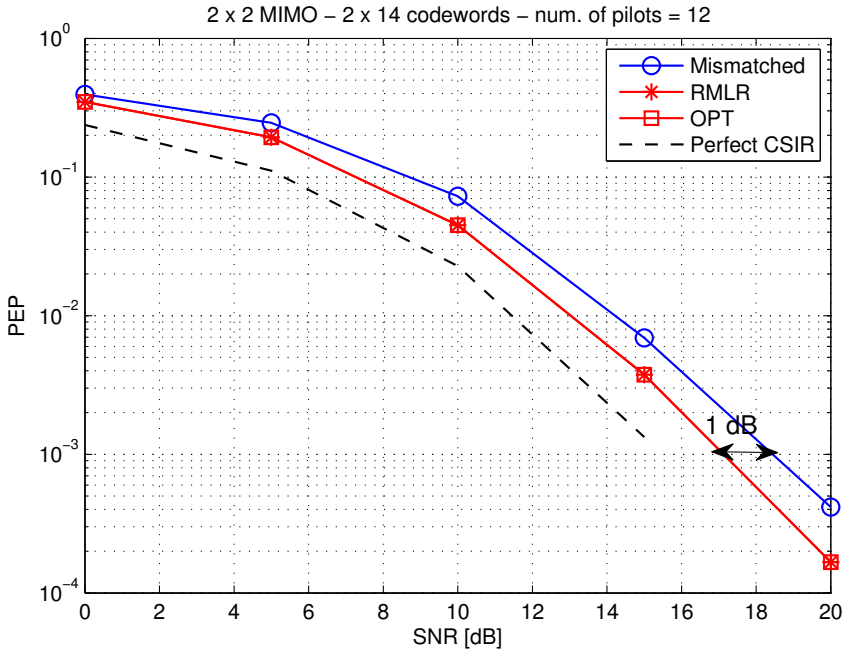

Fig. 4.4 BER vs. SNR for different detection algorithms with $N_p = 12$.

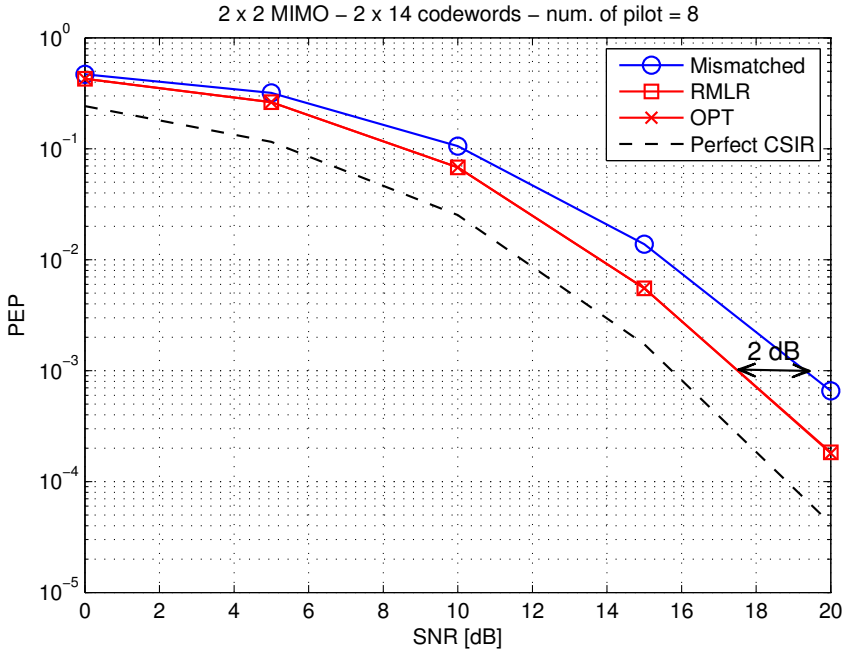

Fig. 4.5 BER vs. SNR for different detection algorithms with $N_p = 8$.

This picture might imply that there is more gain of the proposed receivers with respect to the mismatched receiver, when the CSI quality keeps decreasing.

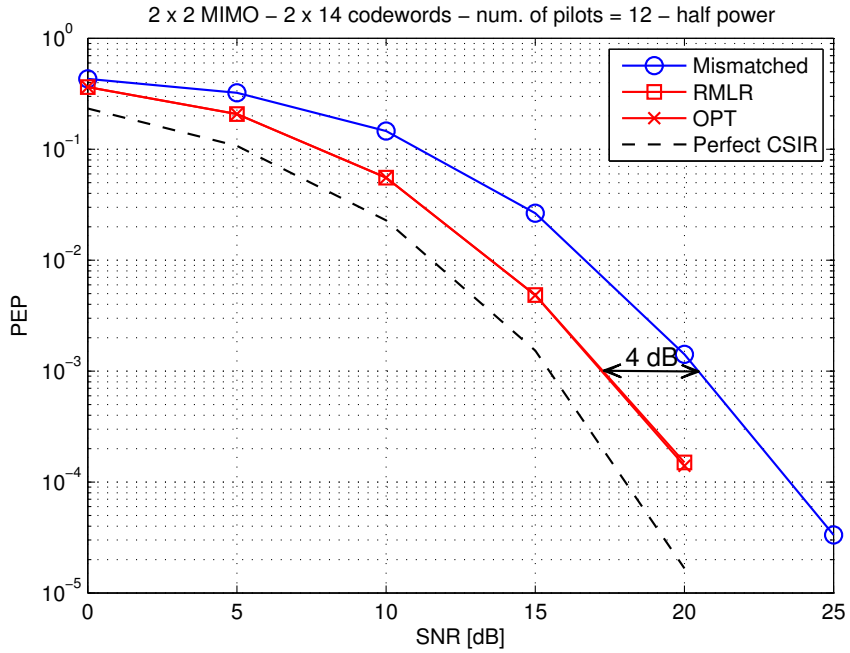

Fig. 4.6 BER vs. SNR for different detection algorithms with $N_p = 12$ and reducing the pilot power by half.

4.4.3 With imperfect CDIR

Fig. 4.7 illustrates the BER performance for different approaches under imperfect CDIR. The BER performance of the proposed scheme is lower- and upper-bounded by that achieved by the perfect CDIR and the worst-case curve. The worst-case curve denotes that the receiver uses the covariance matrices $\mathbf{M_1}$ to optimize the worst case-channel instead of performing model selection. Two selection curves represent the performance using the proposed model selection schemes and different numbers of observations ($n_w = 1$ and $n_w = 4$). Two other cases, perfect CDIR, and ML detection with perfect CSI, are provided for reference purposes. The proposed selection scheme offers an approximately 7 dB gain with respect to the worst-case curve at BER = 10^{-3} when $n_w = 1$. Increasing n_w to 4 and using (4.24), we obtain an additional 3 dB gain at BER = 10^{-4}.

4.5 Conclusion

In this chapter, we considered the effect of imperfect CSI for MIMO-OFDM systems. Two kinds of robust detection strategies have been proposed: 1) RMLR which performs ML

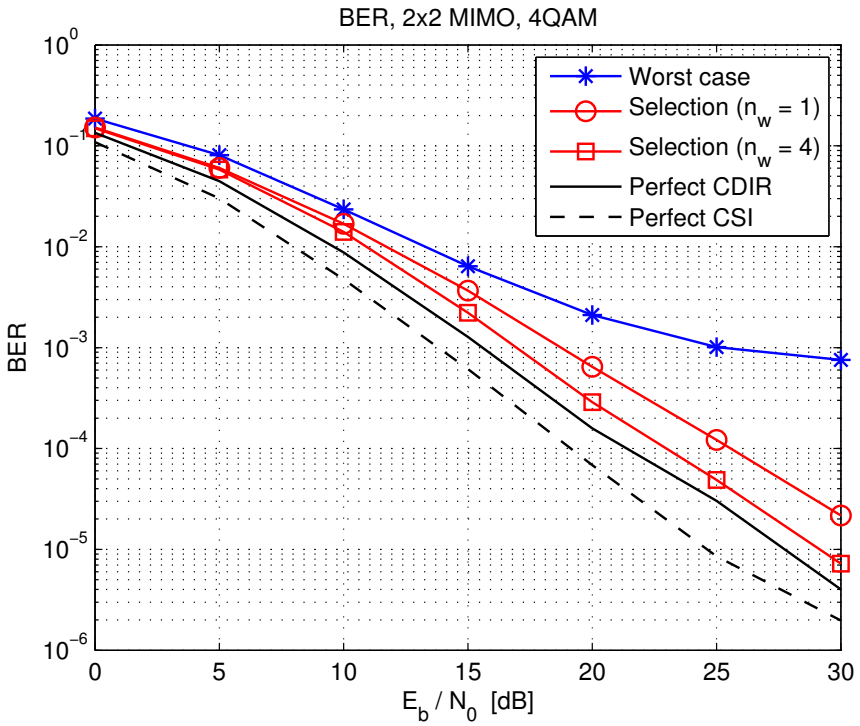

Fig. 4.7 BER performance of various receivers as a function of SNR when the channel is parameterized by $\alpha = 0.215, \beta = -0.304$, EVA, $fd = 100$ Hz.

detection with the uncertainty of channel estimation; 2) the OPT performing the tasks of channel estimation and symbol detection jointly. Numerical results show that these two different criteria come to the same results in terms of the PEP and BER performance. Both of them are better receiver schemes than the conventional mismatched receiver, especially with spatially colored noise and OSTBC, and a limited number of pilots.

In the case of imperfect CDIR, we derived an efficient detection algorithm based on the Bayesian inference. Instead of estimating the covariance matrices, the proposed detector simply compares a few correlation models to obtain sufficient information. Numerical results show that the proposed detector performance is as close as 1 dB to the optimum performance in the presence of imperfect CDIR.

Chapter 5

Interference suppression

In Chapter 4, we have investigated different symbol detection schemes under the assumption of imperfect CSI due to the channel correlations and AWGN. In Chapter 5, the presence of interference is also taken into account, and its impact on both channel estimation and symbol detection is investigated.

Research interest in interference cancellation techniques increased considerably over the past two decades with an upsurge of activities. The main reason was the growing demands on mobile networks to support data applications at higher throughput and spectral efficiencies. This has driven the need to develop a frequency reuse technique in which the BSs, or so called the eNodeBs (eNBs), can transmit on all available time-frequency resource blocks simultaneously. This promising technique relies heavily on its interference mitigation capability. An overview of interference coordination techniques was given in [24], in which viable existing approaches were reviewed, including advanced MIMO receiver processing techniques and iterative decoding algorithms.

The principle of spatial interference rejection in MIMO systems can be found in the seminal works in GSM systems such as [25], where the co-channel interference (CCI) is modeled as a spatial and temporal colored Gaussian noise process. The colored noise assumption leads to the spatial whitening scheme, denoted by interference rejection combining (IRC) [26, 27]. In this scheme, the receiver suppresses the interfering signal statistically instead of decoding it. In [28], it is shown that the IRC receiver provides a spectral efficiency gain up to 24% as compared to the conventional receivers in the system-level evaluations.

In this chapter, we investigate IRC-like receivers in interference limited scenarios. First, we develop efficient schemes, which take into account the channel estimation errors and the errors in covariance estimation. These schemes will focus on different kinds of interference caused by the pilot and the data signals, and suppress them with different strategies. Second, we present a study to show how to estimate the covariance matrix when the interfering signal arrives from a frequency selective channel. In this case, the covariance matrix needs to be estimated by a moving average filter with the optimum number of taps. Finally, we aim at improving the dimensional scalability of IRC-like receivers when additional RX antennas are available. These contributions are organized in three parts:

- In the first part, we consider a two-user interference channel for MIMO-OFDM systems. The main idea is to take into account the difference between the interfering pilots and the interfering data signal in terms of their covariance matrices. Assuming the interference and the desired signal are based on the frame format of the LTE standard [21], we derive three novel receiver structures based on LMMSE and successive interference cancellation (SIC) criteria to improve the BER performance.
- In the second part, we focus on interference from frequency-selective channels. A major difficulty in this case is the accurate estimation of the covariance matrices of interference, which may require knowledge of interference parameters. A similar work can be found in [29], where the proposed covariance estimator is a moving average scheme which chooses 11 taps intuitively. Our contribution is finding the optimal window size (number of taps) of the moving average in a theoretical way.
- In the third part, we propose a scheme that enables the original IRC to use additional RX antennas. A similar work can be found in [30] where the authors combine the IRC with antenna selection. We aim at providing an efficient scheme that jointly processes the received signal by the linear combining. The proposed algorithms are based on CSI and the signal-to-interference-plus-noise ratio (SINR) value from the original IRC equalizer and can provide improvement with a slight complexity increase.

5.1 Interference with covariance mismatches

In the first part of Chapter 5, we start by introducing a general system model and deriving a one-dimensional model for algorithm derivation.

5.1.1 System model

For a two-user interference channel, the received waveform of the user equipment (UE) can be expressed as

$$\mathbf{y}_{tk} = \mathbf{H}_{tk}\mathbf{p}x_{tk} + \alpha\bar{\mathbf{H}}_{tk}\bar{\mathbf{p}}\bar{x}_{tk} + \mathbf{z}_{tk} \in \mathscr{C}^{N_R}, \tag{5.1}$$

where at each time-frequency index (t,k), $\mathbf{H}_{tk}$, $\bar{\mathbf{H}}_{tk}$ are the serving channel matrix and the interfering channel matrix of size $N_R \times N_T$, respectively, $\mathbf{y}_{tk}$ is the N_R dimensional received signal vector, x_{tk}, $\bar{x}_{tk}$ are the transmitted symbols, $\mathbf{p}$, $\bar{\mathbf{p}}$ are the N_T dimensional precoding vectors, $\mathbf{z}_{tk}$ is the N_R dimensional AWGN vector, and α^2 represents the power of interference. To simplify our discussion, each node is equipped with two antennas, i.e., $N_R = 2$ and $N_T = 2$.[1] We further assume that the entries of $\mathbf{z}$ are independent and identically distributed (i.i.d.) Gaussian variables of the form $\mathscr{N}_c(0, N_0)$. Probability density functions of channel matrices $\mathbf{H}^{tk}$, $\bar{\mathbf{H}}^{tk}$ are assumed to be $\text{vec}(\mathbf{H}) \sim \mathscr{N}_c(\mathbf{0}, \mathbf{I})$ and $\text{vec}(\bar{\mathbf{H}}) \sim \mathscr{N}_c(\mathbf{0}, \mathbf{I})$, respectively. The precoding vectors $\mathbf{p}$ and $\bar{\mathbf{p}}$ are chosen from the LTE codebook set $\mathscr{P}$ [21], e.g.,

$$\mathscr{P} = \frac{1}{\sqrt{2}} \cdot \left\{ \begin{bmatrix} 1 \\ 1 \end{bmatrix}, \begin{bmatrix} 1 \\ -1 \end{bmatrix}, \begin{bmatrix} 1 \\ i \end{bmatrix}, \begin{bmatrix} 1 \\ -i \end{bmatrix} \right\}. \tag{5.2}$$

The data-pilot format of the LTE specification is shown in Fig.5.1, where two resource blocks[2] with non-overlapping pilots are considered between the serving evolved node B (eNB) and the interfering eNB.

A one-dimensional model is derived with the following assumption. Assume that the channel is static over the time and frequency spans within one RB, the pilot number is $N_p = 16$ and the number of data symbols is $N_d = 152$. Since the pilot symbols from two eNBs are not placed at the same time-frequency locations, the received signal is subjected to interference with different statistics.

Figs. 5.1 and 5.2 depict a typical relative desired and interfering signal pattern where, without loss of generality, we place the serving pilot symbols at the beginning of the frame

[1] Extensions to different numbers of antennas are straightforward.

[2] Resource block (RB) is defined by a square with 14 time slots and 12 subcarriers.

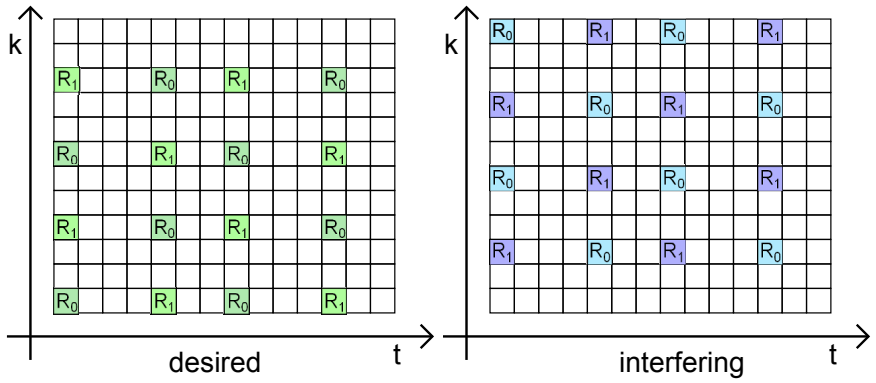

Fig. 5.1 Mapping of the serving and interfering pilot symbols, where R_0 and R_1 indicate the pilot positions.

and the interfering pilot symbols at the end. These two figures suggest that we divide the received samples in a typical frame into four intervals, giving

$$\mathbf{Y}_p = \mathbf{H}\mathbf{X}_p + \alpha\bar{\mathbf{H}}\bar{\mathbf{p}}\bar{\mathbf{X}}_{d1} + \mathbf{Z}_p \in \mathscr{C}^{2\times 16} \tag{5.3}$$

$$\mathbf{Y}_{d1} = \mathbf{H}\mathbf{p}\mathbf{X}_1 + \alpha\bar{\mathbf{H}}\bar{\mathbf{p}}\bar{\mathbf{X}}_{d2} + \mathbf{Z}_{d1} \in \mathscr{C}^{2\times(152-16)} \tag{5.4}$$

$$\mathbf{Y}_{d2} = \mathbf{H}\mathbf{p}\mathbf{X}_2 + \alpha\bar{\mathbf{H}}\bar{\mathbf{X}}_{p1} + \mathbf{Z}_{d2} \in \mathscr{C}^{2\times 8} \tag{5.5}$$

$$\mathbf{Y}_{d3} = \mathbf{H}\mathbf{p}\mathbf{X}_3 + \alpha\bar{\mathbf{H}}\bar{\mathbf{X}}_{p2} + \mathbf{Z}_{d3} \in \mathscr{C}^{2\times 8} \tag{5.6}$$

where $\mathbf{Y}_p, \mathbf{Y}_{d1}, \mathbf{Y}_{d2}, \mathbf{Y}_{d3}$ are the received signal matrices, $\mathbf{X}_p$ is the serving pilot matrix, $\mathbf{X}_1, \mathbf{X}_2, \mathbf{X}_3$ are the serving data matrices, $\bar{\mathbf{X}}_{d1}, \bar{\mathbf{X}}_{d2}$ are the interfering data matrices, $\bar{\mathbf{X}}_{p1}, \bar{\mathbf{X}}_{p2}$ are the interfering pilot matrices, while $\mathbf{Z}_p, \mathbf{Z}_{d1}, \mathbf{Z}_{d2}, \mathbf{Z}_{d3}$ represent AWGN. Note that during the two intervals specified by (5.3) and (5.4), the covariance of interference plus noise is the same. The above model assumes a synchronous network scenario, i.e., all UEs are synchronized with a universal clock such that both the desired and interfering downlink signals arrive at the desired UE simultaneously. We will show that the proposed receivers work in the asynchronous case as well.

In LTE, pilots from a multi-antenna transmitter are transmitted in a time division manner, i.e., when a pilot signal is transmitted by one of the antennas, the other antennas remain silent to avoid self-interference. We further assume that the pilot signal is not spatially precoded so that the matrix products of the pilot signal are

$$\bar{\mathbf{X}}_{p1}\bar{\mathbf{X}}_{p1}^H = \frac{\mathscr{E}_p N_p}{2}\begin{bmatrix} 1 & 0 \\ 0 & 0 \end{bmatrix} \tag{5.7}$$

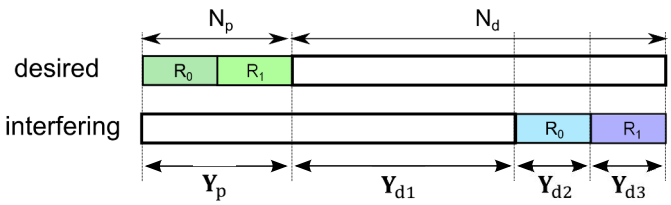

Fig. 5.2 The one-dimensional model which arranges pilot and data symbols.

$$\bar{\mathbf{X}}_{p2}\bar{\mathbf{X}}_{p2}^{H} = \frac{\mathscr{E}_p N_p}{2}\begin{bmatrix} 0 & 0 \\ 0 & 1 \end{bmatrix}, \tag{5.8}$$

where $\bar{\mathbf{X}}_{p1}$ is the transmitted pilot signal from the first antenna and $\bar{\mathbf{X}}_{p2}$ is from the second antenna. The pilot energy is denoted by $\mathscr{E}_p$ and the data energy is $\mathscr{E}_d$. We further define the SNR and SIR as SNR $= 1/N_0$ and SIR $= \alpha^{-2}$ under the unity energy assumption, i.e., $\mathscr{E}_d = \mathscr{E}_p = 1$.

In this work, the goal is to find the linear combination of the received signal for decoding the data of interest $(\mathbf{X}_1, \mathbf{X}_2, \mathbf{X}_3)$. Assuming the CSI from the serving eNB and the interfering eNB are given, the covariance matrices of the received signal $\mathbf{Y}_{d1}, \mathbf{Y}_{d2}, \mathbf{Y}_{d3}$ are as follows:

$$\begin{aligned} \Sigma_{\mathbf{Y}_{d1}} &= \mathbb{E}\left[\mathbf{Y}_{d1} | \mathbf{h}, \bar{\mathbf{h}}, \bar{\mathbf{X}}_{p1}, \bar{\mathbf{X}}_{p2}\right] \\ &= \mathbf{h}\mathbf{h}^H + \bar{\mathbf{h}}\bar{\mathbf{h}}^H + N_0\mathbf{I} \end{aligned} \tag{5.9}$$

$$\Sigma_{\mathbf{Y}_{d2}} = \mathbf{h}\mathbf{h}^H + \bar{\Psi}_{p1} + N_0\mathbf{I} \tag{5.10}$$

$$\Sigma_{\mathbf{Y}_{d3}} = \mathbf{h}\mathbf{h}^H + \bar{\Psi}_{p2} + N_0\mathbf{I}, \tag{5.11}$$

where $\mathbf{h} = \mathbf{H}\mathbf{p}$ and $\bar{\mathbf{h}} = \alpha\bar{\mathbf{H}}\bar{\mathbf{p}}$ are the equivalent channel vectors. The covariance matrices of size 2×2 are given by

$$\bar{\Psi}_{p1} = \alpha^2\bar{\mathbf{H}}\begin{bmatrix} 1 & 0 \\ 0 & 0 \end{bmatrix}\bar{\mathbf{H}}^H \tag{5.12}$$

$$\bar{\Psi}_{p2} = \alpha^2\bar{\mathbf{H}}\begin{bmatrix} 0 & 0 \\ 0 & 1 \end{bmatrix}\bar{\mathbf{H}}^H. \tag{5.13}$$

In this case, the conventional IRC (which treats interference as a single Gaussian process) naturally leads to limited system performance.

5.1.2 IRC with diagonal loading

Treating interference as Gaussian noise, the linear combining based on LMMSE criterion has the following form,

$$\begin{cases} \hat{\mathbf{X}}_1 = \mathbf{h}^H(\Sigma_{\mathbf{Y}_{d1}})^{-1}\mathbf{Y}_{d1} \\ \hat{\mathbf{X}}_2 = \mathbf{h}^H(\Sigma_{\mathbf{Y}_{d2}})^{-1}\mathbf{Y}_{d2} \\ \hat{\mathbf{X}}_3 = \mathbf{h}^H(\Sigma_{\mathbf{Y}_{d3}})^{-1}\mathbf{Y}_{d3} \end{cases} \tag{5.14}$$

where $\hat{\mathbf{X}}_1$, $\hat{\mathbf{X}}_2$, $\hat{\mathbf{X}}_3$ are the estimates of the desired symbols $\mathbf{X}_1$, $\mathbf{X}_2$, $\mathbf{X}_3$. In practice, we substitute the channel and covariance estimations into this theoretical form. The serving channel is assumed to be estimated by the LS estimator:

$$\hat{\mathbf{H}} = \frac{1}{N}\mathbf{Y}_p\mathbf{X}_p^H, \tag{5.15}$$

and the estimated channel vector $\hat{\mathbf{h}} = \hat{\mathbf{H}}\mathbf{p}$ is obtained by the given precoding vector $\mathbf{p}$. The covariance matrices are estimated by the sample covariance:

$$\begin{aligned} \hat{\Sigma}_{\mathbf{Y}_{d1}} &= \hat{\mathbf{h}}\hat{\mathbf{h}}^H + \frac{1}{N_p}\hat{\mathbf{V}}\hat{\mathbf{V}}^H \\ \hat{\Sigma}_{\mathbf{Y}_{d2}} &= \frac{2}{N_p}\mathbf{Y}_{d2}\mathbf{Y}_{d2}^H \\ \hat{\Sigma}_{\mathbf{Y}_{d3}} &= \frac{2}{N_p}\mathbf{Y}_{d3}\mathbf{Y}_{d3}^H \end{aligned} \tag{5.16}$$

where $\hat{\mathbf{V}} = \mathbf{Y}_p - \hat{\mathbf{H}}\mathbf{X}_p$ is the residual matrix. Note that we use $\hat{\mathbf{V}}$ instead of the received signal matrix $\mathbf{Y}_{d1}$ because the former has smaller estimation errors (see Appendix A.1). Using the estimated results in (5.14), the resulting output of IRC with diagonal loading (IRC-DL) is given by

$$\begin{cases} \hat{\mathbf{X}}_{1,dl} = \hat{\mathbf{h}}^H(\hat{\Sigma}_{\mathbf{Y}_{d1}})^{-1}\mathbf{Y}_{d1} \\ \hat{\mathbf{X}}_{2,dl} = \hat{\mathbf{h}}^H(\hat{\Sigma}_{\mathbf{Y}_{d2}} + \nu\mathbf{I})^{-1}\mathbf{Y}_{d2} \\ \hat{\mathbf{X}}_{3,dl} = \hat{\mathbf{h}}^H(\hat{\Sigma}_{\mathbf{Y}_{d3}} + \nu\mathbf{I})^{-1}\mathbf{Y}_{d3}, \end{cases} \tag{5.17}$$

where ν is the diagonal loading value to compensate sample covariance errors. This method is often used in the robust beamforming design for its simplicity [29, 31, 32].

5.1.3 LS with compensation

If the interfering pilot signal is perfectly known at the UE receiver, we can cancel interference to further improve the system performance [2]. We rewrite that part of the received

signal with interfering pilot, $\mathbf{Y}_{d2}$, $\mathbf{Y}_{d3}$, as

$$\mathbf{Y}'_p = \mathbf{h}\mathbf{X}_{d1} + \bar{\mathbf{h}}\bar{\mathbf{X}}_p + \mathbf{Z}'_p \in \mathscr{C}^{2\times N_p}, \tag{5.18}$$

where the received matrix $\mathbf{Y}'_p = [\mathbf{Y}_{d2}, \mathbf{Y}_{d3}]$ is related to the interfering pilot symbols, $\mathbf{X}_{d1} = [\mathbf{X}_2, \mathbf{X}_3]$ denotes the serving data matrix, $\bar{\mathbf{X}}_p = [\bar{\mathbf{X}}_{p1}, \bar{\mathbf{X}}_{p2}]$ denotes the interfering pilot matrix, and $\mathbf{Z}'_p = [\mathbf{Z}_{d2}, \mathbf{Z}_{d3}]$ is the AWGN matrix. A simple LS channel estimator for both serving and interfering channels is thus given by

$$\hat{\mathbf{H}} = \mathbf{Y}_p \mathbf{X}_p^H / N_p = \mathbf{H} + \mathbf{E} \tag{5.19}$$

$$\hat{\mathbf{H}}_b = \mathbf{Y}'_p \bar{\mathbf{X}}_p^H / N_p = \alpha\bar{\mathbf{H}} + \bar{\mathbf{E}}, \tag{5.20}$$

where $\hat{\mathbf{H}}$ is the estimate of the serving channel matrix, $\hat{\mathbf{H}}_b$ is the estimate of the interfering channel matrix, and the channel estimation errors are given by

$$\begin{aligned}\mathbf{E} &= \bar{\mathbf{h}}\bar{\mathbf{X}}_{d1}\mathbf{X}_p^H / N_p + \mathbf{Z}_p \mathbf{X}_p^H / N_p \\ \bar{\mathbf{E}} &= \mathbf{h}\mathbf{X}_{d1}\bar{\mathbf{X}}_p^H / N_p + \mathbf{Z}'_p \bar{\mathbf{X}}_p^H / N_p.\end{aligned}$$

Once the interfering channel estimation is available, we regenerate the received pilot signal via the product of the channel estimate and the given pilot signal as $\hat{\mathbf{H}}_b\bar{\mathbf{X}}_p$. Therefore, the residual matrix of pilot cancellation is obtained as follows:

$$\begin{aligned}\hat{\mathbf{V}}_b &= \mathbf{Y}'_p - \hat{\mathbf{H}}_b\bar{\mathbf{X}}_p \\ &= \mathbf{h}\mathbf{X}_{d1} - \bar{\mathbf{E}}\bar{\mathbf{X}}_p + \mathbf{Z}'_p \in \mathscr{C}^{2\times N_p}.\end{aligned} \tag{5.21}$$

Considering the channel estimation errors on both the serving and interfering channels, we derive the decoding metrics of LS with compensation (LS-C) based on the conditional LMMSE criterion as

$$\hat{\mathbf{X}}_{d1,ls} = \mathbf{w}_{ls}^H \hat{\mathbf{V}}_b \tag{5.22}$$

where we define

$$\begin{aligned}\mathbf{w}_{ls}^H &= \arg\min_{\mathbf{w}^H} \mathbb{E}\left[\|\mathbf{X}_{d1} - \mathbf{w}^H\hat{\mathbf{V}}_b\|^2 \mid \hat{\mathbf{h}}, \hat{\mathbf{h}}_b\right] \\ &= \mathbb{E}\left[\mathbf{X}_{d1}\hat{\mathbf{V}}_b^H \mid \hat{\mathbf{h}}, \hat{\mathbf{h}}_b\right]\mathbb{E}\left[\hat{\mathbf{V}}_b\hat{\mathbf{V}}_b^H \mid \hat{\mathbf{h}}, \hat{\mathbf{h}}_b\right]^{-1} \\ &= \hat{\mathbf{h}}^H\left(\frac{N_p^2(\hat{\mathbf{h}}\hat{\mathbf{h}}^H)}{N_p^2-1} + \frac{N_p(\hat{\mathbf{h}}_b\hat{\mathbf{h}}_b^H)}{N_p^2-1} + N_0\mathbf{I}\right)^{-1},\end{aligned}$$

and $\hat{\mathbf{h}}_b = \bar{\mathbf{p}}\hat{\mathbf{H}}_b$ is the equivalent interfering channel vector.[3]

This result is more complicated than the conventional solution that ignores channel estimation errors. Especially, the LS-C requires the precoding vector $\bar{\mathbf{p}}$ to obtain the term of $\hat{\mathbf{h}}_b$, which is difficult to obtain in practice. Therefore, an alternative way is derived by using the covariance of the residual matrix. To see this, we first notice that the conditional covariance matrix of $\hat{\mathbf{V}}$ is

$$\begin{aligned}\Sigma_v &\triangleq \mathbb{E}\left[\hat{\mathbf{V}}\hat{\mathbf{V}}^H \mid \hat{\mathbf{h}}, \hat{\mathbf{h}}_b\right] \\ &= \frac{N_p^2}{N_p^2-1}\hat{\mathbf{h}}_b\hat{\mathbf{h}}_b^H + \frac{N_p}{N_p^2-1}\hat{\mathbf{h}}\hat{\mathbf{h}}^H + N_0\mathbf{I}. \end{aligned} \tag{5.23}$$

This covariance matrix Σ_v also has the term $\hat{\mathbf{h}}_b\hat{\mathbf{h}}_b^H$. Substituting the covariance matrix Σ_v for the term of $\hat{\mathbf{h}}_b\hat{\mathbf{h}}_b^H$, we have

$$\mathbf{w}_{ls}^H = \hat{\mathbf{h}}^H\left(\hat{\mathbf{h}}\hat{\mathbf{h}}^H + \frac{1}{N_p}\Sigma_v + \frac{N_p-1}{N_p}N_0\mathbf{I}\right)^{-1}, \tag{5.24}$$

which does not depend on the precoding vector $\bar{\mathbf{p}}$. This information can be estimated by the sample covariance estimation as follows

$$\hat{\Sigma}_v = \frac{1}{N_p}\hat{\mathbf{V}}\hat{\mathbf{V}}^H.$$

The resulting output of LS-C becomes

$$\begin{cases} \hat{\mathbf{X}}_{1,ls} = \hat{\mathbf{h}}^H(\hat{\Sigma}_{\mathbf{Y}_{d1}})^{-1}\mathbf{Y}_{d1} \\ \hat{\mathbf{X}}_{d1,ls} = \hat{\mathbf{w}}_{ls}^H\hat{\mathbf{V}}_b. \end{cases} \tag{5.25}$$

where $\hat{\mathbf{w}}_{ls}$ is obtained by using the sample covariance estimation $\hat{\Sigma}_v$ in the theoretical combining vector $\mathbf{w}_{ls}$.

5.1.4 LMMSE with compensation

If perfect SIR is available, we can improve the estimated results of the interfering channel by using the LMMSE channel estimator

$$\mathrm{vec}(\hat{\mathbf{H}}_{b,lm}) = \bar{\mathbf{X}}_{pc}^H(\alpha^2\bar{\mathbf{X}}_{pc}\bar{\mathbf{X}}_{pc}^H + \hat{\Sigma}_{vbc})^{-1}\mathbf{y}_p', \tag{5.26}$$

[3] More details can be found in Appendix A.2.

where $\mathbf{y}'_p = \text{vec}(\mathbf{Y}'_p)$ is the vectorized form of the received matrix, $\hat{\Sigma}_{vbc} = \mathbf{I} \otimes (\hat{\mathbf{V}}_b \hat{\mathbf{V}}_b^H / N_p)$ is the residual matrix, and $\bar{\mathbf{X}}_{pc} = \bar{\mathbf{X}}_p^T \otimes \mathbf{I}$ is the interfering pilot matrix. Replacing the LS channel estimates by the LMMSE channel estimates, we have the resulting output of LMMSE with compensation (LMMSE-C)

$$\begin{cases} \hat{\mathbf{X}}_{1,lm} = \hat{\mathbf{h}}^H (\hat{\Sigma}_{\mathbf{Y}_{d1}})^{-1} \mathbf{Y}_{d1} \\ \hat{\mathbf{X}}_{d1,lm} = \hat{\mathbf{w}}_{ls}^H \hat{\mathbf{V}}_{b,lm}, \end{cases} \tag{5.27}$$

where $\hat{\mathbf{V}}_{b,lm} = \mathbf{Y}'_p - \hat{\mathbf{H}}_{b,lm} \bar{\mathbf{X}}_p$ is the residual matrix of the LMMSE estimate.

5.1.5 Analysis and interpretation

In this section, we try to answer three basic questions: 1) what is the optimum receiver? 2) what is the performance loss of a conventional IRC receiver? and 3) what is the impact of different propagation delays of serving and interfering eNBs?

Optimal receiver (OPT)

We begin by answering the first question of optimal detection of the desired signal $x \in \mathbf{X}_1$ in the presence of interference. The optimal receiver performs ML detection given the following information: the pilot symbols, the received vector $\mathbf{y} \in \mathbf{Y}_{d1}$, precoding vectors, SNR and SIR. Mathematically, the OPT is given by

$$\begin{aligned} \hat{x} &= \arg\max_x \log P(x|\mathbf{y}, \mathbf{Y}_p, \mathbf{Y}'_p, \mathbf{X}_p, \bar{\mathbf{X}}_p, \alpha, N_0, \mathbf{p}, \bar{\mathbf{p}}) \\ &= \arg\max_x \log \sum_{\mathbf{X}_{d1}} \sum_{\bar{\mathbf{X}}_{d1}} \sum_{\bar{x}} \frac{\exp(\mathbf{b}^H \Sigma^{-1} \mathbf{A}^{-1} \mathbf{b})}{\det(\mathbf{A})}, \end{aligned} \tag{5.28}$$

where we apply the Gaussian integral [23] on the conditional probability to obtain the result.[4] We also define the parameters as follows:

$$\mathbf{A} = \mathbf{I}_{2N_T N_R} + \Sigma \left(\left(\mathscr{X} \mathscr{X}^H / N_0 \right)^T \otimes \mathbf{I}_{N_R} \right) \tag{5.29}$$

$$\mathbf{b} = \Sigma \text{vec}(\mathscr{Y} \mathscr{X}^H / N_0) \tag{5.30}$$

$$\mathscr{X} = \begin{bmatrix} \mathbf{X}_p & \mathbf{X}_{d1} & \mathbf{p}x \\ \mathbf{p}\bar{\mathbf{X}}_{d1} & \bar{\mathbf{p}}\bar{\mathbf{X}}_p & \bar{\mathbf{p}}\bar{x} \end{bmatrix} \tag{5.31}$$

[4] See Appendix A.3 for more details

$$\mathscr{Y} = \left(\mathbf{Y}_p, \mathbf{Y}'_p, \mathbf{y}\right) \tag{5.32}$$

$$\Sigma = \begin{bmatrix} 1 & 0 \\ 0 & \alpha^2 \end{bmatrix} \otimes \mathbf{I}_{N_T N_R}. \tag{5.33}$$

The computational load of the OPT is heavy due to the multiple summations over all candidate transmitted signals $\mathbf{X}_{d1}$, $\bar{\mathbf{X}}_{d1}$ and $\bar{\mathbf{x}}$. This formulation implies that we decode (compute all candidates) $\bar{\mathbf{X}}_{d1}$ and $\mathbf{X}_{d1}$ for better CSI estimates; and then decode $\bar{x}$ and x to achieve maximum likelihood detection.

For comparison purposes, we compute the OPT under the assumption that the interfering symbols $\bar{\mathbf{X}}_{d1}$ and the serving symbols $\mathbf{X}_{d1}$ can be decoded perfectly, i.e., both serving and interfering pilots are interference free. In this case, the resulting detector reduces to

$$\hat{x}_{opt} = \arg\max_{x} \log \sum_{\bar{x}} \frac{\exp(\mathbf{b}^H \Sigma^{-1} \mathbf{A}^{-1} \mathbf{b})}{\det(\mathbf{A})}. \tag{5.34}$$

The associated performance will be used as a benchmark for assessing the performance of the proposed algorithms. Note that the log-sum-exp operation can be computed by using the scheme proposed in [33].

The OPT not only provides a performance benchmark, but also helps our understanding of the two-user interference channel. We summarize our observations as follows:

- All interfering symbols $\bar{\mathbf{X}}_{d1}$, $\bar{\mathbf{X}}_{d2}$, and $\bar{\mathbf{X}}_p$ should be decoded and subtracted in a decoding metric. Therefore, both the serving channel $\mathbf{H}$ and the interfering channel $\alpha\bar{\mathbf{H}}$ need to be estimated.

- Good quality of CSI is difficult to obtain because both the pilot symbols $\mathbf{X}_p$ and $\bar{\mathbf{X}}_p$ interfere with the data symbols. These data symbols cannot be decoded and subtracted easily. Therefore, one has to compensate for the channel estimation errors associated with $\mathbf{H}$ and $\bar{\mathbf{H}}$.

Moreover, it is worth noting that all information on the interfering signal is useful, but only some information can be obtained easily, e.g., the SIR value and the positions and the sequences of the interfering pilot symbols. This information is fully exploited in the proposed schemes, i.e., IRC-DL, LS-C, and LMMSE-C.

SINR analysis of IRC

We first consider the conventional IRC scheme [34] which treats interference as a stationary Gaussian process. The IRC detector is

$$\hat{\mathbf{X}}_{irc} = \hat{\mathbf{h}}^H(\hat{\mathbf{h}}\hat{\mathbf{h}}^H + \hat{\mathbf{V}}\hat{\mathbf{V}}^H/N_p)^{-1}\mathbf{Y}_d, \tag{5.35}$$

where $\hat{\mathbf{X}}_{irc}$ is the estimate of the transmitted data matrices $(\mathbf{X}_1, \mathbf{X}_2, \mathbf{X}_3)$ and $\mathbf{Y}_d$ is the received matrix that $\mathbf{Y}_d = (\mathbf{Y}_{d1}, \mathbf{Y}_{d2}, \mathbf{Y}_{d3})$. Unlike the proposed detectors, this scheme decodes $\mathbf{X}_2$ and $\mathbf{X}_3$ with incorrect covariance matrices. The covariance mismatch leads to

$$\begin{aligned} \mathrm{SINR}_{x_1} &= \beta^2/(\beta(1-\beta)) \\ \mathrm{SINR}_{x_2} &= \beta^2/(\beta(1-\beta)+\psi_1) \\ \mathrm{SINR}_{x_3} &= \beta^2/(\beta(1-\beta)+\psi_2). \end{aligned} \tag{5.36}$$

where β^2 is the desired signal power and ψ_1, ψ_2 are the residual interference terms due to the covariance mismatch.[5] If the data energy is much larger than the the noise energy $\mathscr{E}_d \gg N_0$, one can show that $\psi_1 > 0$, $\psi_2 > 0$, and

$$\psi_1, \psi_2 \propto (\mathrm{SNR})^2 \cdot \alpha^2 \cdot \frac{\mathscr{E}_p}{\mathscr{E}_d}. \tag{5.37}$$

Hence, the IRC scheme suffers from mismatch-induced performance degradation when 1) SNR is high, 2) a strong interference is present, and 3) the pilot-to-data power ratio is high, i.e., $\frac{\mathscr{E}_p}{\mathscr{E}_d} \gg 1$. It is worth mentioning the special case when the interfering eNB transmits no data, but pilot symbols only. In this case, we have $\mathscr{E}_d = 0$ such that $\frac{\mathscr{E}_p}{\mathscr{E}_d} = \infty$. This happens in several inter-cell interference coordination (ICIC) approaches [24] and causes significant performance degradation of an IRC receiver.

The asynchronous case

Suppose the length of the DFT window is N_F, the length of the CP is N_{cp}, the maximum channel delay spread is N_L, and the timing difference between two received signals is denoted by τ as shown in Fig. 5.3. All of these parameters are given in terms of the number

[5] See Appendix A.4

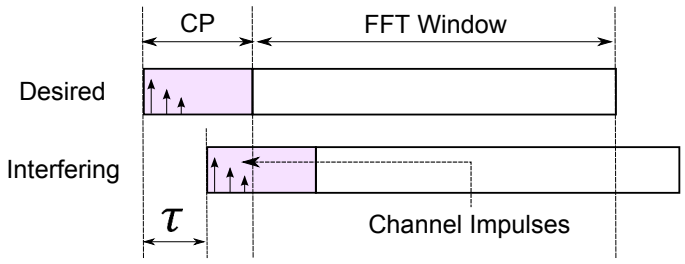

Fig. 5.3 An example of an asynchronous interference

of OFDM samples. We should consider two ranges for the propagation delay τ: 1) those causing no ISI and 2) those which lead to ISI, which are shown in the following.

Case without ISI: The first subset of delays $\tau \in \{0, \cdots, N_{cp} - N_L\}$ does not destroy orthogonality and only introduces a phase rotation in each subcarrier [35]. Assuming the channels are non-selective, the received signal at the (tk)th slot is

$$\mathbf{y} = \mathbf{h}x + e^{\frac{-j2\pi k\tau}{N_F}}\bar{\mathbf{h}}\bar{x} + \mathbf{z}, \tag{5.38}$$

where $0 < \tau \leq N_{cp} - N_L$. Note that the phase rotation $exp(-j2\pi k\tau/N_F)$ is unknown and degrades the interfering channel estimate. On the other hand, since the phase rotation is a function of subcarrier index k instead of time and space, there is no impact on the spatial covariance matrix, i.e., the covariance matrix of $\mathbf{y}$ has no extra distortion due to the timing delay τ, given as follows

$$\Sigma_{\mathbf{y}} = \mathbf{h}\mathbf{h}^H + \bar{\mathbf{h}}\bar{\mathbf{h}}^H + N_0\mathbf{I}, \tag{5.39}$$

Recall that IRC-DL only needs to estimate the covariance matrix without estimating the interfering channel, but both LS-C and LMMSE-C need to estimate the interfering channel. Therefore, we can expect that IRC-DL will perform better than LS-C and LMMSE-C.

Case with ISI: If the delay τ is outside the above range, orthogonality among the subcarriers is destroyed. Mathematically, we have

$$\mathbf{y} = \mathbf{h}x + \kappa e^{\frac{-j2\pi k\tau}{N_F}}\bar{\mathbf{h}}\bar{x} + \alpha\mathscr{I}_{\tau}^{tk} + \mathbf{z},$$

for $\tau < 0$ or $\tau > N_{cp} - N_L$, where $\kappa \approx (N_F - \Delta(\tau))/N_F$, $\Delta(\tau)$ is a positive value related to delay τ, and $\mathscr{I}_\tau^{tk}$ is the ISI term. The impact on the covariance matrices is shown as:

$$\begin{aligned}\Sigma_{\mathbf{y}} &= \mathbf{h}\mathbf{h}^H + \kappa^2\bar{\mathbf{h}}\bar{\mathbf{h}}^H + \alpha^2\mathrm{var}(\mathscr{I}_\tau^{tk}) + N_0\mathbf{I} \\ &\approx \mathbf{h}\mathbf{h}^H + (1 - \frac{\Delta(\tau)}{N_F})^2\bar{\mathbf{h}}\bar{\mathbf{h}}^H \\ &\quad + \alpha^2\left(2\frac{\Delta(\tau)}{N_F} - \left(\frac{\Delta(\tau)}{N_F}\right)^2\right)\mathbf{I} + N_0\mathbf{I}. \end{aligned} \tag{5.40}$$

The ISI term $\mathscr{I}_\tau^{tk}$ is approximated by Gaussian noise as in [36]. In this case, the delay τ degrades the interfering channel estimation by introducing the unknown phase rotation and the distortion term of $\alpha\mathscr{I}_\tau^{tk}$. For the covariance estimation, the delay τ has no impact on the estimate because the covariance matrix $\Sigma_{\mathbf{y}}$ is not a function of time or frequency, i.e., without the index t and the index k after the approximation. Therefore, a similar conclusion can be made that IRC-DL will perform better than LS-C and LMMSE-C, and more gains will be obtained compared to the result in the ISI-free case.

Finally, the performance of the proposed schemes will be evaluated in the numerical section.

5.2 Interference on frequency selective channels

In the second part of this chapter, we consider a two-user interference network on frequency selective channels. Referring to the system model shown in (5.1), the received signal at the time index t can be written as follows

$$\mathbf{y}_k = \mathbf{h}_k x_k + \bar{\mathbf{h}}_k \bar{x}_k + \mathbf{z}_k \in \mathscr{C}^{N_R}, \tag{5.41}$$

where we omit the time index t, and the subcarrier index is denoted by $k = 1, \cdots, N_F$. We also define $\mathbf{h}_k \in \mathscr{C}^{N_R}$ and $\bar{\mathbf{h}}_k \in \mathscr{C}^{N_R}$ are the serving and interfering channel vectors. The frequency selectivity is modelled by the DFT matrix with the time-domain channel impulse response as:

$$(\mathbf{h}_k)_p = \mathscr{F}_k \begin{bmatrix} \mathbf{a}_p \\ \mathbf{0}_{N_F - L} \end{bmatrix} = \mathbf{F}_k \mathbf{a}_p, \tag{5.42}$$

where $(\mathbf{h}_k)_p \in \mathscr{C}$ denotes the p-th element of the channel vector $\mathbf{h}_k$, $\mathscr{F}_k \in \mathscr{C}^{1\times N_F}$ denotes the kth row of the $N_F \times N_F$ DFT matrix, $\mathbf{F}_k \in \mathscr{C}^{1\times L}$ represents the first L entries of $\mathscr{F}_k$ and $\mathbf{a}_p \in \mathscr{C}^{L\times 1}$ is the time-domain channel impulse response. Similarly, the interfering

channel is modelled by the DFT basis with coefficients $(\bar{\mathbf{h}}_k)_p = \mathbf{F}_k \bar{\mathbf{a}}_p$, where $\bar{\mathbf{a}}_p$ denotes the L-tap impulse response of the interfering channel.

We denote the comb-type pilot symbols and the data symbols by using the index of subcarriers with the index sets $\mathscr{P}$ and $\mathscr{D}$ as follows

$$\begin{cases} k \in \mathscr{P}, & \text{if } mod(k, n_p) = 1 \\ k \in \mathscr{D}, & \text{else,} \end{cases} \tag{5.43}$$

where $mod(\cdot)$ denotes the modulus, n_p is the distance between two continuous pilots in the frequency domain, $\mathscr{P}$ is the set of pilot indexes, and $\mathscr{D}$ is the set of data indexes. Note that the comb-type pilots in the set $\mathscr{P}$ is applied for the covariance estimation of interference plus noise.

Suppose the symbols of interest x_k are obtained after the linear processing $\mathbf{w}_k$ as: $\hat{x}_k = \mathbf{w}_k^H \mathbf{y}_k$. To find the optimal combination $\mathbf{w}$, we first introduce the SINR as the measurement. Assuming transmitted symbols with unit power $\mathbb{E}[xx^H] = \mathbb{E}[\bar{x}\bar{x}^H] = 1$, we have the SINR formulation as follows:

$$\text{SINR}_k = \frac{|\mathbf{w}_k^H \mathbf{h}_k|^2}{\mathbf{w}_k^H \mathbf{R}_k \mathbf{w}_k}, \tag{5.44}$$

where $\mathbf{R}_k = \bar{\mathbf{h}}_k \bar{\mathbf{h}}_k^H + N_0 \mathbf{I} \in \mathscr{C}^{N_R \times N_R}$ represents the covariance matrix of interference plus noise, which is unknown and needs to be estimated at the UE receiver.

Suppose the serving channel $\mathbf{h}_k$ and the noise variance N_0 can be accurately estimated. The optimal $\mathbf{w}_k$ and $\mathbf{R}_k$ that maximizes the metric of SINR_k can be written as follows:

$$\begin{aligned} &\max_{\mathbf{w}_k, \mathbf{R}_k} \ \text{SINR}_k \\ &\text{subject to } \mathbf{w}_k^H \mathbf{h}_k = 1, \mathbf{R}_k \in \bar{\nu}, \end{aligned} \tag{5.45}$$

where we assume $\mathbf{R}_k$ belongs to the convex subset $\bar{\nu}$ of Hermitian positive definite matrices of size $N_R \times N_R$ to guarantee that the estimated result is a valid covariance matrix.

5.2.1 Moving-average estimator

Assume that the covariance matrix $\mathbf{R}_k$ is estimated by using the sample covariance via the closest pilot symbols in the index set $\mathscr{P}$ as:

$$\hat{\mathbf{R}}_k = \frac{1}{N} \sum_{m \in \mathscr{P}} \hat{\mathbf{v}}_m \hat{\mathbf{v}}_m^H, \tag{5.46}$$

where $\hat{\mathbf{v}}_m = \mathbf{y}_m - \mathbf{h}_m x_m \in \mathscr{C}^{N_R}$ for $m \in \mathscr{P}$ is the estimated interference plus noise and N is the number of pilots in the moving-average window. We define the estimation errors by $\mathbf{R}_k \triangleq \hat{\mathbf{R}}_k + \Delta_k$ where $\Delta_k \in \mathscr{C}^{N_R \times N_R}$ denotes sample covariance errors.

Lemma 5.2.1. *The entry-wise mean and variance of the sample covariance errors are obtained as follows:*

$$\mathbb{E}[(\Delta_k)_{pq}] = \left(\bar{\mathbf{h}}_k \bar{\mathbf{h}}_k^H - \frac{1}{N}\sum_{m\in\mathscr{P}} \left(\bar{\mathbf{h}}_m \bar{\mathbf{h}}_m^H\right)\right)_{pq}$$

$$var[(\Delta_k)_{pq}] \approx \frac{1}{N^2}\left(\sum_{m\in\mathscr{P}} |(\bar{\mathbf{h}}_m \bar{\mathbf{h}}_m^H)_{pq}|^2 \Psi + N_0 (\Phi)_{pq} + N N_0^2\right)$$

where $(\Phi)_{pq} = \sum_{m\in\mathscr{P}} \left(|(\bar{\mathbf{h}}_m)_p|^2 + |(\bar{\mathbf{h}}_m)_q|^2\right)$ *and* Ψ *is a function of the modulation type of interfering signal* $\bar{x}_k$ *given by*

$$\Psi = \begin{cases} 0 & \text{, PSK} \\ 0.32 & \text{, 16 QAM} \\ 0.3810 & \text{, 64 QAM} \end{cases} \tag{5.47}$$

Proof. See Appendix A.5. □

We found that the variance of the sample covariance errors relies on the following parameters of interference: selectivity of the channel, modulation type, interference strength, and the moving-average window size N. Clearly, more selectivity and higher modulation increase estimation errors. However, the window size N is a trade-off between the selectivity of the interfering channel and the strength of interference plus noise.

Lemma 5.2.2. *Suppose the power delay profile of the interfering channel is given by the equal power assumption (the worst-case assumption) as* $\bar{\mathbf{a}}_p \sim \mathscr{N}_c(\mathbf{0}, (\alpha^2/L)\mathbf{I})$*. Then, the MSE of the sample covariance estimation* $\hat{\mathbf{R}}_k$ *is obtained by*

$$\mathbb{E}[\|\Delta_k\|_F^2] = \sum_{p,q}\left(\frac{\alpha^4}{L^2}\Upsilon\Upsilon^H + \frac{2\alpha^2 N_0}{N} + \frac{N_0^2}{N} + \Psi'\right),$$

where

$$\Upsilon \triangleq \left((\mathbf{F}_k^H)^T \otimes \mathbf{F}_k\right) - \frac{1}{N}\sum_{m\in\mathscr{P}} \left((\mathbf{F}_m^H)^T \otimes \mathbf{F}_m\right) \tag{5.48}$$

$$\Psi' \triangleq \begin{cases} 2 \cdot \alpha^4 \Psi / N & , p = q \\ \alpha^4 \Psi / N & , p \neq q \end{cases} \tag{5.49}$$

Proof. See Appendix A.6. □

Once the power delay profile and the modulation are given, the MSE of sample covariance errors can be obtained by using *Lemma 2*. However, this information is not always available, and an alternative way is as follows: Suppose the length of the channel impulse response L and the modulation function Ψ can be upper bounded, that is

$$L \leq L_w, \text{ and } \Psi \leq \Psi_w. \tag{5.50}$$

Given these bounds, our proposed selection scheme is

$$\begin{aligned} N_w &= \arg\min_N \max_{L,\Psi} \mathbb{E}\|\Delta_k\|_F^2 \\ &= \arg\min_N \sum_{p,q} \left(\frac{\alpha^4}{L_w^2} \Upsilon_w \Upsilon_w^H + \frac{2\alpha^2 N_0}{N} + \frac{N_0^2}{N} + \Psi'_w \right), \end{aligned}$$

where L_w is equal to the CP length n_{cp}. Υ_w is obtained by using $L = n_{cp}$, and Ψ'_w corresponds to a 64-QAM interfering signal ($\Psi = 0.3810$). Note that this metric only relies on the SIR and SNR information, which is available in practice. After the covariance estimation, the linear combination $\mathbf{w}_k$ can be obtained by solving the worst-case problem. Assume the matrix norm of the covariance estimate is upper bounded by a positive value ϵ_k. We can have the solution by the following lemma.

Lemma 5.2.3. *For the following max-min problem:*

$$\arg\max_{\mathbf{w}_k} \min_{\Delta_k} SINR(\mathbf{w}_k) \tag{5.51}$$

$$\textit{subject to } \mathbf{w}_k^H \mathbf{h}_k = 1, \|\Delta_k\| \leq \epsilon_k, \tag{5.52}$$

the solution of $\mathbf{w}_k$ *is given by:*

$$\mathbf{w}_k^* = (\mathbf{h}_k \mathbf{h}_k^H + \hat{\mathbf{R}}_k + \epsilon_k \mathbf{I})^{-1} \mathbf{h}_k. \tag{5.53}$$

Proof. See Appendix A.7. □

This result is equivalent to the IRC (that is based on the LMMSE) with regularization or the so called diagonal loading. The proper upper-bound value ϵ_k can be chosen by the inverse

condition number (ratio of the largest to the smallest singular value) of the covariance estimate [29].

Finally, the performance of the proposed estimator will be evaluated in the numerical results section.

5.3 Interference suppression with additional antennas

In the third part of this chapter, we consider the scheme that enables an IRC receiver to use more RX antennas. Recall the system model shown in (5.1), and add another interfering eNB in this network. The received signal can be characterized by the following equation

$$\mathbf{y}' = \mathbf{h}'_1 x_1 + \sum_{i=2}^{3} \mathbf{h}'_i x_i + \mathbf{z}' \in \mathscr{C}^{N_R}, \tag{5.54}$$

where $x_1 \in \mathscr{C}$ and $\mathbf{h}'_1 = \mathbf{H}'_1 \mathbf{p}'_1 \in \mathscr{C}^{N_R}$ are the serving data symbol and the serving channel response. x_i and $\mathbf{h}'_i = \alpha'_i \mathbf{H}'_i \mathbf{p}'_i$ for $i = 2,3$ are the interfering data symbol and the interfering channel vector, respectively. The desired symbol x_1 is decoded by using the IRC receiver, that is

$$\hat{x}_1 = \mathbf{h}_1^{'H} (\mathbf{h}'_1 \mathbf{h}_1^{'H} + \Sigma'_\nu)^{-1} \mathbf{y}' \triangleq \mathrm{IRC}(\mathbf{y}'), \tag{5.55}$$

where $\Sigma'_\nu = \mathbf{h}'_2 \mathbf{h}_2^{'H} + \mathbf{h}'_3 \mathbf{h}_3^{'H} + N_0 \mathbf{I}$ denotes the covariance of the interference plus AWGN.

Assume that the numbers of TX and RX antennas are $N_T = N_R = 2$ at each node. In this case, if there is no CSI at the transmitter side, the receiver may not have enough RX antennas to efficiently suppress the interference. This necessitates the investigation of efficient schemes to use more antennas. Therefore, suppose we have added some RX antennas that can provide a larger dimensional received signal $\bar{\mathbf{y}} \in \mathscr{C}^{N_a}$ as:

$$\bar{\mathbf{y}} = \bar{\mathbf{h}}_1 x_1 + \sum_{i=2}^{3} \bar{\mathbf{h}}_i x_i + \bar{\mathbf{z}}, \tag{5.56}$$

where we assume the number of the added antennas $N_a = 2$, the intended channel $\bar{\mathbf{h}}_1 = \bar{\mathbf{H}}_1 \bar{\mathbf{p}}_1 \in \mathscr{C}^{N_a}$, the interfering channel vector $\bar{\mathbf{h}}_i = \bar{\alpha}_i \bar{\mathbf{H}}_i \bar{\mathbf{p}}_i \in \mathscr{C}^{N_a}$ for $i = 2,3$, and the AWGN vectors $\bar{\mathbf{z}} \in \mathscr{C}^{N_a}$. The proposed architecture is shown in Fig. 5.5.

In the figure, our goal is to find the optimal combination of the signal $\mathbf{y}'$ and the signal $\bar{\mathbf{y}}$ to reduce the dimension (from four signal streams to two signal streams) for the original

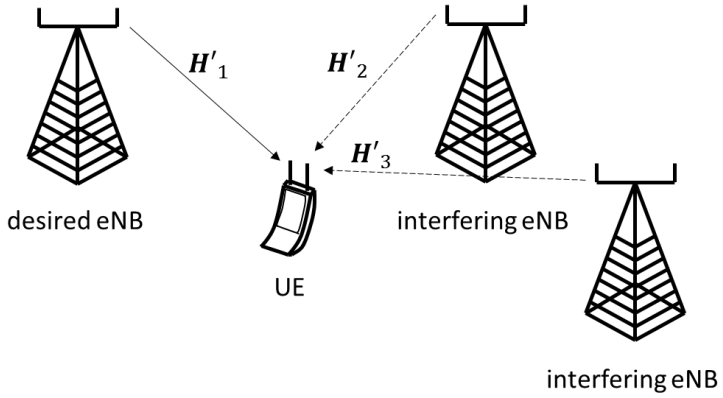

Fig. 5.4 The MIMO interference channel with two antennas on each node transmitting one data stream and sharing the same bandwidth.

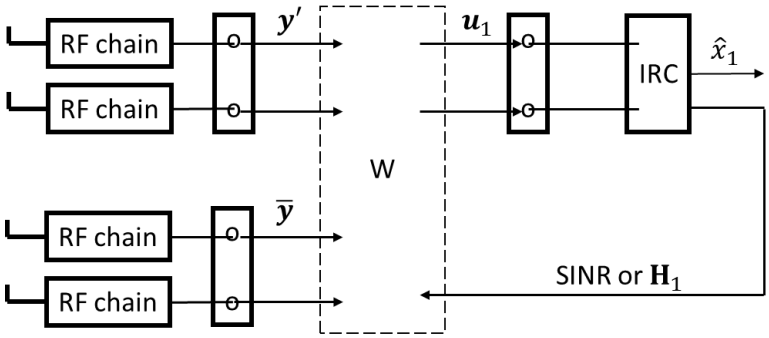

Fig. 5.5 Proposed receiver structure with extra receive antennas and pre-processing **W** on the original IRC receiver

IRC receiver. The optimal combination denoted by **W** can be found based on the SINR maximization as follows:

$$\hat{\mathbf{W}} = \arg\max_{\mathbf{W}} \text{SINR}(\text{IRC}(\mathbf{u}_1)), \tag{5.57}$$

where **W** is an $(N_a + N_R) \times N_R$ pre-processing matrix for the dimension reduction, and the resulting output $\mathbf{u}_1 \in \mathscr{C}^{N_R}$ is given by

$$\mathbf{u}_1 = \mathbf{W}^H \begin{bmatrix} \mathbf{y}' \\ \bar{\mathbf{y}} \end{bmatrix} \triangleq \mathbf{W}^H \left(\mathbf{h}_1 x_1 + \sum_{i=2}^{3} \mathbf{h}_i x_i + \mathbf{z} \right) \tag{5.58}$$

where $\mathbf{h}_i = \alpha_i \mathbf{H}_i \mathbf{p}_i$, $\mathbf{H}_i \in \mathscr{C}^{(N_R+N_a)\times N_R}$ for $i = 1,2,3$ are the stack forms of the channel matrices, and $\mathbf{z} \in \mathscr{C}^{N_R+N_a}$ is the stack form of AWGN vectors of all receive antennas.

5.3.1 Performance enhancement with channel estimates feedback

Suppose IRC has perfect channel estimation and perfect covariance estimation for a two-stream signal. We first derive the resulting output SINR [6]

$$\text{SINR}(\text{IRC}(\mathbf{u}_1)) = \mathbf{h}_1^H \mathbf{W}(\mathbf{W}^H \Sigma_v \mathbf{W})^{-1} \mathbf{W}^H \mathbf{h}_1 \tag{5.59}$$

where $\Sigma_v = \mathbf{h}_2 \mathbf{h}_2^H + \mathbf{h}_3 \mathbf{h}_3^H + N_0 \mathbf{I}$ is the covariance of the interference plus AWGN. Using this result, the SINR maximization can be rewritten as

$$\begin{aligned} &\max_{\mathbf{W}} \mathbf{h}_1^H \mathbf{W}(\mathbf{W}^H \Sigma_v \mathbf{W})^{-1} \mathbf{W}^H \mathbf{h}_1 \\ &\text{subject to } \mathbf{W} \neq \mathbf{0} \end{aligned} \tag{5.60}$$

Since the pre-processing $\mathbf{W}$ is in a matrix form, the optimal solution is not trivial. An alternative solution we found is by omitting the precoding vector $\mathbf{p}_1$ (note that $\mathbf{h}_1 = \mathbf{H}_1 \mathbf{p}_1$) and then separately maximizing the diagonal terms of the matrix. Mathematically, we reformulate the optimization problem as follows:

$$\begin{aligned} &\max_{\mathbf{W}} \left[\mathbf{H}_1^H \mathbf{W}(\mathbf{W}^H \Sigma_v \mathbf{W})^{-1} \mathbf{W}^H \mathbf{H}_1 \right]_k \\ &\text{subject to } \mathbf{W} \neq \mathbf{0} \end{aligned} \tag{5.61}$$

where $k = 1, 2$ is the index of the diagonal terms of the matrix. In this formulation, the closed-form solution can be obtained by

$$\hat{\mathbf{W}}^H = \mathbf{H}_1^H \Sigma_y^{-1}, \tag{5.62}$$

where $\Sigma_y = \mathbf{h}_1 \mathbf{h}_1^H + \Sigma_v$ is the covariance matrix of the received signal from all antennas (more details can be found in Appendix A.9).

In order to obtain $\mathbf{H}_1$, we need the channel estimates from the original IRC. However the original channel estimator of IRC is only designed for a two-stream signal instead of a four-stream signal. Therefore, sequential feedback is needed in order to obtain sufficient CSI. We define two initial pre-processing matrices as:

$$\mathbf{W}_{00} = \begin{bmatrix} \mathbf{I}_2 \\ \mathbf{0}_{2\times 2} \end{bmatrix}, \mathbf{W}_{01} = \begin{bmatrix} \mathbf{0}_{2\times 2} \\ \mathbf{I}_2 \end{bmatrix}. \tag{5.63}$$

[6] See Appendix A.8

Similar to the antenna switching scheme, the IRC receiver estimates the partial CSI sequentially, i.e., using $\mathbf{W}_{00}$ for the first two rows of $\mathbf{H}_1$ then using $\mathbf{W}_{01}$ for the last rows of $\mathbf{H}_1$ in order to obtain a complete matrix of $\mathbf{H}_1$.

5.3.2 Performance enhancement with SINR feedback

If the CSI feedback is unavailable, the performance can still be improved by using the SINR information. In this section, we propose a blind learning scheme which maximizes the output SINR based on a pre-determined unitary codebook as follows: Suppose the 2-stream IRC can provide accurate SINR. We can apply exhaustive search in the solution set $\mathscr{W}$ based on the Grassmannian packing [37].

Using the Cholesky decomposition $\Sigma_v = \mathbf{B}\mathbf{B}^H$, we rewrite the SINR maximization as

$$\hat{\mathbf{W}} = \arg\max_{\mathbf{W}} \mathbf{h}_1^H \mathbf{W}(\mathbf{W}^{\mathbf{H}}\mathbf{B}\mathbf{B}^H\mathbf{W})^{-1}\mathbf{W}^H\mathbf{h}_1 \tag{5.64}$$

$$\approx \arg\max_{\mathbf{W}} \mathrm{tr}\left(\mathbf{W}^H\mathbf{W}\cdot\left(\mathbf{W}^H\mathbf{B}\mathbf{B}^H\mathbf{W}\right)^{-1}\right), \tag{5.65}$$

$$= \arg\max_{\mathbf{W}} \mathrm{tr}\left(\left(\mathbf{W}^H\mathbf{B}\mathbf{B}^H\mathbf{W}\right)^{-1}\right) \tag{5.66}$$

$$\leq \arg\min_{\mathbf{W}} \lambda_{min}^2\left(\mathbf{W}^H\mathbf{B}\right) \tag{5.67}$$

where $\mathrm{tr}(\cdot)$ denotes the trace operation of the matrix, and $\lambda_{min}^2(\cdot)$ denotes the smallest singular value. $\lambda_{min}^2\left(\mathbf{W}^H\mathbf{B}\right) = N_0$ implies that the preprocessor $\mathbf{W}$ is able to suppress all interference and leave AWGN only. The equality holds if $\mathbf{W}$ is $\mathbf{W}_{un} = \bar{\mathbf{U}}_b^H$, where $\bar{\mathbf{U}}_b$ is the $(N_r + N_a - 1)$th and $(N_r + N_a)$th columns of $\mathbf{U}_b$ corresponding to the two minimum singular values. In other words, the optimal unquantized solution is given by $\mathbf{W}_{un} = \bar{\mathbf{U}}_b$.

The optimal quantized codebook $\mathscr{W}$ can be found by the minimization of the average loss from the unquantized solution (see Appendix A.10)

$$\mathscr{W} = \arg\min_{\mathscr{W}'} \mathbb{E}\left[\min_{\mathbf{W}_j \in \mathscr{W}'} \mathrm{d}_{proj}^2(\mathbf{W}_j^H, \bar{\mathbf{U}}_b)\right]. \tag{5.68}$$

Note that this is an equivalent problem to that of [38]. Therefore, we can apply the codebook design criterion of the Grassmannian subspace packing [37].

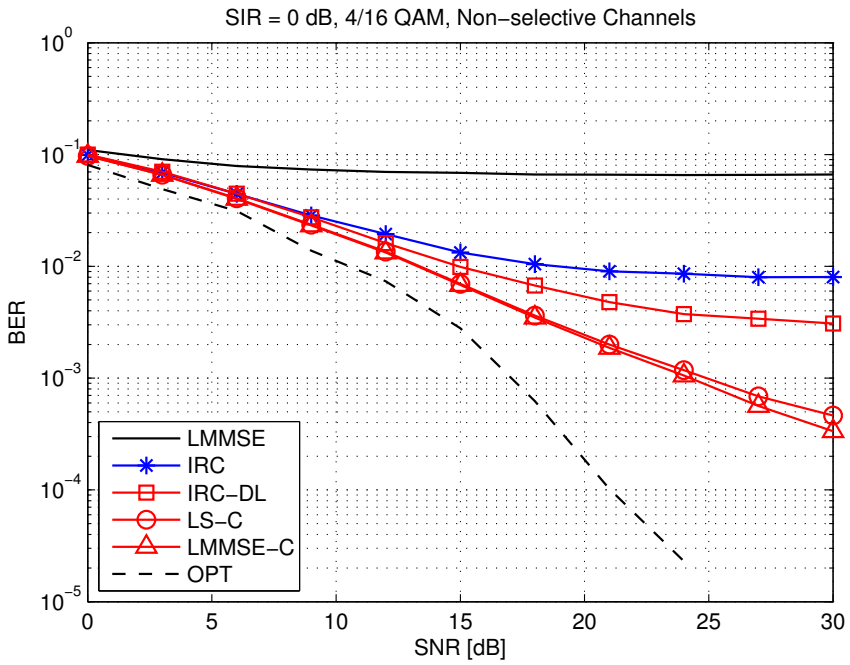

Fig. 5.6 BER vs. SNR in the strong interference region, SIR = 0 dB.

5.4 Numerical results

5.4.1 Interference with covariance mismatches

To evaluate the proposed schemes, we start with a constant channel which is time invariant and frequency non-selective during $N_p + N_d$ intervals (within one RB). The data format follows the LTE FDD specifications [21] where we define $N_p = 16$, and $N_d = 152$. The data of interest $(\mathbf{X}_1, \mathbf{X}_2, \mathbf{X}_3)$ are modulated with Gray-coded 4-QAM. The interfering data matrices $(\bar{\mathbf{X}}_{d1}, \bar{\mathbf{X}}_{d2})$ are modulated with Gray-coded 16-QAM. In what follows, we compare the performance of the conventional schemes: LMMSE (which treats interference as AWGN), IRC, and the proposed approaches: IRC-DL, LS-C, LMMSE-C, and OPT.

Fig. 5.6 shows the BER performance of different SNRs at SIR = 0 dB. These curves show that the proposed IRC-DL, LS-C, and LMMSE-C schemes have better performance than the conventional IRC and LMMSE schemes. The curve of IRC-DL shows the performance gain by suppressing interference with the proper covariance matrices. The curves of LS-C and LMMSE-C show the benefit of decoding the interfering pilot symbols. Besides, OPT shows the possible further improvement if we can decode the interfering data symbols and further improve the channel estimation on both serving and interfering channels.

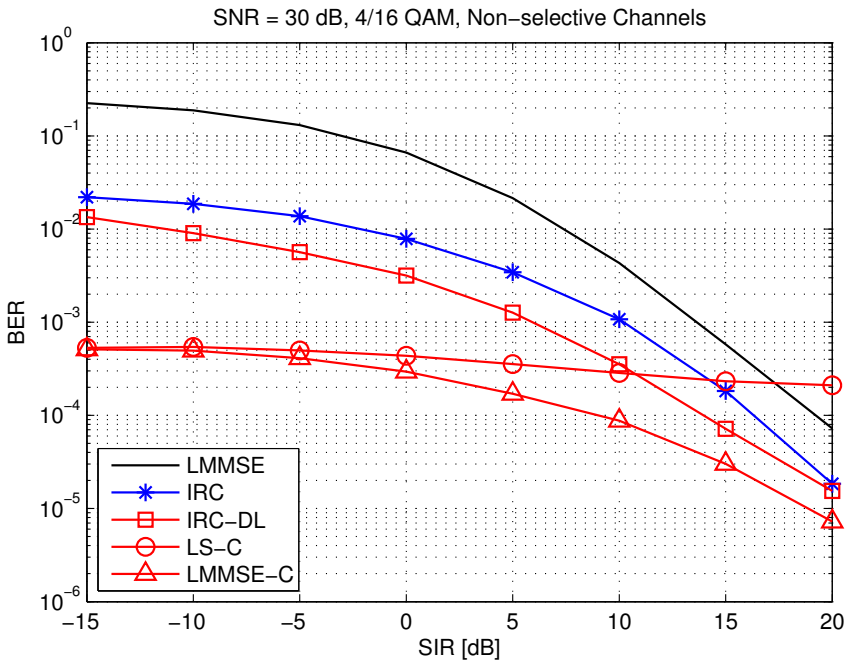

Fig. 5.7 BER vs. SIR in the high SNR region, SNR = 30 dB

Fig. 5.7 shows the BER performance of different SIRs at SNR = 30 dB. These curves demonstrate the advantage of using LMMSE-C compared to LS-C. Note that there is an error floor shown in the LS-C curve. This is due to the fact that an accurate CSI of the interfering channel is difficult to obtain without the correct SIR information. This performance can be improved by using LMMSE-C with the SIR information.

Fig. 5.8 shows a special case in which the interfering eNB only transmits the pilot symbols without sending the data symbols. In this case, the IRC receiver cannot improve the system performance compared to the LMMSE receiver. In contrast, the proposed schemes can still outperform the LMMSE. This result supports our SINR analysis in which the performance loss of IRC is proportional to the pilot-data power ratio $\mathscr{E}_p/\mathscr{E}_d$.

For triply selective channels, we assume that the serving channel distribution information (CDI) is perfectly known but the interfering CDI is unknown. The system parameters are given as follows: normal CP $N_{CP} = 72$, DFT-size $N_F = 1024$, and 2 GHz carrier frequency. All of these parameters are given in terms of OFDM samples. The discrete-time MIMO fading channel is generated using the triply selective channel [39]. In what follows, we denote CDI on both channels by (serving CDI/ interfering CDI) and the UE receiver performs the data detection by the proposed scheme but replacing the serving channel

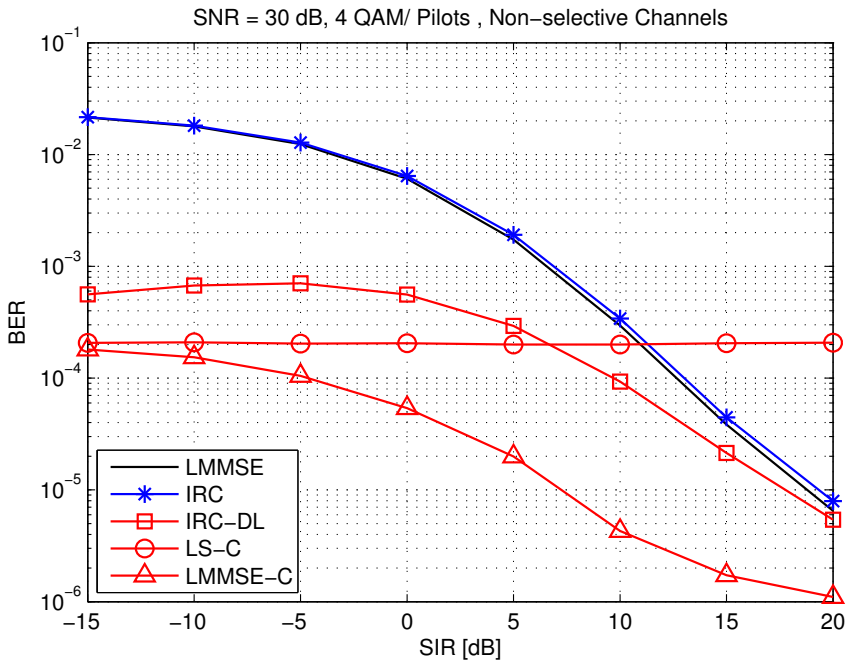

Fig. 5.8 BER vs. SIR for SNR = 30 dB; no interfering data symbols.

estimator by the 2D-minimum mean square error (MMSE) channel estimator instead of the LS channel estimator.

Fig. 5.9 shows the BER performance for SNR = 30 dB on triply selective channels. The CDI of both channels is given by: maximum Doppler frequency fd = 10 Hz, the power delay profiles $\mathbf{C}_{ISI}$ is EPA as defined in LTE specification [21], and no spatial correlation for Ψ_{Tx} and Ψ_{Rx}. In these slow fading and slightly selective assumptions, the resulting curves are similar to the one shown in Fig. 5.7. However, some performance gains are missing in the strong interference region, e.g., in the case of SIR = -15 dB, the LS-C has BER = 10^{-3} over the constant channel shown in Fig. 5.7, but the same scheme only achieves BER = 10^{-2} over the triply selective channel shown in Fig. 5.9. This is due to the fact that the proposed schemes are optimized for the constant channel for its simplicity.

Fig. 5.10 illustrates the asynchronous case on triply selective channels. The CDI of both channels is given as: 10 Hz of the Doppler frequency, the EPA as the power delay profile, and no spatial correlation between antennas. According to EPA, the maximal channel delay spread is given by $N_L = 7$. Therefore, the maximal delay of ISI-free region is $\tau = 65$ shown by the dashed line. These results show different impacts of the timing delay on the proposed schemes. As the delay increases, the LS-C and the LMMSE-C will gain less and less over the conventional IRC. We can find that there is almost no performance gain after

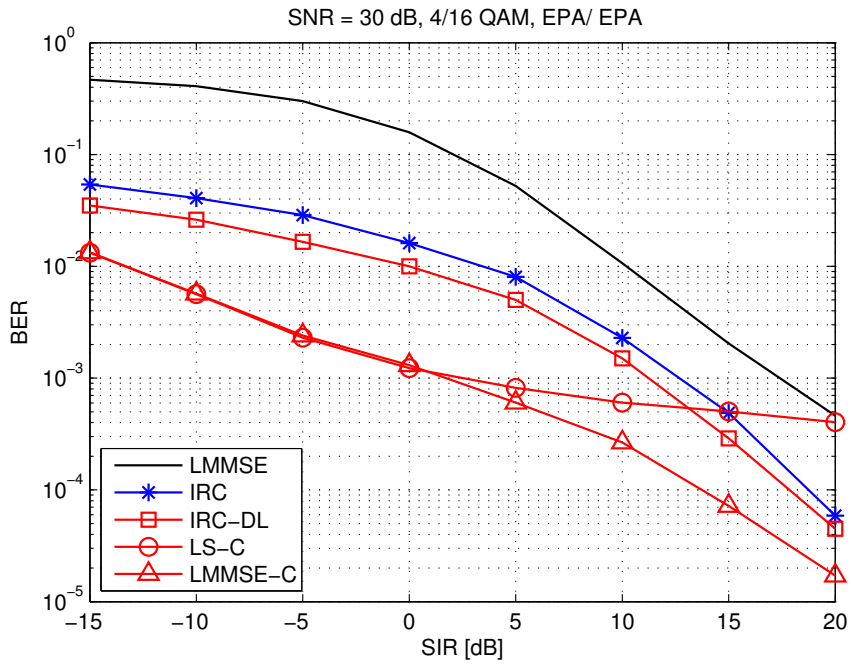

Fig. 5.9 BER vs. SIR with triply selective channels: f_d = 10/ 10 Hz, EPA/ EPA, in the high SNR region, SNR = 30 dB.

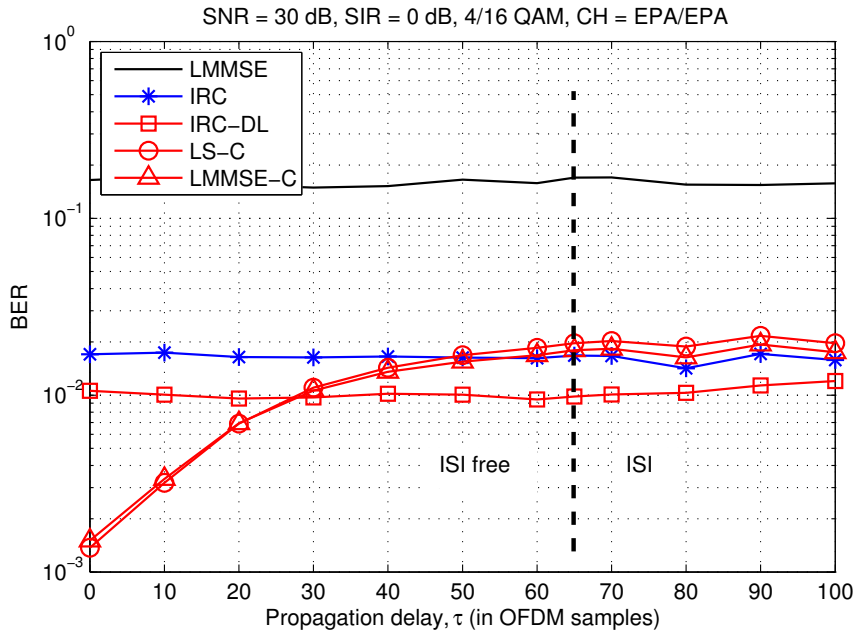

Fig. 5.10 BER vs. propagation delay, τ for SNR = 30 dB and SIR = 0 dB on triply selective channels: f_d = 10/ 10 Hz, EPA/ EPA.

$\tau > 50$. In contrast, the IRC-DL can maintain the same performance gain in the ISI-free region and degrades very slowly in the ISI region.

5.4.2 Interference on frequency selective channels

We generate OFDM symbols with the following parameters: number of subcarriers $N_F = 1024$, central frequency of 2 GHz, normal cyclic prefix of $n_{CP} = 72$ OFDM samples, number of receive antennas $N_R = 2$, and distance between two pilots $n_p = 6$. Transmitted data symbols x_k and $\bar{x}_k$ are modulated with Gray-coded 16-QAM, and the pilot symbols are modulated with QPSK. The time-domain channel impulse response is assumed to be block fading, i.e., flat in one OFDM symbol and i.i.d. between different OFDM symbols, and their power delay profiles are defined by the ETU model according to the LTE specifications [21]. The data of interest is decoded by the linear receivers as follows:

$$\text{LMMSE: } \hat{x}_k = \mathbf{h}_k^H (\mathbf{h}_k \mathbf{h}_k^H + N_0 \mathbf{I})^{-1} \mathbf{y}_k, \tag{5.69}$$

$$\text{OPT: } \hat{x}_k = \mathbf{h}_k^H (\mathbf{h}_k \mathbf{h}_k^H + \mathbf{R}_k)^{-1} \mathbf{y}_k, \tag{5.70}$$

$$\text{Others: } \hat{x}_k = \mathbf{h}_k^H (\mathbf{h}_k \mathbf{h}_k^H + \hat{\mathbf{R}}_k + \epsilon_k \mathbf{I})^{-1} \mathbf{y}_k, \tag{5.71}$$

where LMMSE denotes the interference non-aware scheme (which treats interference as AWGN), OPT denotes the optimal result as a benchmark, and Others denote the suppression schemes with different window sizes for covariance estimation $\hat{\mathbf{R}}_k$. We further compare two possible ways to select the pilots index m for the covariance estimation 1) block partitions (BL), and 2) moving average (MA). The BL is to separate the symbol frame into several non-overlapped clusters and the MA is to separate the symbol frame into overlapped clusters instead. In both schemes, the number which appears in the acronym (see Fig. 5.11) designates the number of pilot symbols available within the window for covariance estimation.

Fig. 5.12 validates *Lemma 2* for SIR = 0 dB. We plot the MSE with different window sizes, MA-2 and MA-4. Note that the variance of *Lemma 1* is obtained by ignoring partial terms related to AWGN. However, the closed-form analysis precisely matches the numerical results even for SNR = 0 dB. These curves also illustrate the impact on different SNR levels, i.e., a longer window is required at low SNR.

Fig. 5.13 shows the BER performance for SIR = 0 dB with the ETU model (the length of the channel impulse response is around 39 OFDM samples) on both serving and interfering channels. We show different approaches where IRC uses all available pilots without

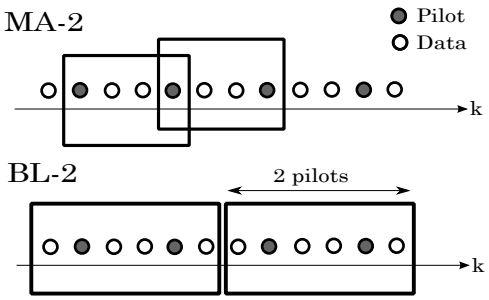

Fig. 5.11 An illustration of sample covariances algorithms: BL-2 and MA-2 with the period of pilot $n_p = 3$

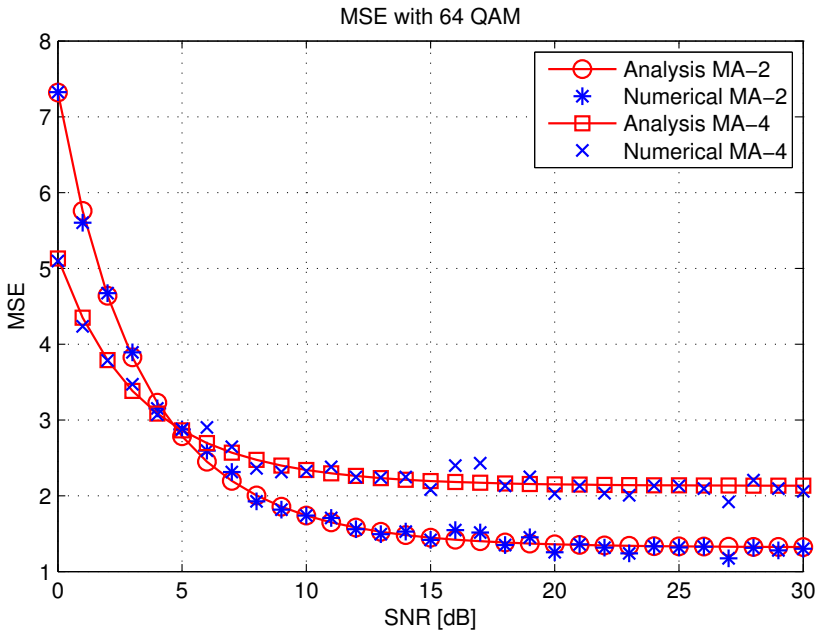

Fig. 5.12 Approximation of MSE in *Lemma 2 with 64 QAM and* $L = n_{cp}$

partition, MA-2 uses 2 pilots within a sliding window, BL-6 uses 6 pilots in a block window, and Selection denotes the proposed window selection scheme with MA. First of all, these curves show that the MA schemes outperform the BL schemes. Second, we found that using a longer window is not always the best option, e.g., MA-2 outperforms MA-6 due to using a smaller window size. Finally, our proposed scheme can provide the correct window size (i.e., $N = 2$) at different SNR values.

Fig. 5.14 shows the BER performance for different interference levels and SNR = 15 dB. These curves indicate that the proposed scheme can always find the optimal window size, e.g., as SIR increases, the selected size starts from a small window $N = 2$ to a large window $N = 8$. Note that there is a crossing point at $SIR = SNR = 15$ dB. Before this point $SIR < 15$

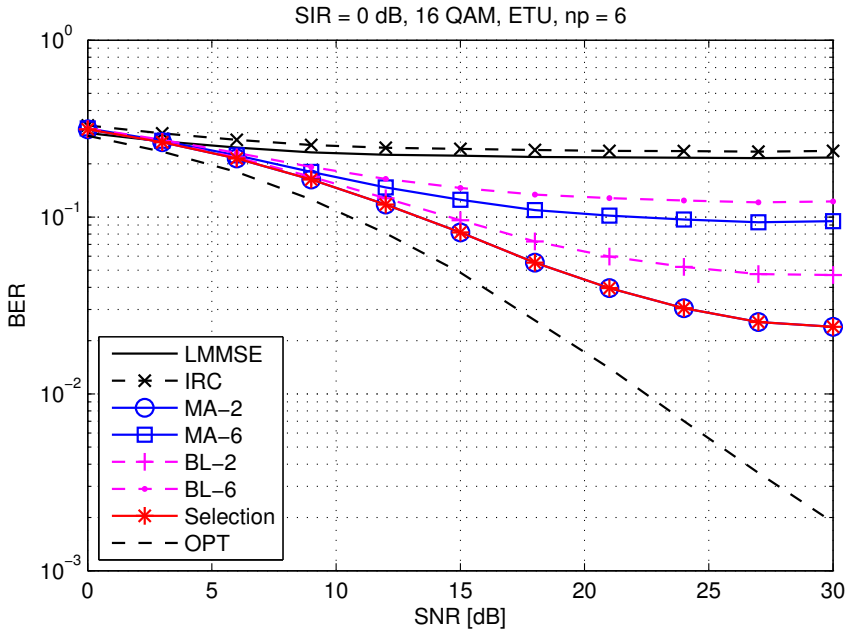

Fig. 5.13 System performance for SIR = 0 dB with different SNR values

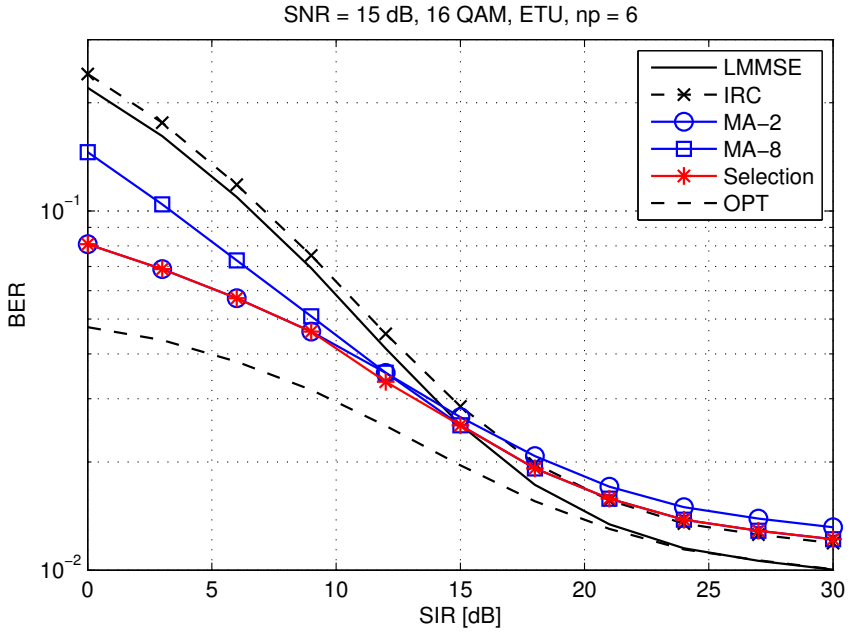

Fig. 5.14 System performance for SNR = 15 dB with different SIR values

dB, the window selector must use a small size ($N = 2$) to suppress the strong interference over the frequency-selective channel. On the contrary, after the point $SIR > 15$ dB, the selector turns to use a large window ($N = 8$) to suppress AWGN.

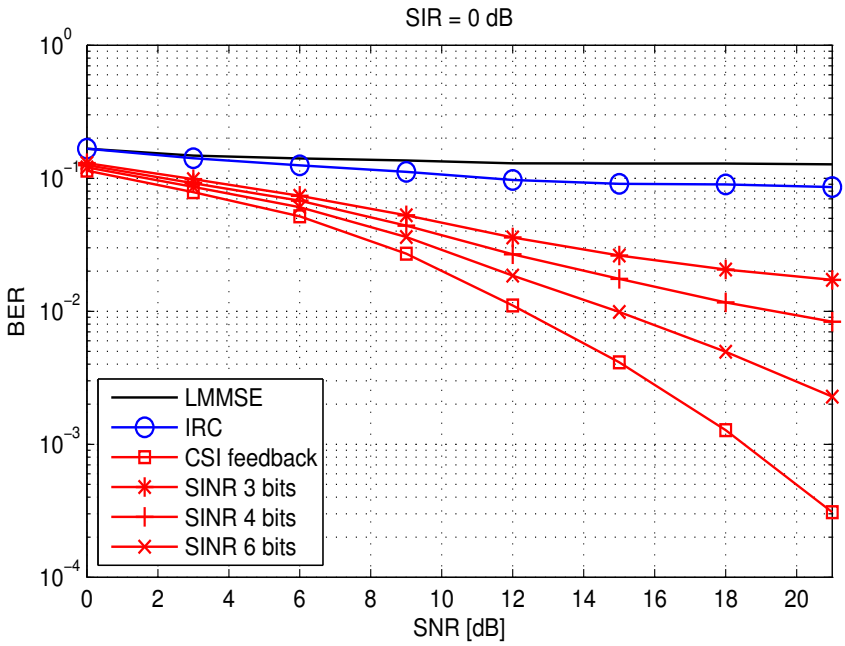

Fig. 5.15 BER vs. SNR for SIR = 0 dB; with three users, two antennas, and transmitting one data stream from each user.

5.4.3 Interference suppression with additional antennas

Consider a three-user downlink MIMO channel with block fading. The transmitted data symbol and the interfering symbols x_i for $i = 1,2,3$ are modulated with Gray-coded 16-QAM. The precoding vectors $\mathbf{p}_i$ for $i = 1,2,3$ are selected randomly. We compare the following approaches: i) LMMSE denotes the interference non-aware receiver (which treats interference as AWGN), ii) IRC is the conventional IRC with the 2-stream detector, iii) CSI feedback is the proposed scheme using 4 receive antennas and the preprocessor, and iv) Proposed SINR (3,4,6) bits are given with the Grassmannian codebook [37].

Fig. 5.15 reports the BER performance vs. SNR in the presence of strong interference (SIR = 0 dB). We first show the conventional approaches, i.e., LMMSE and IRC, which are unable to suppress the interference due to the lack of RX antennas. Second, the blind learning algorithms, i.e., SINR 3 bits 4 bits and 6 bits, result in different improvements according to different codebook sizes. Finally, the Proposed CSI feedback scheme outperforms the conventional schemes and the blind learning schemes by using the additional training phrase shown in (5.63) to obtain full CSI.

Fig. 5.16 shows the BER curves at SNR = 20 dB for different SIR values in order to show the impact of different interference levels. As in the previous figure, the proposed solutions

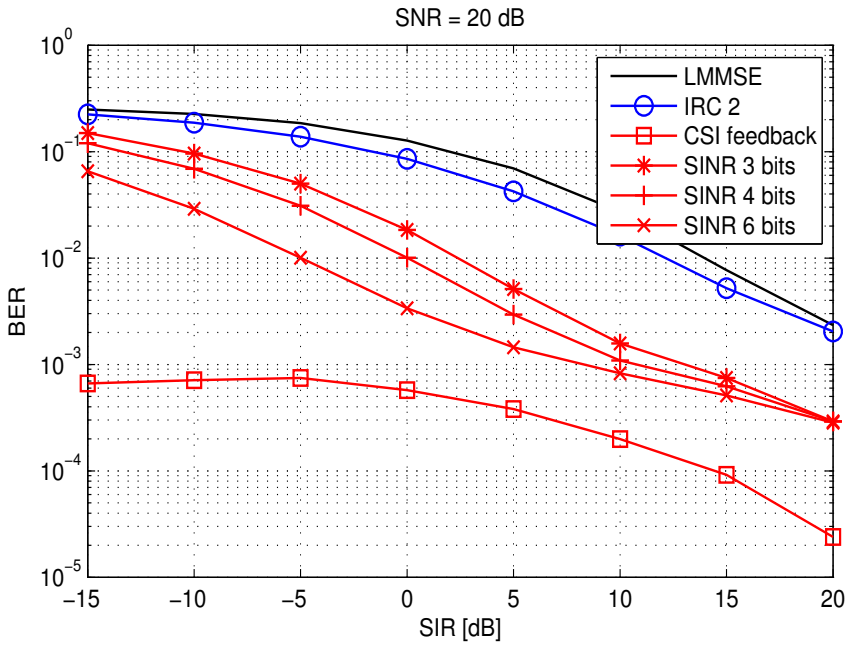

Fig. 5.16 BER vs. SIR for SNR = 20 dB; with three users, two antennas, and transmitting one data stream from each user.

show improvements compared to the conventional schemes. Moreover, we can expect more improvements for the SINR scheme with a larger codebook size, e.g., 8 bits and 10 bits, in the strong interference region.

Finally, we need to point out that the proposed scheme can be applied for different kinds of receivers. The general idea is to create an equivalent channel matrix for the original receiver. For example, we generate a 2×2 equivalent channel matrix for the original IRC receiver by using 4 physical antennas and linear combining. This equivalent 2×2 channel matrix enhances SINR by exploiting some information from the original IRC.

5.5 Conclusion

This study considers interference suppression schemes for MIMO-OFDM systems. In such systems, the statistical property of interference impacts its suppression schemes. The main concern in this chapter is how to properly estimate the statistical information and how to update this information in an efficient way.

In the first part of our study, some novel schemes have been derived by the LMMSE and the SIC criteria, which are based on using the pilot-data structure of interference.

Numerical results have demonstrated that separately handling the interfering pilot and data signals allows substantial improvements, which also clearly reveal the importance of judicious exploitation of the structure and statistics of interfering signal (such as those from neighboring cells).

The numerical results include flat and triply selective channels with/without timing delays of arrival signals. In the synchronous case, we find that the proposed LMMSE-C provides better performance than the other schemes. This scheme is based on the SIC criterion that decodes interfering pilots by estimating the interfering channel. In the asynchronous case, since estimating the interfering channel becomes difficult, the proposed IRC-DL based on the LMMSE criterion provides reliable and stable performance. This scheme only estimates the distinct statistical properties based on the pilot-data structure, treating interference as noise without decoding it.

In the second part, we focus on interference over a frequency selective channel. The interference suppression scheme becomes challenging because of the trade-off between handling the channel selectivity and AWGN. We first make an analysis of means and variances of covariance estimation errors, and then derive the closed-form MSE of covariance estimation. Based on the analysis results, we proposed a window-size selection scheme which only depends on the knowledge of SIR and SNR. Numerical results demonstrate that the selection scheme can find the optimal window size for different SIRs.

Finally, to improve IRC in its dimensional scalability, we propose two approaches to scale the number of RX antennas in order to provide extra spatial diversity. The proposed schemes maximize the resulting SINR by the CSI or the SINR feedback from the original receiver. Numerical results are presented, confirming the performance improvements by exploiting the additional spatial dimension in the presence of interference.

Chapter 6

Spatial Modulation Design

MIMO technologies are now commonplace in wireless communications systems in order to increase throughput, performance, or both. The basic principle of these technologies is well described in Chapter 2, and the proposed reception schemes can be found in Chapter 3, Chapter 4, and Chapter 5. The main limitation of MIMO systems is related to their implementation complexity, which increases with the number of antennas. In some MIMO systems, cost and energy consumption considerations lead to the implementation of a smaller number of RF chains in the transmitter than the number of TX antennas. This is often the case in mobile and fixed user equipment, because the number of antennas is dictated by the performance requirements of the downlink signal, and cost and energy consumption limitations may not allow the implementation of as many RF chains.

When the number of RF chains in the transmitter is smaller than the number of TX antennas, we essentially have two options to exploit the inherent antenna redundancy: The classic approach is to use antenna switching to improve system performance. Indeed, if the channels are known at the transmitter side, the antennas corresponding to the best channels can be selected for transmission. This is called switching diversity, and it is well known that this technique can approach the performance of optimum diversity [40]. The second approach, which is called SM, does not aim at creating diversity. Instead, the active antenna indices in this technique are used to transmit information. The first papers on SM considered a single active antenna [41–43]. In that simple case, selection of 1 out of N_T TX antennas requires $\log_2(N_T)$ bits, assuming that N_T is an integer power of 2. Next, m information bits are used to transmit one symbol from that antenna, assuming that the signal constellation has $M = 2^m$ points. In summary, such a scheme transmits $m + \log_2(N_T)$ bits per channel use (bpcu). The SM technique was simplified in [44] by

using only the spatial constellation diagram (the index of the active antenna) to transmit information bits. This scheme is known as space-shift keying (SSK). Further work on SM and SSK generalized these techniques by relaxing the single RF-chain constraint and allowing more than one antenna to transmit simultaneously. The resulting schemes are known as generalized SM (GSM) [45–48] and generalized SSK (GSSK) [49–51] in the literature. Further work on the subject introduced space-time block codes to improve system performance as in conventional MIMO systems. Examples of this type of work can be found in [52–54].

In terms of spectral efficiency, it should be noted that SM is quite poor compared to spatial multiplexing (SMX) that is commonly used in wireless communications standards. SMX consists of transmitting independent data streams from all TX antennas simultaneously [2]. For example, with 2 TX antennas, conventional SM (with one RF chain) transmits $m+1$ bpcu, whereas SMX transmits $2m$ bpcu (where m is the number of bits per symbol of the constellation used). Similarly, with 4 TX antennas, SM transmits $m+2$ bpcu, whereas SMX transmits $4m$ bpcu. This inherent throughput loss of conventional SM is the main motivation for this work to introduce a new SM scheme, which we refer to as ESM.

ESM was devised by combining several ideas. The first one is to transmit symbols from a primary constellation when a single TX antenna is activated and to transmit symbols from a secondary constellation when two TX antennas are activated. The second idea is to define a set of secondary constellations whose size is half of the primary constellation size in order to transmit the same number of bits during the single active antenna periods and the two active antenna periods. The third idea is to design the secondary constellations through geometric interpolation in the signal space in such a way as to maximize the minimum Euclidean distance between transmitted signal vectors.

The concept of using multiple signal constellations is the basic deviation of ESM from conventional MIMO schemes including single-RF SM and GSM. Here, instead of the active antenna index, or the indices of active antennas, information bits are transmitted by antenna and constellation combinations. The number of those combinations is the double or the quadruple of the number of active antenna indices (or index combinations) in conventional SM systems, and this increases the number of bits transmitted per channel use by 1 or 2, when the signal constellation of conventional SM is used as a primary constellation in ESM. Alternatively, when the signal constellations are selected in such a way that ESM operates at the same spectral efficiency as conventional SM, ESM achieves higher performance.

6.1 System model

For a MIMO system, the received signal can be expressed as:

$$\mathbf{y} = \mathbf{H}\mathbf{x} + \mathbf{n}, \tag{6.1}$$

where $\mathbf{H}$ is the $N_R \times N_T$ channel matrix, N_R denotes the number of receive antennas, N_T is the number of transmit antennas, $\mathbf{x}$ is the $N_T \times 1$ transmitted symbol vector, and $\mathbf{n}$ designates the AWGN. Assume that the entries of the channel matrix $\mathbf{H}$ are i.i.d. complex circularly symmetric Gaussian variables of the form $\mathcal{N}_c(0,1)$ and the entries of AWGN, $\mathbf{n}$, are i.i.d. Gaussian noise of the form $\mathcal{N}_c(0,N_0)$. The transmit energy is $\mathbb{E}[\mathbf{x}^H\mathbf{x}] = E_s$, and the average SNR is defined as SNR $= E_s/N_0$. Note that the main difference between SM and conventional MIMO is that in the former not all transmit antennas are activated simultaneously, which means that there are some zero elements in the transmit symbol vector $\mathbf{x}$ to present the silent TX elements.

6.1.1 A brief review of SMX and conventional SM

For SMX with N_T transmit antennas, the transmitted symbol vector $\mathbf{x}$ can be written as:

$$\mathbf{x} \in \left\{ \begin{Bmatrix} \mathscr{C} \\ \vdots \\ \mathscr{C} \end{Bmatrix} \right\} = \mathscr{C}^{N_T}, \tag{6.2}$$

where the entries $\mathscr{C}$ represent the complex signal constellation used. When this MIMO scheme uses a signal constellation with $M = 2^m$ points, it transmits mN_T bits per channel use, and the total energy per transmitted symbol vector is N_T times the average energy per symbol of the signal constellation.

In conventional SM with N_T TX antennas (out of which only one antenna is active at a time), the transmitted symbol vectors $\mathbf{x}$ are of the form:

$$\mathbf{x} \in \left\{ \begin{Bmatrix} \mathscr{C} \\ 0 \\ \vdots \\ \cdot \\ 0 \end{Bmatrix}, \begin{Bmatrix} 0 \\ \mathscr{C} \\ 0 \\ \vdots \\ 0 \end{Bmatrix}, \cdots, \begin{Bmatrix} 0 \\ \vdots \\ \cdot \\ 0 \\ \mathscr{C} \end{Bmatrix} \right\}, \tag{6.3}$$

where, as previously, the entry $\mathscr{C}$ denotes the symbol constellation used, and the zero entries correspond to the silent TX elements. Assuming that this scheme uses a signal constellation with $M = 2^m$ points, a total of $m + \lfloor \log_2(N_T) \rfloor$ information bits are sent per channel use: $\lfloor \log_2(N_T) \rfloor$ bits select the index of the active antenna and m bits select a particular symbol from the signal constellation to be transmitted from that antenna. For example, with the QPSK signal constellation, SM transmits 3 bpcu when $N_T = 2$, and it transmits 4 bpcu when $N_T = 4$. Note that the corresponding numbers for SMX are 4 bpcu with $N_T = 2$ and 8 bpcu with $N_T = 4$.

Clearly, when both transmission schemes use the same signal constellation, SM transmits significantly less information than SMX, and this motivated us to search for an enhanced SM scheme that increases the transmitted data rate. In the following section, we describe the general principle and the construction of the introduced ESM scheme for $N_T = 2$ and $N_T = 4$ before outlining its generalizations to a higher number of antennas. In terms of signal constellations, we start with QPSK as primary modulation, and then we describe ESM designs using 16QAM and 64QAM.

6.2 ESM with multiple signal constellations

6.2.1 ESM-QPSK

With two TX antennas and QPSK as primary modulation, the transmitted signal vector in our proposed ESM technique is of the form:

$$\mathbf{x} \in \left\{ \begin{bmatrix} \mathscr{C}_4 \\ 0 \end{bmatrix}, \begin{bmatrix} 0 \\ \mathscr{C}_4 \end{bmatrix}, \begin{bmatrix} \mathscr{B}_2^0 \\ \mathscr{B}_2^0 \end{bmatrix}, \begin{bmatrix} \mathscr{B}_2^1 \\ \mathscr{B}_2^1 \end{bmatrix} \right\}, \tag{6.4}$$

where $\mathscr{C}_4$ denotes the QPSK signal constellation used as primary constellation, and $\mathscr{B}_2^0$ and $\mathscr{B}_2^1$ represent two secondary signal constellations given by $\mathscr{B}_2^0 = \{\pm 1\}$ and $B_2^1 = \{\pm i\}$. Clearly, the first two elements in the signal space given by (6.4) are those of conventional SM with QPSK signal constellation and they correspond to the transmission of a QPSK symbol from the first and the second antenna, respectively. The third and the fourth signal elements correspond to the simultaneous transmission of symbols from both antennas, but those symbols take their values from a secondary constellation, which carries only 1 bit. The purpose of this is to have the same number of transmitted bits as with the first and the second elements of the signal space. We refer to the secondary signal constellations

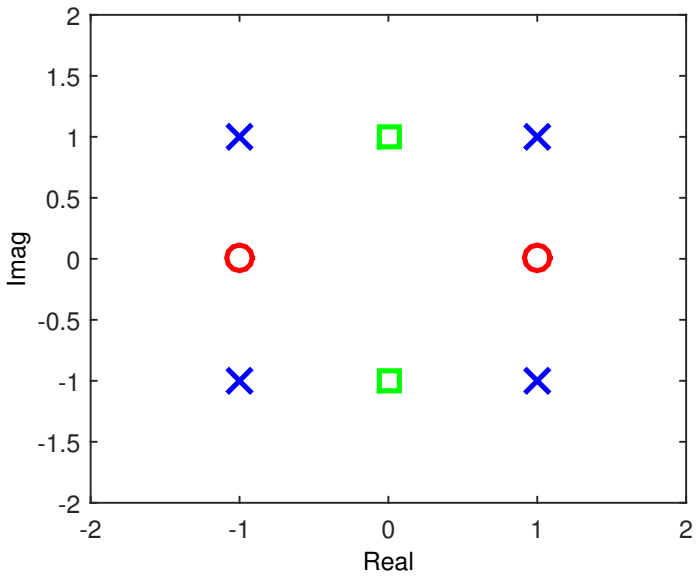

Fig. 6.1 The constellations used: The crosses represent QPSK and the circles (resp. squares) represent the BPSK0 (resp. BPSK1) signal constellation.

as BPSK0 and BPSK1, respectively. The three signal constellations used in this design are shown in Fig. 6.1, and the four antenna constellation combinations, which respectively determine the four signal space elements in (6.4), are illustrated in Table 6.1. This scheme transmits 4 bpcu, because selection of one combination out of four requires two bits, and two other bits are required to select either a QPSK symbol, or two symbols from one of the secondary constellations (BPSK0, BPSK1). Compared to conventional SM with the same modulation and number of TX antennas, we have thus increased the number of bits per channel use by one.

Two main features of the proposed ESM scheme are very evident from the description above: The first is the increased number of combinations compared to conventional SM by the inclusion of a set of secondary modulations in addition to the primary modulation. The second feature is that the size of the secondary modulations is exactly half of the primary modulation size and therefore the number of transmitted bits is the same for all combinations. At this point, it is important to describe a third feature, which is related to the derivation of the secondary signal constellations. The principal criterion in this derivation is to maximize the minimum Euclidean distance between the three constellations involved without increasing the transmitted signal energy.

As evidenced from Fig. 6.1, the minimum Euclidean distance is the same for all three signal constellations used in the design. It is given by $\delta_0 = 2$. Obviously, δ_0 is also the

Table 6.1 ESM-QPSK with 2 TX antennas

	TX1	TX2
C1	QPSK	0
C2	0	QPSK
C3	BPSK0	BPSK0
C4	BPSK1	BPSK1

Table 6.2 ESM-QPSK with 4 TX antennas

	TX1	TX2	TX3	TX4
C1	QPSK	0	0	0
C2	0	QPSK	0	0
C3	0	0	QPSK	0
C4	0	0	0	QPSK
C5	BPSK0	BPSK0	0	0
C6	BPSK0	0	BPSK0	0
C7	BPSK0	0	0	BPSK0
C8	0	BPSK0	BPSK0	0
C9	0	BPSK0	0	BPSK0
C10	0	0	BPSK0	BPSK0
C11	BPSK1	BPSK1	0	0
C12	BPSK1	0	BPSK1	0
C13	BPSK1	0	0	BPSK1
C14	0	BPSK1	BPSK1	0
C15	0	BPSK1	0	BPSK1
C16	0	0	BPSK1	BPSK1

minimum distance between two signal vectors corresponding to the same combination. Next, δ_0 is also the minimum distance between a signal vector from combination C1 and a signal vector from combination C2. The same applies to the minimum distance between a signal vector from combination C3 and a vector from combination C4. However, the distance between a signal vector from $C1 \cup C2$ and a signal vector from $C3 \cup C4$ is $\delta_0/\sqrt{2}$. This is the minimum distance of the entire signal space, but this 3-dB reduction of the minimum Euclidean distance is limited to ESM which uses QPSK as primary modulation. The ESM designs described in the following subsections with 16QAM and 64QAM as primary modulations do not have such a problem.

As indicated earlier, with $N_T = 4$ and the QPSK signal constellation, conventional SM transmits 4 bpcu, because two bits determine the active antenna index and two other bits determine a QPSK symbol to be transmitted from that antenna. In this case, our ESM uses 16 combinations of active antennas and constellations transmitted from these antennas, which are shown in Table 6.2. The first four combinations in this table are those of conventional SM. They simply correspond to the transmission of a QPSK symbol from one of the four TX antennas. Next, we have 6 combinations for transmission of two simultaneous BPSK0 symbols from two TX antennas, and as many combinations for simultaneous transmission of two BPSK1 symbols. Therefore, ESM transmits 6 bpcu, compared to the 4 bpcu capacity of conventional SM: 4 information bits are needed to select one of those 16 combinations, and 2 bits are used to select a QPSK symbol, or a pair of BPSK0 symbols, or a pair of BPSK1 symbols.

6.2.2 ESM-16QAM

Conventional SM with 16QAM modulation and 2 TX antennas consists of selecting one of the two TX antennas using one information bit and transmitting a 16QAM symbol from that antenna. The throughput is 5 bpcu.

For ESM, we use the following constellation combinations, which provide 6 bpcu transmission:

$$\mathbf{x} \in \left\{ \begin{Bmatrix} \mathscr{C}_{16} \\ 0 \end{Bmatrix}, \begin{Bmatrix} 0 \\ \mathscr{C}_{16} \end{Bmatrix}, \begin{Bmatrix} \mathscr{Q}_4^0 \\ \mathscr{Q}_4^0 \end{Bmatrix}, \begin{Bmatrix} \mathscr{Q}_4^1 \\ \mathscr{Q}_4^1 \end{Bmatrix} \right\}, \tag{6.5}$$

where $\mathscr{C}_{16}$ denotes the 16QAM signal constellation used as primary modulation, and $\mathscr{Q}_4^0$ and $\mathscr{Q}_4^1$ represent two reduced-size signal constellations defined as $\mathscr{Q}_4^0 = \{\pm 1 \pm i\}$ and $\mathscr{Q}_4^1 = \{\pm 1, \pm i\}$. We refer to the secondary signal constellations as QPSK0 and QPSK1, respectively.

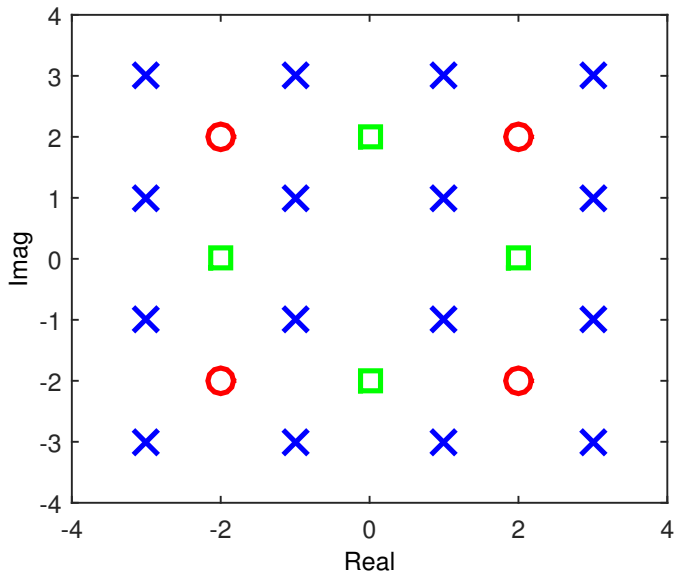

Fig. 6.2 The constellations used: The crosses represent 16QAM and the circles (resp. squares) represent the QPSK0 (resp. QPSK1) signal constellations.

These constellations are shown in Fig. 6.2. The antenna/modulation combinations used in ESM are those of Table 6.1, when QPSK, BPSK0 and BPSK1 are replaced by 16QAM, QPSK0 and QPSK1, respectively.

It should be noted that the average transmit energy in the proposed ESM scheme is slightly larger than in the corresponding conventional SM scheme. Indeed, conventional SM transmits one 16QAM symbol from the selected active antenna, and the average transmit energy is $E_s = 10$. This also holds for the first two combinations in ESM. But the third combination of ESM transmits two QPSK0 symbols and the corresponding average energy is 16. Finally, the fourth combination transmits two QPSK1 symbols and the corresponding average energy is 8. Therefore, the overall average energy is $E_s = 11$, which represents a 0.4 dB increase with respect to conventional SM.

The design methodology of the secondary modulations used in ESM-16QAM follows the same rules as in ESM-QPSK. More specifically, their size is half of the size of the primary modulation, so that transmitting two symbols in parallel from a secondary modulation corresponds to the same number of bits per channel use as the transmission of a symbol from a primary modulation. Next, the points of the QPSK0 and QPSK1 constellations are placed at the centers of the square grid representing the original 16QAM constellation in order to maximize the minimum Euclidean distance between symbol vectors belonging to combinations based on the primary modulation and those belonging to combinations

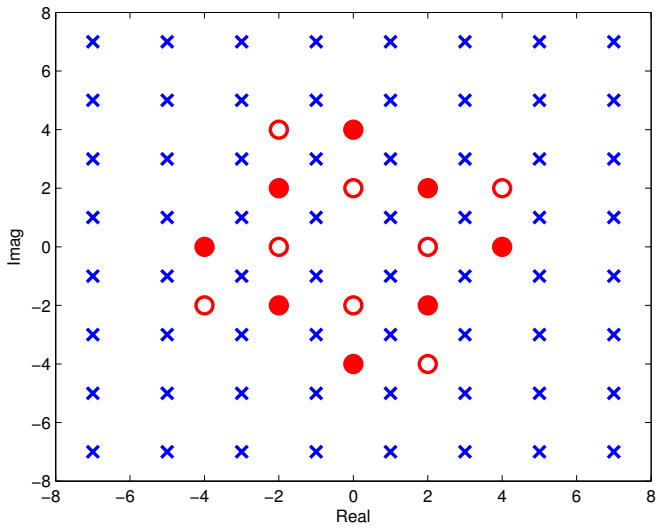

Fig. 6.3 The constellations used: The blue crosses represent 64QAM, and the heavy/empty red circles represent the 8APK0/8APK1 signal constellations.

that are based on the secondary modulations. It can be easily verified by hand that the minimum distance δ_0 of the 16QAM modulation is also the minimum distance of the signal vector space in this design.

Extension of ESM-16QAM to the 4-TX case follows the same process as with ESM-QPSK, i.e., by substituting in Table 6.2 16QAM, QPSK0, and QPSK1 for QPSK, BPSK0, and BPSK1, respectively. Using 16QAM and 4 TX antennas, ESM transmits 8 *bpcu*, and the resulting scheme is denoted 4TX8b. This is to be compared to the 6 bpcu spectral efficiency of conventional SM with the same number of TX antennas and the 16QAM modulation.

6.2.3 ESM-64QAM

To achieve higher throughputs, we now describe ESM schemes using higher-level signal constellations. The design process is similar to that with the previous constellations, but here we have more degrees of freedom, and we will describe two different ESM schemes using 64QAM as primary modulation and two TX antennas. The first one of those, referred to as 2TX8b, is based on the following signal space:

$$\mathbf{x} \in \left\{ \begin{Bmatrix} \mathscr{C}_{64} \\ 0 \end{Bmatrix}, \begin{Bmatrix} 0 \\ \mathscr{C}_{64} \end{Bmatrix}, \begin{Bmatrix} \mathscr{A}_8^0 \\ \mathscr{A}_8^0 \end{Bmatrix}, \begin{Bmatrix} \mathscr{A}_8^1 \\ \mathscr{A}_8^1 \end{Bmatrix} \right\} \triangleq \mathscr{S}_{2TX8b}, \tag{6.6}$$

where $\mathscr{C}_{64}$ denotes the 64QAM signal constellation used as primary modulation, and $\mathscr{A}_8^0$ and $\mathscr{A}_8^1$ represent two different secondary signal constellations of 8 points each. The secondary signal constellations are respectively given by $\mathscr{A}_8^0 = \{\pm 2 \pm 2i, \pm 4i, \pm 4\}$ and $\mathscr{A}_8^1 = \{\pm 2, \pm 2i, 4+2i, -4-2i, 2-4i, -2+4i\}$. These constellations are referred to as 8-level amplitude-phase-keying (8APK)0 and 8APK1, respectively, and the resulting ESM scheme is referred to as 2TX8b, because it transmits 8 bpcu. It can be verified that the average transmit signal energy in this ESM scheme is $E_s = 33$. The constellations used are shown in Fig. 6.3, where the signal points in 8APK0 and 8APK1 are placed close to the origin with the purpose of average energy reduction. The combinations are the same as those of Table 6.1 when QPSK, BPSK0 and BPSK1 are replaced by 64QAM, 8APK0 and 8APK1, respectively.

Another ESM scheme based on two TX antennas and 64QAM as primary modulation is the 2TX9b scheme in which the transmitted signal vector $\mathbf{x}$ takes its values from the signal space given below:

$$\mathbf{x} \in \left\{ \mathscr{S}_{2TX8b}, \begin{Bmatrix} \mathscr{A}_8^2 \\ \mathscr{A}_8^2 \end{Bmatrix}, \begin{Bmatrix} \mathscr{A}_8^3 \\ \mathscr{A}_8^3 \end{Bmatrix} \begin{Bmatrix} \mathscr{A}_8^4 \\ \mathscr{A}_8^4 \end{Bmatrix}, \begin{Bmatrix} \mathscr{A}_8^5 \\ \mathscr{A}_8^5 \end{Bmatrix} \right\}, \tag{6.7}$$

In addition to the signal space of 2TX8b, this one includes 4 other combinations. They correspond to the transmission in parallel of two symbols taking their values from one of 4 other secondary constellations. So, in summary, compared to 2TX8b this design doubles the number of combinations and involves 6 secondary constellations instead of 2. We denote the 4 secondary signal constellations used in this design as 8APK2, 8APK3, 8APK4, and 8APK5, respectively. These signal constellations are shown in Fig. 6.4. A simple inspection indicates that the average transmit signal energy in this scheme is $E_s = 59.5$. The 8 combinations of TX antenna and the constellations transmitted from them are explicitly shown in Table 6.3.

Extension of 2TX8b to 4 TX antennas is straightforward. We simply replace QPSK, BPSK0, and BPSK1 in Table 6.2 by 64QAM, 8APK0, and 8APK1, respectively. The resulting scheme is referred to as 4TX10b, because it transmits 10 bpcu. However, extension of 2TX9b to 4 TX antennas is not straightforward. In 4TX11b, there are 32 combinations of the antennas and constellations requiring 5 bits for combination selection, and each combination transmits 6 bits, leading to a throughput of 11 bpcu. Note that we have 40 combinations if we follow the same extension as in 4TX10b, which is more than what is required. From those, we choose 32 combinations as follows: $C1 - C4$ with 64QAM transmitted from a single antenna, $C5 - C10$ with 8APK0 transmitted from two antennas, $C11 - C16$ with 8APK1,

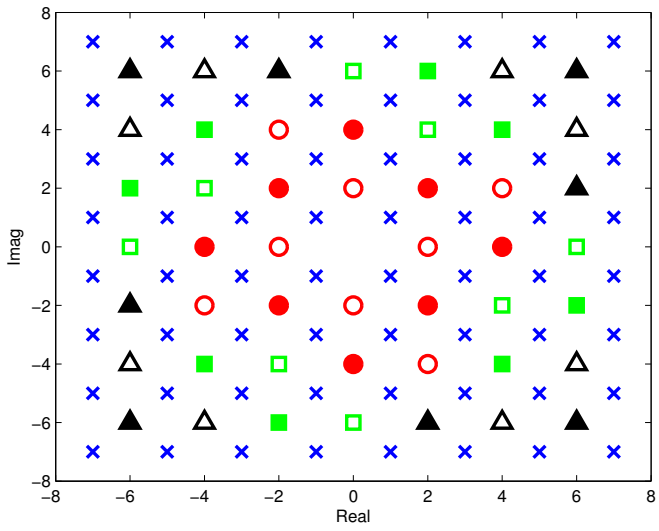

Fig. 6.4 The crosses are 64QAM, the heavy/empty circles are the 8APK0/8APK1, the heavy/empty squares are the 8APK2/8APK3, and the heavy/empty triangles are 8APK4/8APK5 signal constellations.

$C17-C22$ with 8APK2, $C23-C28$ with 8APK3, $C29-C30$ with 8APK4, and $C31-C32$ with 8APK5. Note that the 8APK4 and 8APK5 signal constellations whose average energy is higher than the other signal constellations are only used in two combinations each, whereas the 8APK0-8APK3 constellations are used in 6 combinations each. The purpose of this is to limit the average transmit energy. The resulting average signal energy is 51.75.

6.2.4 Generalizations

In the previous subsections, we described ESM using primary modulations from QPSK to 64QAM, for a number of transmit antennas $N_T = 2$ and $N_T = 4$. Since our reference was conventional SM with a single active antenna ($N_A = 1$), the primary modulation was used for transmission from a single antenna, and the (half-size) secondary modulations were used for simultaneous transmission from two antennas.

First, generalization of the proposed technique to $N_T > 4$ is straightforward. The number of combinations to select one active antenna out of N_T transmit antennas is N_T. For convenience, we consider the number of transmit antennas N_T to be an integer power of 2. In this case, selection of one transmit antenna in conventional SM requires exactly $\log_2(N_T)$ bits. Like conventional SM, ESM features N_T combinations with one active transmit antenna. But ESM also features $\mathbb{C}_2^{N_T} = N_T(N_T-1)/2$ active antenna combinations

Table 6.3 ESM-64QAM with 2 TX antennas and 9 bpcu

	TX1	TX2
C1	64QAM	0
C2	0	64QAM
C3	8APK0	8APK0
C4	8APK1	8APK1
C5	8APK2	8APK2
C6	8APK3	8APK3
C7	8APK4	8APK4
C8	8APK5	8APK5

for transmitting two symbols in parallel from the first secondary modulation. It also involves as many combinations for transmitting two symbols from the other secondary modulation. Therefore, the total number of active antennas and modulation combinations in ESM is $N_T + \mathbb{C}_2^{N_T} + \mathbb{C}_2^{N_T} = N_T^2$. Selection of one combination out of N_T^2 requires $2\log_2(N_T)$ bits. In other words, the number of bits required to select one combination is the double of that in the case of conventional SM. For example, with $N_T = 8$, the number of bits for active antenna selection in conventional SM is 3, and the number of bits for selection of a particular antenna and modulation combination is 6 in ESM.

Generalization to larger numbers of active antennas ($N_A > 1$) is quite simple. Consider a GSM system with N_T transmit antennas, two of which are active ($N_A = 2$). The total number of antenna combinations is $\mathbb{C}_2^{N_T}$, but note that this number is not an integer power of 2. For addressing the active antenna combinations with an integer number of bits, the number of combinations used in GSM is the largest integer power of 2 that is smaller than $\mathbb{C}_2^{N_T}$. In the simplest case, the signal vector space L in the corresponding ESM system is composed of 3 subspaces: $L = L_1 \cup L_2 \cup L_3$. The first one is the signal vector space of GSM, in which the number of combinations is given above ($\text{card}(L_1) = \mathbb{C}_2^{N_T}$). The second subspace L_2 corresponds to the simultaneous transmission of 4 symbols using 4 active antennas and the first secondary modulation. The number of combinations in this subspace is $\mathbb{C}_4^{N_T} = N_T(N_T-1)(N_T-2)(N_T-3)/24$. The third subspace L_3 corresponds to the transmission of 4 symbols using 4 active antennas and the other secondary modulation. The number of combinations in this subspace is the same as the number of combinations in the second subspace. Therefore, the total number of combinations in this ESM scheme

is given by

$$\text{card}(L) = \mathbb{C}_2^{N_T} + \mathbb{C}_4^{N_T} + \mathbb{C}_4^{N_T} \tag{6.8}$$

For $N_T = 8$, $\text{card}(L) = 28(1+5) = 168$. The largest integer power of 2 that is smaller than this number is 128. We therefore include 128 combinations in the signal space, which require 7 bits for selection of a particular combination. The corresponding numbers in GSM are 16 combinations and 4 address bits.

In fact, the signal space can be expanded by realizing that when 4 transmit antennas are simultaneously active, 2 of them can transmit symbols from the first secondary constellation while the other 2 antennas transmit symbols from the other secondary constellation. This expansion does not involve any reduction of the minimum distance. The additional number of combinations corresponding to this signal space expansion is given by

$$\text{card}(L_4) = \mathbb{C}_2^{N_T}\mathbb{C}_2^{N_T-2} \tag{6.9}$$

For $N_T = 8$, $\text{card}(L_4) = 420$, and therefore the addition of this subspace leads to $\text{card}(L) = 588$. The integer power of 2 that is immediately below this number being 512, 512 combinations are included in the signal space and the number of bits needed to select a particular combination is 9. This ESM scheme increases the number of address bits by 5.

Further expansions of the signal space are possible by transmitting from one antenna a symbol taken from the primary constellation and transmitting in parallel two symbols from a secondary constellation. It can be easily verified that those expansions do not reduce the minimum Euclidean distance of the signal space, and therefore, the asymptotic performance at high SNR must be essentially the same.

6.2.5 Performance analysis

When the CSI is perfectly known at the receiver, the ML decoder estimates the transmitted symbol vector according to:

$$\hat{\mathbf{x}} = \arg\min_{\mathbf{x}\in\mathbb{X}} \|\mathbf{y} - \mathbf{H}\mathbf{x}\|^2, \tag{6.10}$$

where $\mathbb{X}$ denotes the constellation of the normalized transmitted symbols, and the minimization is performed over all possible transmitted symbol vectors. We define the PEP as the probability that the ML decoder decodes a symbol vector $\mathbf{x}'$ instead of the transmitted

symbol vector **x**. The average PEP (APEP) can be computed by using the union bound as

$$APEP \leq \frac{1}{|\mathbb{X}|} \sum_{\mathbf{x}\in\mathbb{X}} \sum_{\mathbf{x}'\in\mathbb{X}} PEP(\mathbf{x} \rightarrow \mathbf{x}'). \tag{6.11}$$

For Rayleigh fading channels, the PEP is given by [55]:

$$\begin{aligned} & PEP(\mathbf{x} \rightarrow \mathbf{x}') \\ & = \mathbb{E}_{\mathbf{H}} \left[\mathcal{Q}\left(\sqrt{\frac{E_s \cdot \gamma_{x\rightarrow x'}}{2N_0}} \right) \right] \\ & = \frac{1}{\pi} \int_0^{\frac{\pi}{2}} \mathscr{L}_{\gamma_{s\rightarrow s'}} \left(\frac{E_s}{4N_0 \sin^2(\theta)} \right) d\theta \\ & = \left(\frac{1-\mu}{2} \right)^{N_R} \sum_{k=0}^{N_R-1} \mathbb{C}_k^{N_R-1+k} \left(\frac{1+\mu}{2} \right)^k, \end{aligned} \tag{6.12}$$

where $\mathcal{Q}(\cdot)$ denotes the Gaussian $\mathcal{Q}$-function, $\gamma_{x\rightarrow x'} = \|\mathbf{Hx} - \mathbf{Hx}'\|^2$ represents a random variable with the chi-squared distribution, $\mathscr{L}_{\gamma_{x\rightarrow x'}}$ is the moment-generating function (MGF) of $\gamma_{x\rightarrow x'}$, $\mu = \sqrt{E_s \cdot \tau/(4N_0 + \tau)}$, and $\tau = \|\mathbf{x} - \mathbf{x}'\|^2$. At high SNR, the asymptotic system performance is determined by the worst-case PEP, which corresponds to the minimum value of the squared Euclidean distance between symbol vectors in the signal space:

$$L_{min}^2 = \min_{\mathbf{x}\neq\mathbf{x}'} \|\mathbf{x} - \mathbf{x}'\|^2 \tag{6.13}$$

To analyze asymptotic performance (at high SNR), it is instructive to compare the different MIMO schemes at hand (SMX, SM, and ESM) in terms of the squared minimum Euclidean distance between transmit symbol vectors divided by their required transmit energy, denoted as $\frac{L_{min}^2}{E_s}$. The comparisons were made at identical spectral efficiency and the results are represented in Table 6.4. The first part of the table corresponds to MIMO schemes with 2 TX antennas, and the second part corresponds to schemes with 4 TX antennas. Different columns correspond to different spectral efficiencies. Labeling of the MIMO schemes in this table is based on the number of TX antennas and the number of bits per channel use. For instance, 4TX8b means 4 TX antennas and 8 bpcu.

The normalized squared minimum Euclidean distances which appear in this table are given in the form of a fraction or using a decimal representation. The reason is that some of the considered schemes use the 8PSK signal constellation, and the distance is best expressed using decimal representation in this case. In contrast, fractional number

Table 6.4 The normalized minimum squared Euclidean distance, $\frac{L_{min}^2}{E_s}$

	2TX4b	**2TX6b**	**2TX8b**	**2TX9b**
SM	0.5858	4/20	4/82	4/170
SMX	4/4	0.2929	4/20	4/30
ESM	2/2	0.3636	4/33	4/59.5
QSM	2/2	2/10	2/42	2/82
	4TX6b	**4TX8b**	**4TX10b**	**4TX11b**
SM	4/10	4/42	4/170	4/330
SMX(2TX)	0.2929	4/20	4/40	4/62
ESM	2/2	4/11.5	4/28.5	4/51.75
QSM	2/2	2/10	2/42	2/82

representation of the distances is more convenient for the schemes based on QAM signal constellations, and this holds for most cases which appear in the table. In all schemes using QAM signal constellations, the comparison in terms of squared minimum distances is rather straightforward. For example, the average transmit signal vector energy in the 2TX8b case are 82 for SM, 20 for SMX, 33 for ESM, and 42 for Quadrature SM (QSM)[56], respectively (when the minimum distance is set to 2 in all of the signal constellations). Therefore, the normalized squared minimum Euclidean distances are 4/82, 4/20, 4/33, and 2/42, respectively, when the transmitted average signal energy is normalized by 1. These values appear in the 2TX8b column of the table. Note that SMX is restricted to two active antennas, because our assumption is that the number of RF chains is limited to 2 as in the proposed ESM schemes. The conventional SM schemes considered here actually involve a single RF chain, because the number of active antennas is 1. As for QSM, the number of active antennas is 2 as in ESM, but the authors of [56] claim that this technique can be implemented using a single RF chain. Comparing the distances displayed in Table 6.4, we can see that ESM has a significantly larger L_{min}^2 than SM in all cases. It also has a larger L_{min}^2 than QSM except in the trivial case where ESM uses QPSK as primary modulation (the 2TX4b and 2TX6b cases in the table). Finally, ESM provides a larger L_{min}^2 than SMX in the 4-TX cases due to restricting the system to 2 RF chains. These results indicate that ESM reduces the worst-case PEP compared to SM, SMX, and QSM and leads to the best system performance in most cases.

In terms of worst-case PEP, the gain of a scheme with a normalized squared minimum distance of $\frac{L_{min}^2}{E_s}$ over a scheme with a squared minimum distance of $\frac{\bar{L}_{min}^2}{\bar{E}_s}$ is given by:

$$\mathscr{G} = 10\log_{10}\left(\frac{L_{min}^2}{\bar{L}_{min}^2} \times \frac{\bar{E}_s}{E_s}\right) \tag{6.14}$$

For example, the expected gain of ESM over conventional SM in the case of 2TX4b is given by:

$$\mathscr{G}_{SM,ESM} = 10\log_{10}(1/0.5858) = 2.32 \text{ dB}$$

Note that with QPSK as primary modulation, bit mapping is important in ESM, because the squared minimum distance in the signal space arises between symbol vectors that belong to different combinations, e.g., between C1 and C3 in Table 6.1 and between C1 and C5 in Table 6.2, and this distance is smaller than the minimum distance of QPSK. In this case, separately labeling the signal constellations and the active antennas patterns is not optimum for ESM. However, this is an isolated case, and the Euclidean distance is preserved with higher level modulations, e.g., with 16QAM as primary modulation and QPSK0/QPSK1 as secondary modulations.

6.2.6 Receiver complexity analysis

In this section, we show that in addition to improving performance over conventional SM, the proposed ESM also reduces the complexity of the ML decoder. Reduction of the receiver complexity will be demonstrated by explicitly evaluating the respective complexities of SM and ESM in the 4TX8b case before summarizing the complexity figures of the two transmission schemes for different spectral efficiencies. In this analysis, we define complexity as the number of complex multiplications required per ML decoder decision

For 4TX8b SM, the ML decoder needs to compute $\mathbf{w}_{ij} = \mathbf{y} - \mathbf{h}_i s_j$, where $\mathbf{h}_i$ with $i = 1,2,\cdots,4$ denotes the i-th column of the channel matrix $\mathbf{H}$, and s_j with $j = 1,2,\cdots,64$ denotes a 64QAM symbol. This step involves 256 complex multiplications. Next, it needs to compute the squared modulus of each one of the $\mathbf{w}_{ij}$ terms, and this step involves another 256 complex multiplications. In other words, the total number of complex multiplications in this scheme is 512 per channel use.

In the case of 4TX8b ESM, we need to consider separately 3 groups of antenna and constellation combinations. First, in combinations C1 - C4, a 16QAM symbol is transmitted from one of the 4 TX antennas. For those combinations, the ML decoder needs to com-

Table 6.5 Receiver Complexity ($N_R = 1$)

	2TX4b	**2TX6b**	**2TX8b**	**2TX9b**
SM	32	128	512	1024
ESM	32	112	416	836
	4TX6b	**4TX8b**	**4TX10b**	**4TX11b**
SM	128	512	2048	4096
ESM	96	352	1344	2912

pute $\mathbf{w}_{ij} = \mathbf{y} - \mathbf{h}_i s_j$, with $i = 1,2,3,4$ and $j = 1,2,\cdots,16$, and this involves 64 complex multiplications. Next, in combinations C5 - C10, two QPSK0 symbols are transmitted from two active antennas. For those combinations, the ML decoder needs to compute $\mathbf{w}_{ijkl} = \mathbf{y} - \mathbf{h}_i s_j^0 - \mathbf{h}_k s_l^0$, with $i,k = 1,2,3,4$ and where s_j^0 and s_l^0 $(j,l = 1,2,3,4)$ denote two symbols taken from the Q_4^0 signal constellation. The number of complex multiplications involved in this step is only 16. Finally, in combinations C11 - C16, two QPSK1 symbols are transmitted from two active antennas. For those combinations, the ML decoder needs to compute $\mathbf{w}_{ijkl} = \mathbf{y} - \mathbf{h}_i s_j^1 - \mathbf{h}_k s_l^1$, with $i,k = 1,2,3,4$ and where s_j^1 and s_l^1 $(j,l = 1,2,3,4)$ denote two symbols taken from the Q_4^1 signal constellation. Here, the number of complex multiplications is also 16. So, the total number of complex multiplications involved in the steps above is 96, although the number of $\mathbf{w}_{ij}$ and $\mathbf{w}_{ijkl}$ values computed is 256 (64 values corresponding to combinations C1 - C4, 96 values corresponding to combinations C5 - C10, and 96 values corresponding to combinations C11 - C16). Next, the decoder needs to compute the squared modulus of all $\mathbf{w}_{ij}$ and $\mathbf{w}_{ijkl}$ values to determine the 256 metrics involved. So, the total number of complex multiplications per decoding step in the ML decoder is 352, which is significantly smaller than the corresponding number in SM. In this particular case, the decoder complexity reduction with respect to conventional SM is 31.2%.

The complexity analysis reported above for the 4TX8b case was also made for all SM and ESM schemes and the results are reported in Table 6.5. The results indicate that ESM significantly reduces the ML decoder complexity compared to conventional SM, particularly in the case of 4 TX antennas. Note that in the 4TX10b case, the ML decoder complexity of ESM is 34.4% smaller than that of conventional SM.

6.3 ESM with two active antennas

In this section, the ESM concept was modified by restricting two active antennas to transmit simultaneously, which will provide an increased spectral efficiency. Before describing our proposed ESM schemes, we first briefly describe the baseline multistream SM (MSM) scheme [57], which will be used as basis for comparisons.

MSM with 4 TX antennas ($N_T = 4$) out of which two are active and transmitting 16QAM symbols can be described using the following signal space representation:

$$\text{MSM: } \mathbf{x} \in \left\{ \begin{bmatrix} P_{16} \\ P_{16} \\ 0 \\ 0 \end{bmatrix}, \begin{bmatrix} 0 \\ 0 \\ P_{16} \\ P_{16} \end{bmatrix}, \begin{bmatrix} P_{16} \\ 0 \\ P_{16} \\ 0 \end{bmatrix}, \begin{bmatrix} 0 \\ P_{16} \\ 0 \\ P_{16} \end{bmatrix} \right\}, \tag{6.15}$$

where the entry P_{16} denotes the 16QAM signal constellation and the zero entries correspond to the silent TX elements. In this example, MSM achieves a throughput of 10 bits channel per use (*bpcu*): Indeed, 2 information bits are assigned to select one of four combinations of the active TX antennas and 8 bits select two particular symbols from the signal constellation P_{16} to be transmitted from those antennas. The total energy per transmitted symbol vector in this example is $E_{msm} = 20$, because the energy corresponding to the transmission of each 16QAM symbol is 10.

6.3.1 ESM-Type1

For the same spectral efficiency as the MSM scheme described above, the transmitted symbol vectors in ESM-Type1 are given by:

$$\text{ESM-Type1: } \mathbf{x} \in \left\{ \begin{bmatrix} P_{16} \\ S_8 \\ 0 \\ 0 \end{bmatrix}, \begin{bmatrix} P_{16} \\ 0 \\ 0 \\ S_8 \end{bmatrix}, \begin{bmatrix} 0 \\ P_{16} \\ S_8 \\ 0 \end{bmatrix}, \begin{bmatrix} 0 \\ 0 \\ P_{16} \\ S_8 \end{bmatrix}, \begin{bmatrix} S_8 \\ P_{16} \\ 0 \\ 0 \end{bmatrix}, \begin{bmatrix} S_8 \\ 0 \\ 0 \\ P_{16} \end{bmatrix}, \begin{bmatrix} 0 \\ S_8 \\ P_{16} \\ 0 \end{bmatrix}, \begin{bmatrix} 0 \\ 0 \\ S_8 \\ P_{16} \end{bmatrix} \right\}, \tag{6.16}$$

In this case, we have a total of 8 antenna and constellation combinations: As in MSM, there are 4 active antenna combinations, but while one of the active antennas transmits a symbol from the primary 16QAM constellation, the other antenna transmits a symbol from a secondary constellation referred to as S_8. Both of these signal constellations are

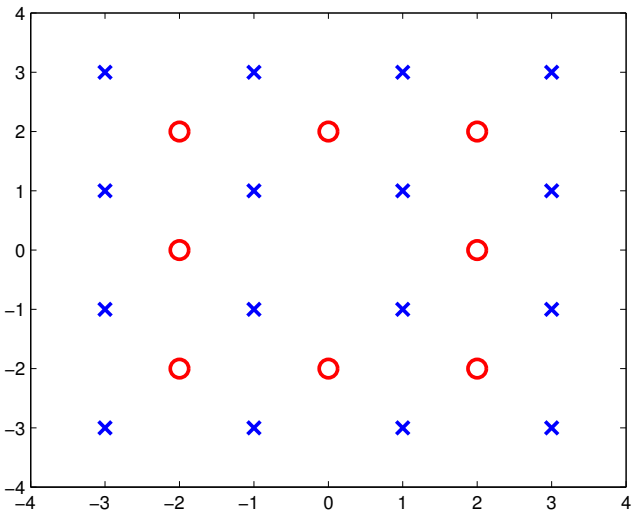

Fig. 6.5 The constellations used in ESM-Type1: The blue crosses represent 16QAM, and the red circles represent constellation S_8.

shown in Fig. 6.5, and the antenna/modulation combinations are shown in Table 6.6. The secondary signal constellation S_8 has the following mathematical representation:

$$S_8 = \{\pm 2 \pm 2i, \pm 2, \pm 2i\}.$$

Similar to MSM, this design achieves 10 bpcu despite the fact that one of the antennas transmits symbols from a reduced-size signal constellation. Indeed, the two symbols transmitted in parallel from the two active TX antennas convey 7 bpcu only, but the number of antenna constellation combinations (pairs of indexes along with the assigned signal constellations) is 8, and therefore 3 bits must be assigned to select one of these combinations.

A simple inspection indicates that the energy per symbol for the S_8 constellation is $E_{S8} = 6$ and since the average energy per 16QAM symbol is $E_{16QAM} = 10$, the total energy per transmitted symbol vector in this scheme is

$$E_{ESM-Type1} = 16.$$

This means that in terms of total transmit energy, ESM-Type1 saves 20% (approx. 1 dB) compared to MSM. The final remark to make at this point is that the S_8 constellation in the proposed scheme is designed in such a way as not to reduce minimum Euclidean

Table 6.6 The antenna/modulation combinations used in ESM-Type1

	Tx1	Tx2	Tx3	Tx4
C1	16QAM	S_8	0	0
C2	16QAM	0	0	S_8
C3	0	16QAM	S_8	0
C4	0	0	16QAM	S_8
C5	S_8	16QAM	0	0
C6	S_8	0	0	16QAM
C7	0	S_8	16QAM	0
C8	0	0	S_8	16QAM

distance between transmitted symbol vectors compared to MSM, as can be easily verified by making a simple exhaustive search.

6.3.2 ESM-Type2

By using a primary constellation and a reduced-size secondary constellation, ESM-Type1 reduced the total transmit energy to some extent. This idea can be further extended using more than two constellations. We will now describe an ESM scheme that is based on first discarding the corner points of the 16QAM signal constellation and then partitioning the resulting 12-point constellation into two subsets, one with 8 points denoted P_8 and another one with 4 points denoted Q_4. This scheme will be referred to as ESM-Type2. The constellations used in this ESM scheme are depicted in Fig. 6.6. Mathematically, the P_8 and Q_4 constellations can be represented as follows:

$$P_8 = \{\pm 1 \pm i, 3+i, 1-3i, -3-i, -1+3i\}$$
$$Q_4 = \{1+3i, 3-i, -1-3i, -3+i\}.$$

A simple inspection reveals that the average energy is 6 for the P_8 constellation and 10 for the Q_4 constellation. Clearly, constellation P_8 must be used more frequently than constellation Q_4 in order to reduce average transmitted energy. The design procedure is described in the following. The transmitted symbol vectors belong to a symbol space L,

which can be written as:

$$\text{ESM-Type2: } \mathbf{x} \in L = \{L_1, L_2, L_3, L_4\}, \tag{6.17}$$

where each $L_{j\in\{1,2,3,4\}}$ subspace is defined by a set of active antenna combinations and associated signal constellations. The first three subspaces are defined as:

$$L_1 = \left\{ \begin{bmatrix} P_8 \\ S_8 \\ 0 \\ 0 \end{bmatrix}, \begin{bmatrix} S_8 \\ P_8 \\ 0 \\ 0 \end{bmatrix}, \begin{bmatrix} 0 \\ 0 \\ P_8 \\ S_8 \end{bmatrix}, \begin{bmatrix} 0 \\ 0 \\ S_8 \\ P_8 \end{bmatrix} \right\}, L_2 = \left\{ \begin{bmatrix} P_8 \\ 0 \\ S_8 \\ 0 \end{bmatrix}, \begin{bmatrix} S_8 \\ 0 \\ P_8 \\ 0 \end{bmatrix}, \begin{bmatrix} 0 \\ P_8 \\ 0 \\ S_8 \end{bmatrix}, \begin{bmatrix} 0 \\ S_8 \\ 0 \\ P_8 \end{bmatrix} \right\}, L_3 = \left\{ \begin{bmatrix} P_8 \\ 0 \\ 0 \\ S_8 \end{bmatrix}, \begin{bmatrix} S_8 \\ 0 \\ 0 \\ P_8 \end{bmatrix}, \begin{bmatrix} 0 \\ P_8 \\ S_8 \\ 0 \end{bmatrix}, \begin{bmatrix} 0 \\ S_8 \\ P_8 \\ 0 \end{bmatrix} \right\}$$

Different subspaces use different antenna combinations, but in all of these three subspaces one active antenna transmits symbols from the P_8 signal constellation, and the other active antenna transmits symbols from the S_8 constellation. Note that 6 information bits are conveyed by the transmitted symbols, and 2 information bits are used to select one antenna combination in each subspace. Also, 2 prefix bits select a particular L_j subspace, and hence the total number of bits per channel use is 10.

The fourth signal subspace L_4 is given by:

$$L_4 = \left\{ \begin{bmatrix} Q_4 \\ S_8 \\ 0 \\ 0 \end{bmatrix}, \begin{bmatrix} S_8 \\ Q_4 \\ 0 \\ 0 \end{bmatrix}, \begin{bmatrix} 0 \\ 0 \\ Q_4 \\ S_8 \end{bmatrix}, \begin{bmatrix} 0 \\ 0 \\ S_8 \\ Q_4 \end{bmatrix}, \begin{bmatrix} Q_4 \\ 0 \\ S_8 \\ 0 \end{bmatrix}, \begin{bmatrix} S_8 \\ 0 \\ Q_4 \\ 0 \end{bmatrix}, \begin{bmatrix} 0 \\ Q_4 \\ 0 \\ S_8 \end{bmatrix}, \begin{bmatrix} 0 \\ S_8 \\ 0 \\ Q_4 \end{bmatrix} \right\} \tag{6.18}$$

In this subspace, one of the active antennas transmits a symbol from the S_8 constellation, while the other antenna transmits a symbol from the Q_4 signal constellation. The two symbols convey 5 information bits, but here we need 3 information bits to select one antenna combination out of 8, and together with the 2 prefix bits assigned to the L_4 subspace the number of bits per channel use is 10 as in the other cases.

In subspaces L_1, L_2, and L_3, the average transmitted energy is 12, because both of the constellations used have an average energy of 6. In contrast, the average transmitted energy is 16 in L_4, because constellation Q_4 has an average energy of 10. Therefore, the average total energy per transmitted symbol vector is given by:

$$E_{ESM-Type2} = \frac{3}{4} \times 12 + \frac{1}{4} \times 16 = 13.$$

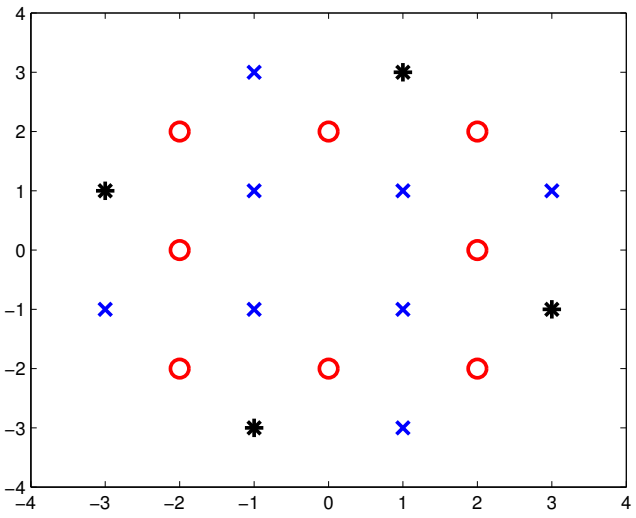

Fig. 6.6 The constellations used in ESM-Type2: The blue crosses represent P_8, the red circles represent S_8, and the black stars represent Q_4.

This indicates that ESM-Type2 saves approximately 35% in terms of total energy transmitted (13 instead of 20), which reads approximately 1.9 dB gain in the decibel scale.

6.3.3 ESM-Type3

By using a primary constellation and a reduced-size secondary constellation, the ESM scheme described above reduced the total transmit energy to some extent. This idea can be extended to using more than two constellations in the design and defining the constellations through two interpolation steps instead of one. The design is based on the ESM-Type2 signal constellations shown in Fig. 6.6 and two additional 8-point constellations T_8 and F_8 that are obtained through a second geometric interpolation step between the points of the ESM-Type2 constellations. The T_8 and F_8 constellations are defined as $T_8 = \{T_c \cup T_4 \cup T_2\}$ and $F_8 = \{F_c \cup F_4 \cup F_2\}$ using the six constellations shown in Fig. 6.7 and mathematically defined as follows:

$$T_c = \{\pm i\},\ T_4 = \{\pm 2 \pm i\},\ T_2 = \{\pm 3i\}$$
$$F_c = \{\pm 1\},\ F_4 = \{\pm 1 \pm 2i\},\ F_2 = \{\pm 3\}.$$

Note that the minimum Euclidean distance between the points of anyone of these four constellations (P_8, S_8, T_8, F_8) is $\delta_0 = 2$. Next, the minimum distance between the P_8 and

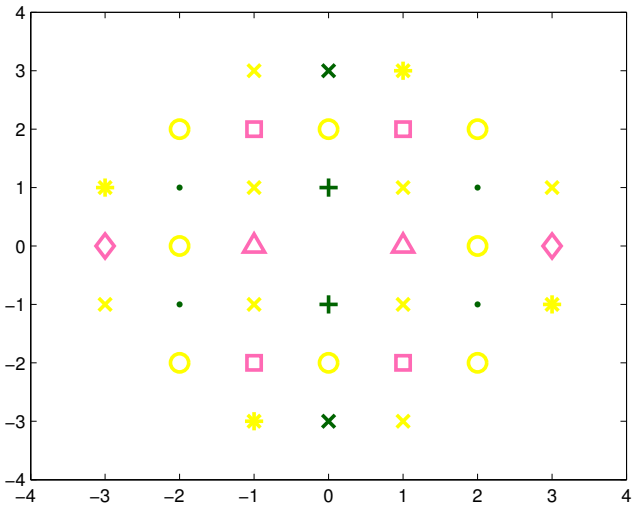

Fig. 6.7 The constellations used in ESM-Type3: The yellow constellations are those used in ESM-Type2, the green pluses represent Tc, the pink triangles represent F_c, the green points represent T_4, the pink squares represent F_4, the green crosses represent T_2, and the pink diamonds denote F_2.

S_8 constellations (resp. the T_8 and F_8 constellations) is $(\delta_0/\sqrt{2})$. This can be easily seen by checking Figs. 6.6 and 6.7. Finally, the minimum distance between a point taken from $P_8 \cup S_8$ and a point taken from $T_8 \cup F_8$ is $(\delta_0/2)$. Since the number of active antennas is limited to 2, a particular care must be exercised to preserve a minimum distance of $\delta_0 = 2$ in the signal space.

More specifically, the use of different constellations cannot be made independently from a channel use to the next. Instead, the antenna and constellation combinations must be jointly defined over a block of two consecutive channel uses. The minimum distance can be preserved in the following two cases: In the first case, the P_8 and S_8 constellations (resp. the T_8 and F_8 constellations) are employed during both channel uses. In the second case, the P_8 and S_8 constellations are used during the first channel use, and the T_8 and F_8 constellations are used during the second channel use, or vice versa. In this work, we take the second approach, because the number of bits transmitted per block is not constant in the first.

For presenting our ESM-Type3 scheme, we first extend the system model by stacking two consecutive received signal vectors. Assuming slow-fading channels essentially constant over two consecutive channel uses, then the transmitted and received signals are related

by the following equation:

$$\mathbf{Y} = \mathbf{H}\mathbf{X} + \mathbf{N}, \tag{6.19}$$

where $\mathbf{Y} = [\mathbf{y}_1, \mathbf{y}_2]$ denotes the $N_R \times 2$ received signal matrix, $\mathbf{X} = [\mathbf{x}_1, \mathbf{x}_2]$ is the $N_T \times 2$ transmitted matrix, $\mathbf{N}$ is the $N_R \times 2$ AWGN matrix, and the subscript $k \in \{1,2\}$ denotes the time index of the symbol vector.

For ESM-Type3, the transmitted symbol matrix $\mathbf{X}$ belongs to the following signal subsets:

$$\text{ESM-Type3: } \mathbf{X} \in \{\mathbb{S}_1, \mathbb{S}_2\}, \tag{6.20}$$

where

$$\begin{aligned} \mathbb{S}_1 &= \{\mathbf{x}_1 \in \mathbb{S}_{PS}, \mathbf{x}_2 \in \mathbb{S}_{TF}\} \\ \mathbb{S}_2 &= \{\mathbf{x}_1 \in \mathbb{S}_{TF}, \mathbf{x}_2 \in \mathbb{S}_{PS}\}. \end{aligned} \tag{6.21}$$

In this representation, $\mathbb{S}_{PS}$ denotes the set of symbol vectors based on the primary and the secondary constellations, and $\mathbb{S}_{TF}$ denotes the set of symbol vectors based on the third and the fourth constellations. The transmitted symbol vector takes its values from the set $\mathbb{S}_{PS}$ during the first channel use in the block and from the set $\mathbb{S}_{TF}$ during the second channel use, or vice versa. From the 20 bits per $N_T \times 2$ symbol matrix, 1 bit selects subset $\mathbb{S}_1$ or subset $\mathbb{S}_2$. Next, 10 bits select a vector from $\mathbb{S}_{PS}$ and 9 bits select a vector from $\mathbb{S}_{TF}$, and these two vectors are transmitted in the order determined by the first bit.

The details of the proposed design process are presented as follows. First, the set of symbol vectors $\mathbb{S}_{PS}$ is actually the signal space of ESM-Type2 described in the previous section. A signal vector is therefore of the form:

$$\mathbb{S}_{PS} : \mathbf{x} \in \{L_1, L_2, L_3, L_4\}, \tag{6.22}$$

where the subsets $L_1 - L_4$ are given by eqn. (6.18). As shown in the previous section, this scheme transmits 10 bits per channel use, and the average total energy per transmitted symbol vector is $E_s = 13$. Next, the set of symbol vectors $\mathbb{S}_{TF}$ is based on the third and the fourth constellations T_8 and F_8, but symbol vectors in $\mathbb{S}_{TF}$ only transmit 9 bpcu instead of the 10 bpcu transmitted in the case of $\mathbb{S}_{PS}$. The set $\mathbb{S}_{TF}$ is constructed by the union L' of four subsets as:

$$\mathbb{S}_{TF} : \mathbf{x} \in L' = \{L'_1, L'_2, L'_3, L'_4\}, \tag{6.23}$$

where each set is corresponding to different antenna combinations and associated signal constellations. The first subset is defined as:

$$L_1' = \left\{ \begin{bmatrix} T_8 \\ F_8 \\ 0 \\ 0 \end{bmatrix}, \begin{bmatrix} F_8 \\ T_8 \\ 0 \\ 0 \end{bmatrix}, \begin{bmatrix} 0 \\ 0 \\ T_8 \\ F_8 \end{bmatrix}, \begin{bmatrix} 0 \\ 0 \\ F_8 \\ T_8 \end{bmatrix} \right\} \tag{6.24}$$
$$\triangleq \{L_1 | P_8 \rightarrow T_8, S_8 \rightarrow F_8\}.$$

Subset L_1' has the same antenna combinations as L_1 shown in eq. (6.18), but instead of P_8 and S_8, it uses the T_8 and F_8 constellations. The L_1' subset can transmit 8 bits: 2 bits select one of the four combinations of active TX antennas and associated constellations, 3 bits select a symbol from the T_8 constellation, and 3 bits select a symbol from the F_8 constellation. The other three subsets $L_2' - L_4'$ are defined as follows:

$$\begin{aligned} L_2' &= \{L_4 | P_4 \rightarrow T_4, S_8 \rightarrow F_4\}, \\ L_3' &= \{L_4 | P_4 \rightarrow T_4, S_8 \rightarrow F_2\} \\ L_4' &= \{L_4 | P_4 \rightarrow T_2, S_8 \rightarrow F_4\} \end{aligned} \tag{6.25}$$

This representation indicates that the combinations of active antennas in subset L_2' are the same as those in L_4 shown in eq. (6.18), but here constellation P_4 is replaced by constellation T_4 and constellation S_8 is replaced by constellation F_4. Similarly, subset L_3' is obtained from L_4 by substituting constellation T_4 for P_4 and substituting F_2 for S_8. Finally, subset L_4' is obtained from L_4' by substituting constellation T_2 for P_4 and constellation F_4 for S_8.

The signal subset L_2' transmits 7 bits per symbol vector: 3 bits are needed to select one of the 8 combinations, 2 bits to select a symbol from T_4, and 2 bits to select a symbol from F_4. Next, since the L_3' subset is derived from L_2' by substituting F_2 for F_4, it transmits 6 bits per symbol vector. Again, 3 bits select one of the 8 combinations, and then 1 bit selects a symbol from F_2, and 2 bits select a symbol from T_4. Similarly, since the L_4' subset is derived from L_2' by substituting T_2 for T_4, it also transmits 6 bits per symbol vector. Here, 3 bits select one of the 8 combinations, 1 bit selects a symbol from T_2, and 2 bits select a symbol from F_4.

The discussion above indicates that the number of bits transmitted per symbol vector is not uniform across the $L_1' - L_4'$ subsets. The implication of this is that the prefix of these subsets in $\mathbb{S}_{TF}$ must have a variable number of bits. Subset L_1' must have a 1-bit prefix,

subset L_2' must have a 2-bit prefix, and subsets L_3' and L_4' must have a 3-bit prefix. With these variable-length prefixes, it can be seen that all symbol vectors in $\mathbb{S}_{TF}$ carry 9 bits.

At this point, it is important to clarify the difference between the construction of the L_1' subset and that of the $L_2' - L_4'$ subsets included in $\mathbb{S}_{TF}$. Notice that the innermost points of the T_8 and F_8 constellations, namely T_c and F_c, are only used in the first subset L_1'. These points cannot be used in L_2', because otherwise the minimum Euclidean distance in the signal space would be $\delta_0/\sqrt{2}$, which is 3 dB smaller than the minimum Euclidean distance in $\mathbb{S}_{PS}$. This is the case, for instance, between the symbol vectors $[1,i,0,0] \in L_1'$ and $[1,0,i,0] \in L_2'$. Similarly, the innermost points are not allowed in the subsets L_3' and L_4' in order to preserve the minimum Euclidean distance. As a result, the signal vectors in $\mathbb{S}_{TF}$ carry only 9 bits, while the signal vectors in $\mathbb{S}_{PS}$ carry 10 bits. The average total energy per transmitted symbol vector from $\mathbb{S}_{TF}$ is $E_s = 11$.

Since the signal vector sets in $\mathbb{S}_{PS}$ and $\mathbb{S}_{TF}$ are used with the same probability, the average energy of the transmitted signal vectors in ESM-Type3 is

$$E_{ESM-Type3} = \frac{1}{2}(13+11) = 12$$

This represents a 2.2 dB SNR gain over MSM, and a 0.4 dB gain over the ESM-Type2.

6.3.4 ESM with 64QAM as primary modulation

In order to achieve higher throughputs, we now describe ESM schemes that are equivalent to MSM with 64QAM in terms of spectral efficiency. In all of them, the number of transmit antennas is 4, two of which are active, and the spectral efficiency is 14 bpcu. The design process is similar to that in the previous subsections, but here we have more degrees of freedom due to the fact that the primary modulation has a larger number of constellation points. As previously, we will describe here three ESM schemes, starting with the description of the baseline MSM with 64QAM, which we use as reference.

For MSM with 4 TX antennas ($N_T = 4$) and 14 bpcu, the transmitted symbol vector can be written as:

$$\text{MSM: } \mathbf{x} \in \left\{ \begin{bmatrix} P_{64} \\ P_{64} \\ 0 \\ 0 \end{bmatrix}, \begin{bmatrix} 0 \\ 0 \\ P_{64} \\ P_{64} \end{bmatrix}, \begin{bmatrix} P_{64} \\ 0 \\ P_{64} \\ 0 \end{bmatrix}, \begin{bmatrix} 0 \\ P_{64} \\ 0 \\ P_{64} \end{bmatrix} \right\}, \tag{6.26}$$

where P_{64} denotes the 64QAM symbols. The number of antenna combinations being four, 2 bits must be assigned for selection of a particular combination. Next, the transmitted 64QAM symbols convey 12 information bits, and therefore the spectral efficiency is 14 bpcu. The total average energy per transmitted symbol vector in this scheme is $E_{MSM} = 84$, because each 64QAM symbol has an average energy of 42.

ESM-Type1 with 14 bpcu

In this scheme, the transmitted symbol vectors can be represented as:

$$\text{ESM-Type1: } \mathbf{x} \in \left\{ \begin{bmatrix} P_{64} \\ S_{32} \\ 0 \\ 0 \end{bmatrix}, \begin{bmatrix} P_{64} \\ 0 \\ 0 \\ S_{32} \end{bmatrix}, \begin{bmatrix} 0 \\ P_{64} \\ S_{32} \\ 0 \end{bmatrix}, \begin{bmatrix} 0 \\ 0 \\ P_{64} \\ S_{32} \end{bmatrix}, \begin{bmatrix} S_{32} \\ P_{64} \\ 0 \\ 0 \end{bmatrix}, \begin{bmatrix} S_{32} \\ 0 \\ 0 \\ P_{64} \end{bmatrix}, \begin{bmatrix} 0 \\ S_{32} \\ P_{64} \\ 0 \end{bmatrix}, \begin{bmatrix} 0 \\ 0 \\ S_{32} \\ P_{64} \end{bmatrix} \right\}, \tag{6.27}$$

The symbol transmitted from the antenna with index m takes its values from 64QAM which is the primary modulation, and the symbol transmitted from the antenna with index $n \neq m$ takes its values from the secondary modulation that is denoted by S_{32}. These signal constellations are shown in Fig. 6.8, where the entries of the secondary modulation are given by:

$$S_{32} = \left\{ \begin{array}{c} S_8, \pm 4, \pm 4i, \pm 6, \pm 6i \\ \pm 4 \pm 2i, \pm 4 \pm 4i, \pm 2 \pm 4i \\ 2+6i, 6-2i, -6+2i, -2-6i \end{array} \right\}.$$

The S_{32} constellation is obtained through geometric interpolation between the points of the primary constellation with the constraint of transmitting minimum energy.

In this ESM scheme, the transmitted symbol pair conveys 11 bits only (because the S_{32} symbols carry 5 bits), but the number of combinations is 8 and so 3 bits must be assigned to selection of a particular combination. Therefore, the spectral efficiency is 14 bpcu as in the baseline MSM. As for the total energy per transmitted symbol vector, it is given by:

$$E_{ESM-Type1} = 64,$$

because the transmitted symbol vector includes one 64QAM symbol with ($E_{64QAM} = 42$) and one S_{32} symbol ($E_{S32} = 22$). Consequently, ESM-Type1 reduces the transmitted

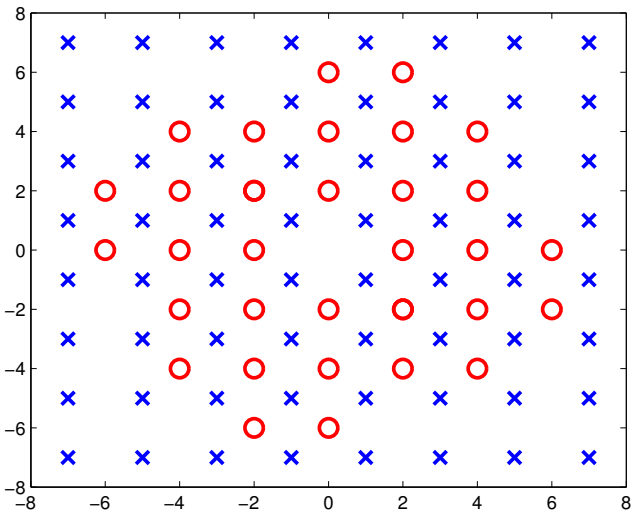

Fig. 6.8 The constellations used in ESM-Type1 with 14 bpcu: The blue crosses represent 64QAM, and the red circles represent S_{32}.

average energy by approximately 24% compared to MSM. In the decibel scale, this gives a gain of 1.2 dB.

ESM-Type2 with 14 bpcu

In this scheme, the transmitted symbol vectors are defined by the following set:

$$\text{ESM-Type2: } \mathbf{x} \in \left\{ L_1, L_2, L_3, L_4, L_5, L_6, L_7, L_8 \right\}, \tag{6.28}$$

where the signal subspaces L_1 to L_6 are defined as:

$$L_1 = \left\{ \begin{bmatrix} P_{32} \\ S_{32} \\ 0 \\ 0 \end{bmatrix}, \begin{bmatrix} S_{32} \\ P_{32} \\ 0 \\ 0 \end{bmatrix} \right\}, L_2 = \left\{ \begin{bmatrix} P_{32} \\ 0 \\ S_{32} \\ 0 \end{bmatrix}, \begin{bmatrix} S_{32} \\ 0 \\ P_{32} \\ 0 \end{bmatrix} \right\}, L_3 = \left\{ \begin{bmatrix} P_{32} \\ 0 \\ 0 \\ S_{32} \end{bmatrix}, \begin{bmatrix} S_{32} \\ 0 \\ 0 \\ P_{32} \end{bmatrix} \right\}, \tag{6.29}$$

$$L_4 = \left\{ \begin{bmatrix} 0 \\ P_{32} \\ S_{32} \\ 0 \end{bmatrix}, \begin{bmatrix} 0 \\ S_{32} \\ P_{32} \\ 0 \end{bmatrix} \right\}, L_5 = \left\{ \begin{bmatrix} 0 \\ P_{32} \\ 0 \\ S_{32} \end{bmatrix}, \begin{bmatrix} 0 \\ S_{32} \\ 0 \\ P_{32} \end{bmatrix} \right\}, L_6 = \left\{ \begin{bmatrix} 0 \\ 0 \\ P_{32} \\ S_{32} \end{bmatrix}, \begin{bmatrix} 0 \\ 0 \\ S_{32} \\ P_{32} \end{bmatrix} \right\}.$$

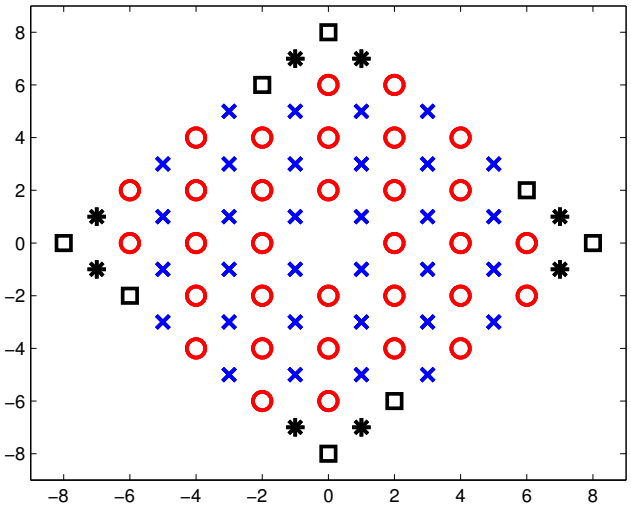

Fig. 6.9 The constellations used in ESM-Type2 with 14 bpcu: The blue crosses represent 32QAM, the red circles represent S_{32}, the black stars represent R_8, and the black squares represent Q_8.

Different L_j subspaces correspond to different combinations of active antennas, and in all cases one of the transmitted symbols takes its values from the 32QAM signal constellation while the other symbol takes its values from the S_{32} constellation illustrated in Fig. 6.9. The other two signal subspaces (L_7 and L_8) are given by:

$$L_7 = \left\{ \begin{bmatrix} P_{32} \\ Q_8 \\ 0 \\ 0 \end{bmatrix}, \begin{bmatrix} Q_8 \\ P_{32} \\ 0 \\ 0 \end{bmatrix}, \begin{bmatrix} 0 \\ 0 \\ P_{32} \\ Q_8 \end{bmatrix}, \begin{bmatrix} 0 \\ 0 \\ Q_8 \\ P_{32} \end{bmatrix}, \begin{bmatrix} P_{32} \\ 0 \\ Q_8 \\ 0 \end{bmatrix}, \begin{bmatrix} Q_8 \\ 0 \\ P_{32} \\ 0 \end{bmatrix}, \begin{bmatrix} 0 \\ P_{32} \\ 0 \\ Q_8 \end{bmatrix}, \begin{bmatrix} 0 \\ Q_8 \\ 0 \\ P_{32} \end{bmatrix} \right\}, \tag{6.30}$$

$$L_8 = \{L_7 | P_{32} \rightarrow P_{32}, Q_8 \rightarrow R_8\}.$$

In subspace L_7, one of the transmitted symbols takes its values from 32QAM and the other takes its values from the Q_8 constellation, also illustrated in Fig. 6.9. Finally, In subspace L_8, one of the transmitted symbols takes its values from the S_{32} constellation, and the other takes its values from R_8 constellation (again, see Fig. 6.9). The Q_8 and R_8 constellations can be mathematically written as:

$$Q_8 = \left\{ \pm 8, \pm 8i, 2-6i, -2+6i, 6+2i, -6-2i \right\}$$
$$R_8 = \left\{ \pm 7 \pm i, \pm 1 \pm 7i \right\}.$$

In signal subspaces L_1 to L_6, symbol selection requires 10 bits (one symbol from the 32QAM constellation and one from S_{32}). Each of these subsets has two antenna constellation combinations, and therefore a single bit is needed to select a particular combination. In subspaces L_7 and L_8, symbol selection requires 8 bits, because the R_8 and Q_8 constellations have only 8 points and their symbols carry 3 bits). But since each of these subspaces has 8 index combinations, 3 bits are needed to select one of them, and so 11 bits are needed in total to select a particular combination and the symbols to transmit from each active antenna, in each of these signal subspaces. Finally, since the signal space includes 8 subspaces, 3 bits must be assigned to selection of a particular subspace, and hence the described scheme transmits 14 bpcu.

To compute the total energy per transmitted symbol vector, we first evaluate the average energy of the constellations used in this design: A simple inspection shows that the average energy is $E_{32QAM} = 20$ for 32QAM, $E_{S32} = 22$ for S_{32}, $E_{Q8} = 52$ for Q_8, and $E_{R8} = 50$ for R_8. Since the symbols take their values from {32QAM,S_{32}} in 6 out of the 8 subspaces, from {32QAM,Q_8} in one subspace, and from $\{S_{32},R_8\}$ in the remaining subspace, the average total transmit energy is given by:

$$E_{ESM-Type2} = \frac{6}{8} \times 42 + \frac{1}{8} \times 72 + \frac{1}{8} \times 72 = 49.5.$$

Compared to the baseline MSM scheme, this ESM scheme saves approximately 41% in terms of transmit energy. This represents a SNR gain of 2.3 dB.

ESM-Type3 with 14 bpcu

In this scheme, the transmitted symbol is represented as:

$$\text{ESM-Type3: } \mathbf{X} \in \{\mathbb{S}_1, \mathbb{S}_2\}, \tag{6.31}$$

where we define $\mathbb{S}_1 = \{\mathbf{x}_1 \in \mathbb{S}_{PS}, \mathbf{x}_2 \in \mathbb{S}_{TF}\}$ and $\mathbb{S}_2 = \{\mathbf{x}_1 \in \mathbb{S}_{TF}, \mathbf{x}_2 \in \mathbb{S}_{PS}\}$. Similarly, the set of symbol vectors $\mathbb{S}_{PS}$ is defined as the signal space of ESM-Type2 described in the previous section. A signal vector is therefore of the form:

$$\mathbb{S}_{PS} : \mathbf{x} \in \Big\{L_1, L_2, L_3, L_4, L_5, L_6, L_7, L_8\Big\}, \tag{6.32}$$

where the subsets $L_1 - L_8$ are given by eqns. (6.29) – (6.30). As shown in the previous section, this scheme transmits 14 bits per channel use, and the average total energy per transmitted symbol vector is $E_s = 49.5$.

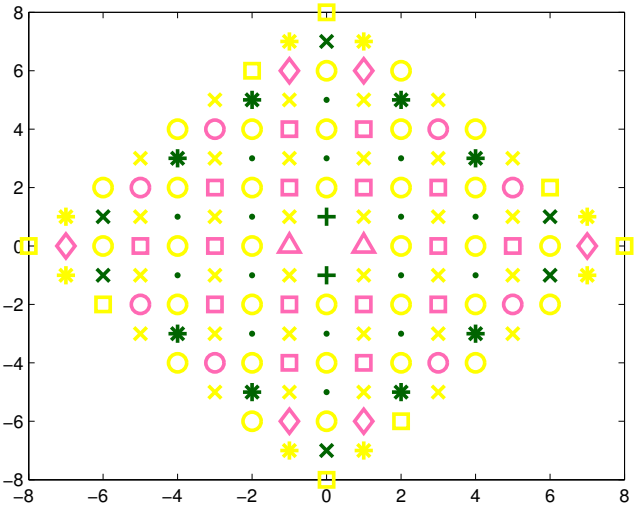

Fig. 6.10 The constellations used in ESM-Type3 with 14 bpcu: The yellow constellations are those of ESM-Type2, the green pluses represent T_c, the pink triangles represent F_c, the green points represent T_{16}, the pink squares represent F_{16}, the green starts represent T_8, the pink circles denote F_8, the green crosses are T_o, and the pink diamonds are F_o.

Next, the signal set $\mathbb{S}_{TF}$ is constructed by the union L' of four subsets as follows:

$$\mathbb{S}_{TF} : \mathbf{x} \in L' = \{L'_1, L'_2, L'_3, L'_4\}, \tag{6.33}$$

where each set is corresponding to different antenna combinations and associated signal constellations. The first subset is defined as:

$$L'_1 = \left\{ \begin{bmatrix} T_{32} \\ F_{32} \\ 0 \\ 0 \end{bmatrix}, \begin{bmatrix} F_{32} \\ T_{32} \\ 0 \\ 0 \end{bmatrix}, \begin{bmatrix} 0 \\ 0 \\ T_{32} \\ F_{32} \end{bmatrix}, \begin{bmatrix} 0 \\ 0 \\ F_{32} \\ T_{32} \end{bmatrix} \right\} \tag{6.34}$$

The constellations are illustrated in Fig. 6.10, where the T_{32} and F_{32} constellations can be mathematically written as:

$$\begin{aligned} T_{32} &= T_c \cup T_{16} \cup T_8 \cup T_o \\ F_{32} &= F_c \cup F_{16} \cup F_8 \cup F_o. \end{aligned} \tag{6.35}$$

Specifically, the third constellations are given by $T_c = \{\pm i\}$, $T_{16} = \{\pm 2 \pm i, \pm 2, \pm 3i, \pm 4 \pm i, \pm 3i, \pm 5i\}$, $T_8 = \{\pm 2 \pm 5i, \pm 4 \pm 3i\}$, and $T_o = \{\pm 6 \pm i, \pm 7i\}$. The fourth constellations are

written as $F_c = \{\pm 1\}$, $F_{16} = \{\pm 1 \pm 2i, \pm 3 \pm 2i, \pm 1 \pm 4i, \pm 3, \pm 5\}$, $F_8 = \{\pm 3 \pm 4, \pm 5 \pm 2i\}$, and $F_o = \{\pm 1 \pm 6i, \pm 7\}$.

The L'_1 subset can transmit 12 bits: 2 bits select one of the four combinations of active TX antennas and associated constellations, 5 bits select a symbol from the T_{32} constellation, and 3 bits select a symbol from the F_{32} constellation. The other three subsets $L'_2 - L'_4$ are defined as follows:

$$L'_2 = \left\{ \begin{bmatrix} T_{16} \\ F_{16} \\ 0 \\ 0 \end{bmatrix}, \begin{bmatrix} F_{16} \\ T_{16} \\ 0 \\ 0 \end{bmatrix}, \begin{bmatrix} 0 \\ 0 \\ T_{16} \\ F_{16} \end{bmatrix}, \begin{bmatrix} 0 \\ 0 \\ F_{16} \\ T_{16} \end{bmatrix}, \begin{bmatrix} T_{16} \\ 0 \\ F_{16} \\ 0 \end{bmatrix}, \begin{bmatrix} F_{16} \\ 0 \\ T_{16} \\ 0 \end{bmatrix}, \begin{bmatrix} 0 \\ T_{16} \\ 0 \\ F_{16} \end{bmatrix}, \begin{bmatrix} 0 \\ F_{16} \\ 0 \\ T_{16} \end{bmatrix} \right\}, \tag{6.36}$$

$$L'_3 = \{L'_2 | T_{16} \rightarrow T_8, F_{16} \rightarrow F_{16}\}.$$

$$L'_4 = \{L'_2 | T_{16} \rightarrow T_{16}, F_{16} \rightarrow F_8\}.$$

The T_{16}, F_{16}, T_8 and F_8 constellations are also shown in Fig. 6.10. This representation indicates that the combinations of active antennas in subset L'_3 are the same as those in L'_2, but here constellation F_{16} is replaced by constellation F_8. Similarly, subset L'_4 is obtained from L'_2 by substituting constellation T_8 for T_{16}.

The signal subset L'_2 transmits 11 bits per symbol vector: 3 bits are needed to select one of the 8 combinations, 4 bits to select a symbol from T_{16}, and 4 bits to select a symbol from F_{16}. Next, since the L'_3 subset transmits 10 bits per symbol vector. Again, 3 bits select one of the 8 combinations, and then 3 bit selects a symbol from T_8, and 4 bits select a symbol from T_{16}. Similarly, since the L'_4 subset also transmits 10 bits per symbol vector. Here, 3 bits select one of the 8 combinations, 4 bit selects a symbol from T_{16}, and 3 bits select a symbol from F_8.

The prefix of these subsets in $\mathbb{S}_{TF}$ must have a variable number of bits. Subset L'_1 has a 1-bit prefix, subset L'_2 has a 2-bit prefix, and subsets L'_3 and L'_4 have a 3-bit prefix. With these variable-length prefixes, it can be seen that all symbol vectors in $\mathbb{S}_{TF}$ carry 13 bits. The average total energy per transmitted symbol vector from $\mathbb{S}_{TF}$ is $E_s = 37.5$.

The signal vector sets in $\mathbb{S}_{PS}$ and $\mathbb{S}_{TF}$ are used with the same probability, the average energy of the transmitted signal vectors in ESM-Type3 is

$$E_{ESM-Type3} = \frac{1}{2}(49.5 + 37.5) = 43.5$$

This represents a 2.9 dB SNR gain over MSM.

Table 6.7 Expected gain of the ESM schemes over MSM

	10-bpcu	**14-bpcu**
ESM-Type1	1 dB	1.2 dB
ESM-Type2	1.9 dB	2.3 dB
ESM-Type3	2.2 dB	2.9 dB

6.3.5 Performance and complexity analysis

The minimum Euclidean distance: Assuming the CSI is perfectly known at the receive side, the ML decoder estimates the transmitted codeword according to:

$$\hat{\mathbf{X}} = \arg\min_{\mathbf{X}\in\mathbb{X}} \|\mathbf{Y} - \mathbf{H}\mathbf{X}\|^2, \tag{6.37}$$

where the minimization is performed over all possible transmitted symbol vectors from the signal codeword space $\mathbb{X}$.

In ML detection using exhaustive search, the receiver computes the Euclidean distance between the received noisy signal and the set of all possible signal vectors transmitted over the channel matrix. At high SNR, the receiver performance is dominated by the minimum squared Euclidean distance over the signal space [58]:

$$L^2_{min} = \min \|\mathbf{X} - \mathbf{X}'\|^2. \tag{6.38}$$

The ESM schemes introduced in this work were designed in such a way as to preserve the minimum squared Euclidean distance of the primary modulation $L^2_{min} = \delta_0^2$. The same minimum distance being also valid for MSM, comparison of the asymptotic performance of the different schemes is reduced to comparing their average transmit energy E_s. We therefore define the expected gain $\mathscr{G}$ of a scheme over another as the ratio of their average transmit energies expressed in the dB scale as follows:

$$\mathscr{G} = 10\log_{10}\left(\frac{E_s}{E'_s}\right). \tag{6.39}$$

For example, the expected gain of ESM-Type3 over MSM with 10 bpcu is $10\log_{10}(20/12) =$ 2.2 dB. The expected asymptotic gains of the proposed ESM schemes over MSM are reported in Table 6.7.

Receiver complexity: Defining the receiver complexity as the number of complex multiplications required per ML decoder decision, we found that the first two of the proposed ESM schemes have essentially the same receiver complexity as MSM, while the third has a 50% higher complexity. Using the system model given by eqn. (6.1), the ML decoder needs to compute 2^b decision metrics $w_k = \|\mathbf{y} - \mathbf{H}\mathbf{x}_k\|^2$, where b is the total number of transmitted bits per channel use. This holds for MSM as well as for ESM-Type1 and ESM-Type2. Obviously, the number of antenna/modulation combinations is higher in ESM-Type2 than in ESM-Type1, which in turn has a higher number of combinations than in MSM, but as the number of combinations increases, the ESM schemes use smaller constellations, and the number of the vectors in the signal space remains the same. Computation of each metric by the decoder involves one norm calculation, which requires a single complex multiplication. The difference between the three schemes lies in the number of multiplications needed prior to norm calculations. But this number is of second order compared to the number of metrics, and therefore the receiver complexities of MSM, ESM-Type1, and ESM-Type2 only differ by a few percent.

A close look at ESM-Type3 reveals that the decoder complexity is more involved than in the first two ESM schemes, because the ML decoder must jointly decide two consecutive symbols. For 10 bpcu, the signal space is described by eqn. (6.20). The ML decoder must search in this space using two consecutive received signal samples $\mathbf{y}_1$ and $\mathbf{y}_2$ and computing metrics of the form $w_k = \|\mathbf{y}_1 - \mathbf{H}\mathbf{x}_i\|^2 + \|\mathbf{y}_2 - \mathbf{H}\mathbf{x}_j\|^2$, where $\mathbf{x}_i \in \mathbb{S}_{PS}$, $\mathbf{x}_j \in \mathbb{S}_{TF}$, or $\mathbf{x}_i \in \mathbb{S}_{TF}$, $\mathbf{x}_j \in \mathbb{S}_{PS}$. The number of norm calculations (and complex multiplications) per decoder decision is $2 \times [\text{card}(\mathbb{S}_{PS}) + \text{card}(\mathbb{S}_{TF})]$, where the sign $\text{card}(\cdot)$ indicates the cardinality of the signal set involved. But since only one decision is made every two channel uses, the number of norm calculations (and complex multiplications) per channel use is $\text{card}(\mathbb{S}_{PS}) + \text{card}(\mathbb{S}_{TF}) = 2^b + 2^{b-1}$. This is 50% higher than in the first two ESM schemes. The number of complex multiplications required before the norm calculations is essentially the same as in the previous schemes, but as indicated earlier, these numbers are of second order, and the decoder complexity is essentially given by the number of norm calculations, and therefore, the ML decoder complexity is approximately 50% higher in ESM-Type3 than in MSM, ESM-Type1, and ESM-Type2.

But in any case, implementation of the ML decoder using exhaustive search involves a very high complexity and becomes prohibitive at very high spectral efficiencies in any MIMO scheme. In practice, the ML decoder can be implemented efficiently using the sphere decoding (SD) technique. This technique reduces the complexity of the ML decoder by shrinking the search space to an acceptable level and counting those combinations that

lie within a sphere centered on the received signal. The general SD scheme for SM was described in [59], and it was shown that it significantly reduces computational complexity with no performance loss. In the simulations section which follows, we use the complex-valued SD for ESM, which takes the signal space of ESM into account and uses an infinity search radius to guarantee the ML performance.

6.4 Simulation results

We report here the results of Monte Carlo simulations, which were obtained using Rayleigh fading MIMO channels with 4 receive antennas ($N_R = 4$) and assuming perfect CSI at the receiver. We also assume perfect synchronization and rectangular pulse shaping. That is, we neglect the problems of antenna switching with Nyquist pulse shaping, which may be challenging in practice. This problem was addressed in some recent papers, which proposed solutions such as employing a multiple-RF antenna switching architecture [60] or simply using a large roll-off factor in the pulse shaping filters to ensure that the energy is concentrated in a short period of time [61].

6.4.1 ESM with multiple signal constellations

In the simulations, symbol vectors were randomly generated and transmitted over the channel, ML detection was performed using the received noisy signal samples, and symbol vector error events were counted. The obtained symbol vector error rate (SVER) was used to compare the respective performances of conventional SM and ESM. Unlike BER performance evaluation, the SVER does not need to define the bit mapping, and the simulations are much quicker. In the first part of the simulations, we compared the BER and the SVER performance results of SM, SMX, and ESM in the 2TX4b case.

The BER results are reported in Fig. 6.11. The constellation used in each scheme is given in the legend. For example, SM uses 8PSK and is denoted SM-8PSK, SMX uses 4QAM and is denoted SMX-4QAM, and finally ESM uses 4QAM as primary modulation, and it is denoted ESM-4QAM. These results show that ESM gains 1.5 dB over conventional SM and gives the same performance as SMX at $BER = 10^{-4}$. Next, the SVER performance of the 3 MIMO schemes at hand was evaluated, and the results are given in Fig. 6.12. Comparison of Fig. 6.11 and Fig. 6.12 shows that the gains in terms of SVER performance perfectly match those given in terms of BER. On the basis of this observation, SVER

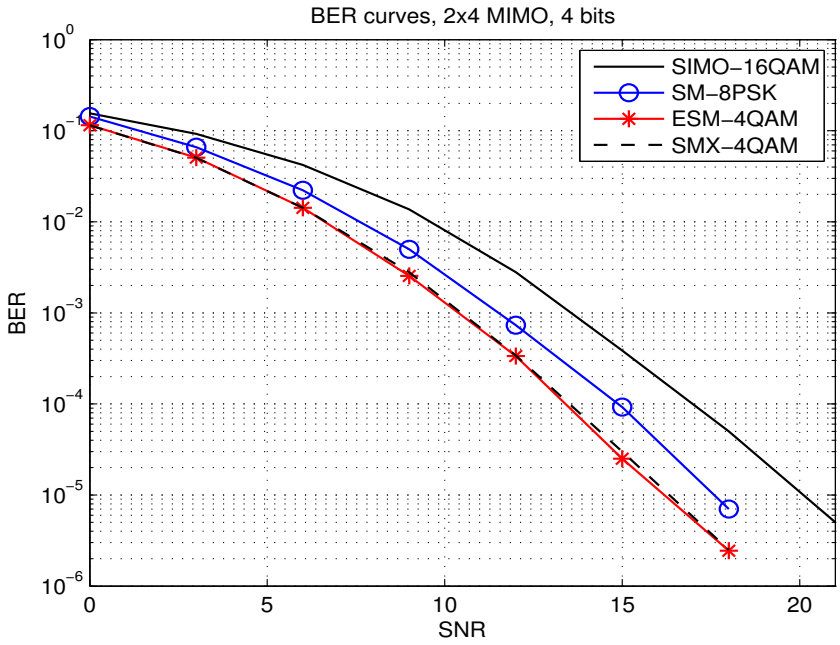

Fig. 6.11 BER performance of 2TX4b.

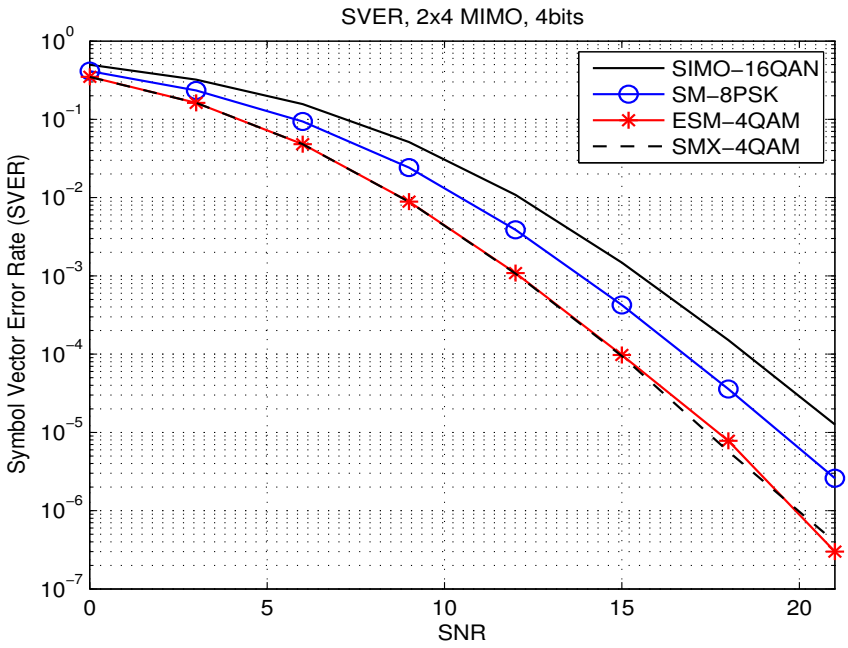

Fig. 6.12 SVER performance of 2TX4b.

performance evaluations were used in all subsequent comparisons of the MIMO schemes under investigation, because they are simpler to evaluate than BER performance and they provide very accurate performance comparisons.

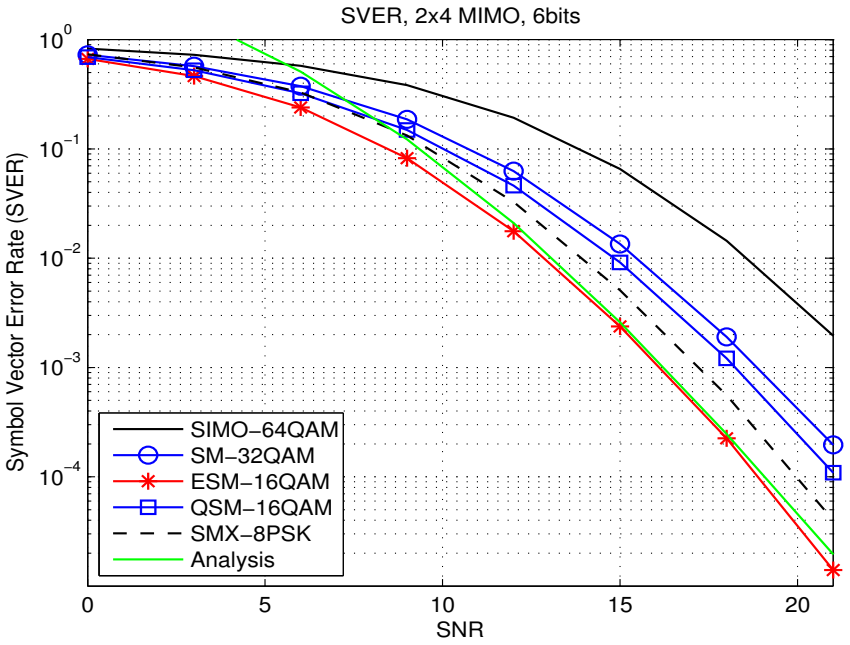

Fig. 6.13 SVER performance of 2TX6b.

The SVER curves corresponding to 2TX6b are presented in Fig. 6.13. As predicted by the L^2_{min} analysis, the simulation results confirm that ESM outperforms all other MIMO schemes at hand. Specifically, ESM gains more than 1 dB over SMX, 2 dB over QSM, and close to 3 dB over SM at $SVER = 10^{-3}$. In this figure, we also give the analytic bound of ESM obtained using (6.11) to show its tightness in the high SNR region.

Next, in Fig. 6.14, we show the SVER performance of 2TX8b schemes in which ESM uses 64QAM as primary modulation. The results indicate that ESM gains around 4 dB over QSM and 5 dB over SM, but loses close to 1 dB with respect to SMX at $SVER = 10^{-3}$. The average SNR loss of ESM with respect to SMX is mainly due to the fact that combinations $C1 - C2$ use the 64QAM signal constellation while SMX uses 16QAM in that case.

In Fig. 6.15, the SVER curves of 2TX9b show that ESM gains around 4 dB over QSM and 6 dB over SM and has about 0.8 dB loss compared to SMX at $SVER = 10^{-3}$. Again, the average SNR loss of ESM with respect to SMX can be attributed to the use of 64QAM in combinations $C1 - C2$, while SMX uses one 16QAM stream and one 32QAM stream in parallel to achieve a spectral efficiency of 9 *bpcu*.

In Fig. 6.16, the SVER curves of 4TX6b show substantial improvements of the SM family (both SM and ESM) over SMX. Specifically, ESM gains around 3 dB over SM and approximately 4 dB over SMX at $SVER = 10^{-3}$. This means that SM gains about 1 dB over SMX

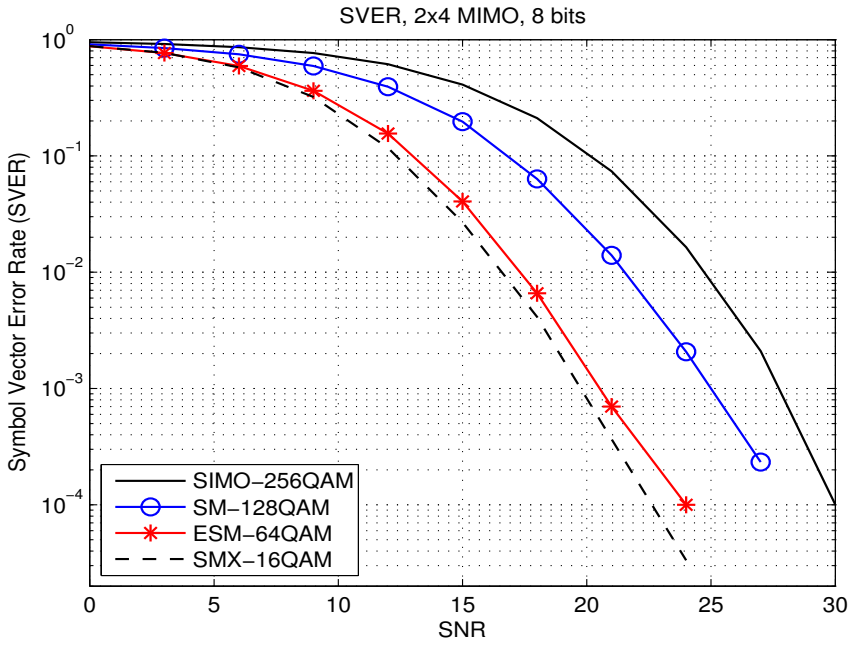

Fig. 6.14 SVER performance of 2TX8b.

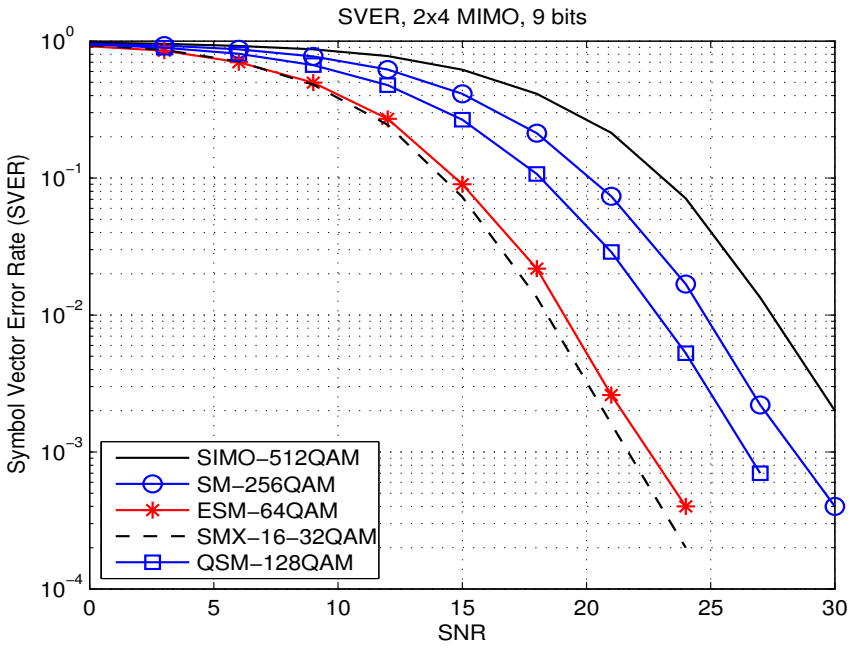

Fig. 6.15 SVER performance of 2TX9b.

while using fewer RF chains. Similarly, the SVER curves of 4TX8b are shown in Fig. 6.17, which indicates that ESM gains around 3 dB over SMX and QSM and approximately 6 dB over SM at $SVER = 10^{-3}$. In other words, SM loses 3 dB over SMX in this case.

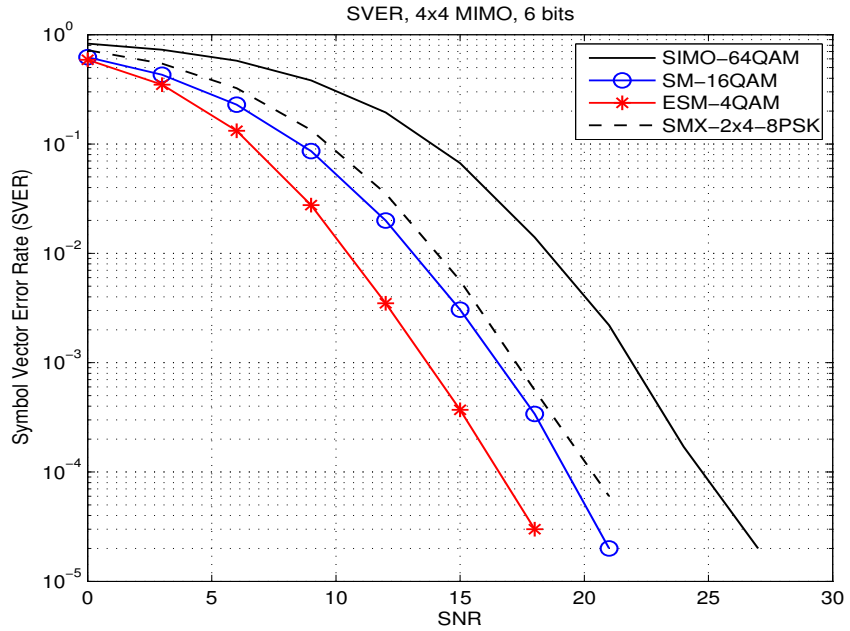

Fig. 6.16 SVER performance of 4TX6b.

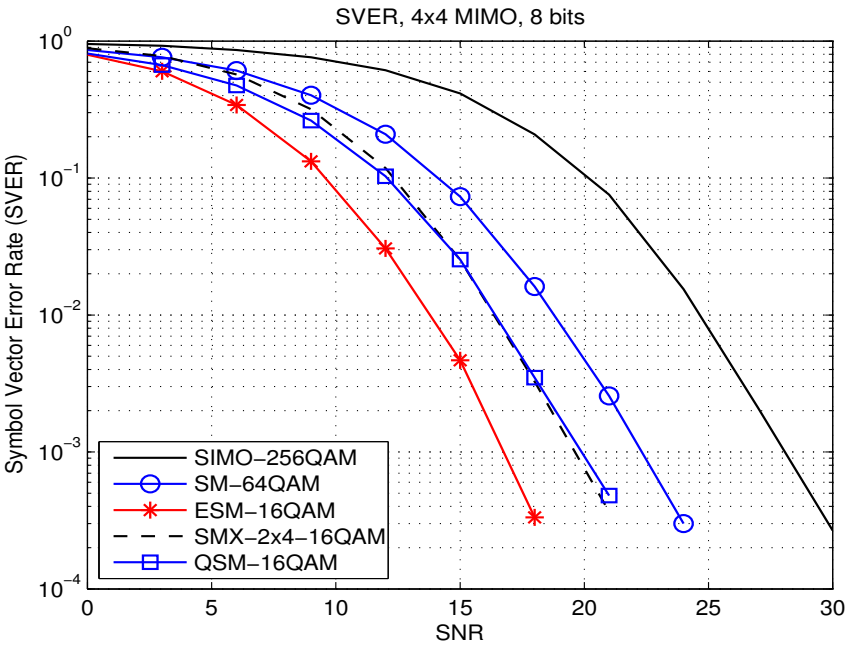

Fig. 6.17 SVER performance of 4TX8b.

Fig. 6.18 shows the SVER performance results of 4TX10b in which ESM uses 64QAM as primary modulation. Here, ESM gains around 3 dB over SMX, 5 dB over QSM, and more than 7.5 dB over conventional SM at $SVER = 10^{-3}$. Finally, the SVER performances of the

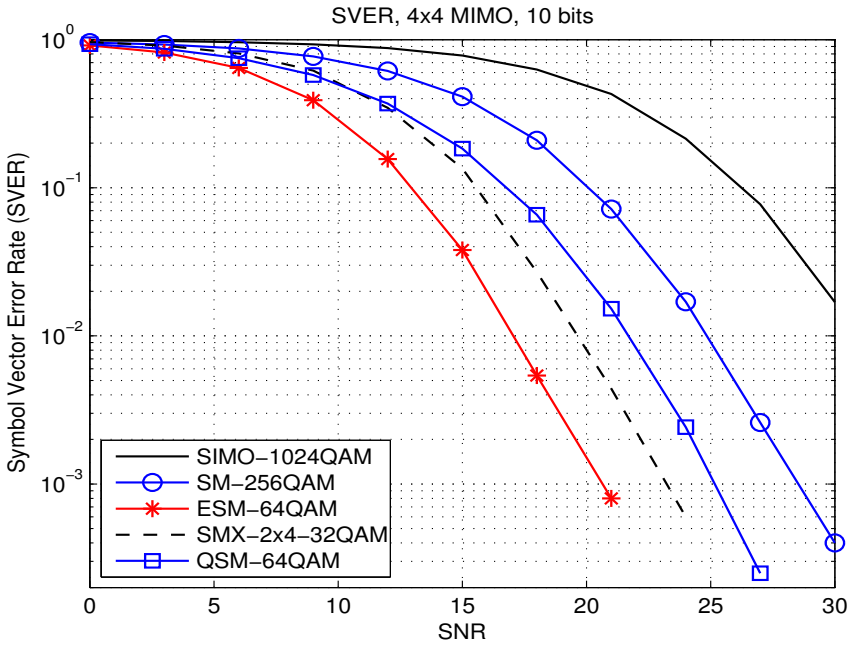

Fig. 6.18 SVER performance of 4TX10b.

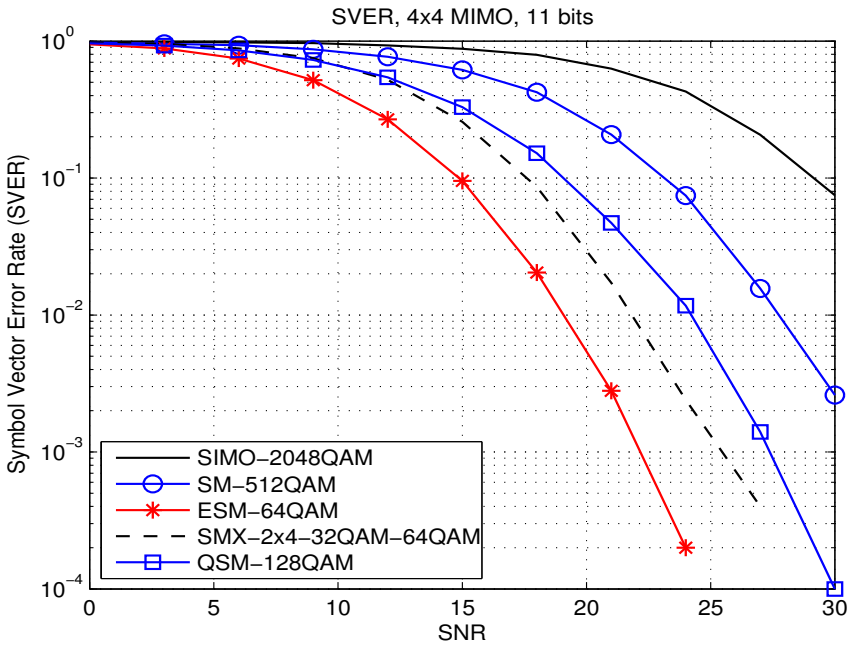

Fig. 6.19 SVER performance of 4TX11b.

4TX11b schemes are depicted in Fig. 6.19, which shows that ESM gains around 3 dB over SMX, 5 dB over QSM, and as much as 9 dB over SM at $SVER = 10^{-2}$. The substantial gain of ESM over SM in the 4TX11b case can be explained by the fact that SM requires 512QAM

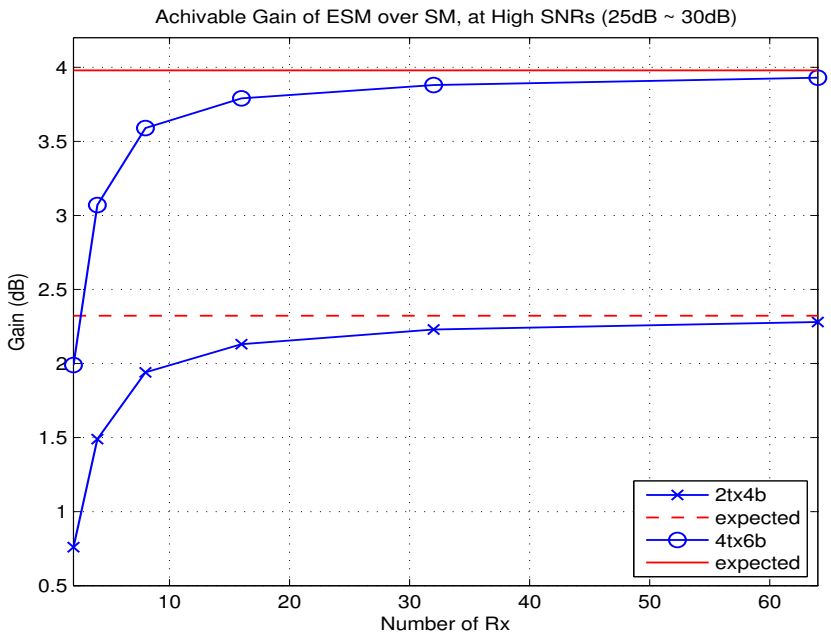

Fig. 6.20 Impact of the number of RX antennas.

for transmitting 11 bpcu, while ESM only needs 64QAM as primary modulation to achieve the same spectral efficiency.

A final investigation in this work concerned the relation between the expected gains from the minimum distance analysis and the gains achieved with a finite number of RX antennas. The results are reported in Fig. 6.20. The specific numbers of RX antennas used here are 2, 4, 8, 16, 32, and 64. The average SNR gains which appear in this figure are those of ESM over SM. The expected gains corresponding to the 2TX4b and 4TX6b cases are indicated by the dotted line and the solid line, respectively. The curve with crosses gives the gain as a function of the number of RX antennas for the 2TX4b case. It shows that the expected gain of 2.32 dB can be approached when the number of RX antennas increases. Specifically, the gain is virtually to 2 dB with 8 RX antennas and 2.3 dB with 16 RX antennas. A similar observation can be made for the 4TX6b case. Here, the expected gain (the solid-line curve) is 4 dB, and the curve with circles, which gives the gain as a function of the number of RX antennas indicate that the gain achieved with 8 RX antennas is 3.6 dB and the gain with 16 RX antennas is 3.8 dB.

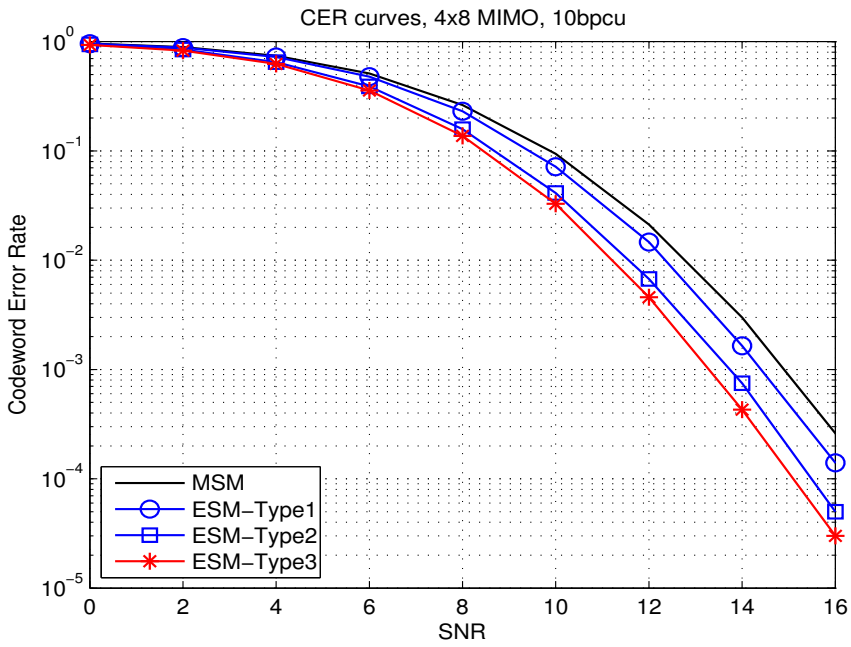

Fig. 6.21 CER performance of MSM and ESMs: 4 TX antennas and 8 RX antennas with 10 bpcu.

6.4.2 ESM with two active antennas

In the simulations, the symbol codewords $\mathbf{X}$ were randomly generated transmitted over the channel, the SD was performed using the received noisy signal samples, and error events $\mathbf{X} \neq \mathbf{X}'$ were counted. The obtained codeword error rate (CER) was used to compare the respective performances of conventional MSM and the presented ESMs.

Fig. 6.21 gives the Monte-Carlo simulation results of the system performance for 10-bpcu transmission. These results show that at $CER = 10^{-3}$ the presented ESM schemes achieve SNR gains over MSM of around 0.6 dB, 1.3 dB and 1.8 dB, respectively. In Fig. 6.22, we report the CER performance of MSM and the proposed ESM schemes providing 14 bpcu. Here, we can see that at $CER = 10^{-3}$ the ESM schemes achieve gains of around 0.9 dB, 1.9 dB and 2.2 dB, respectively, over MSM. Note that the gains are higher than those achieved in the 10 bpcu case. This is due to the fact that the average energy of the secondary constellations used in our signal design becomes lower (relatively to the primary constellation) when higher spectral efficiencies are considered.

A final investigation in this work concerned the relation between the expected gains and the practical gains achieved with a finite number of RX antennas. The results are reported in Fig. 6.23 for the case of 10 bpcu. The specific numbers of RX antennas used in this

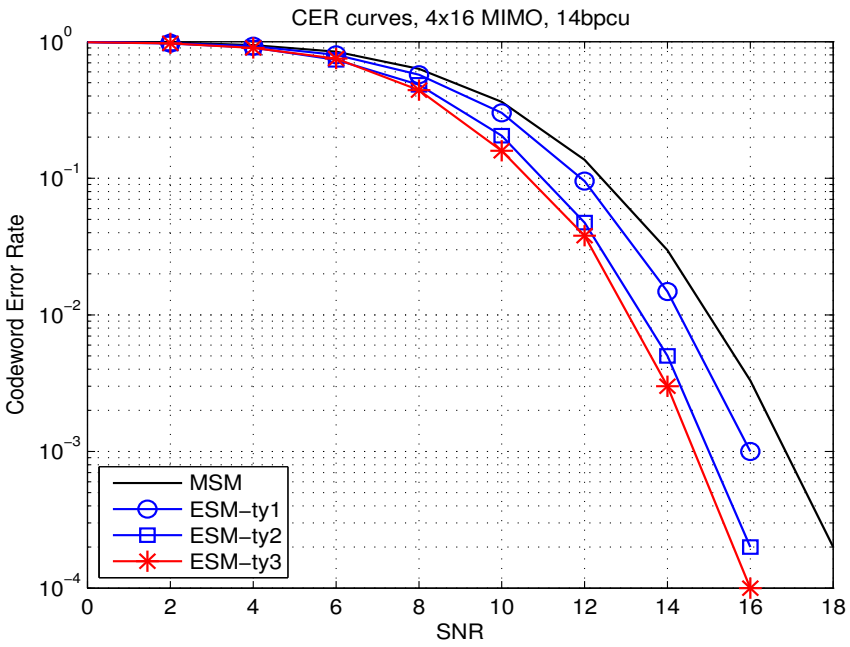

Fig. 6.22 CER performance of MSM and ESMs: 4 TX antennas and 16 RX antennas with 14 bpcu.

investigation are 2, 4, 8, 16, 32, and 64. The results show that the expected gain can be approached when the number of RX antennas increases. In fact, 80% of the expected gain can be achieved with 16 RX antennas.

6.5 Conclusion

In the first part of this chapter, we have introduced an ESM scheme by enabling one or two active TX antennas and using multiple signal constellations. Compared to conventional SM, this scheme transmits one or two additional information bits per channel use. On Rayleigh fading channels, both the closed-form performance analysis and the simulation results showed that the proposed technique outperforms conventional SM when the signal constellations are selected so as to have the same number of bits per channel use. It was found that with two TX antennas ESM potentially gains up to 6 dB over conventional SM. It was also found that with four TX antennas, ESM leads to higher gains: it gains up to 9 dB over SM. Moreover, the receiver complexity analysis of ML detection revealed that while ESM achieves a substantial performance gain over conventional SM, it also significantly reduces the complexity of the optimum decoder.

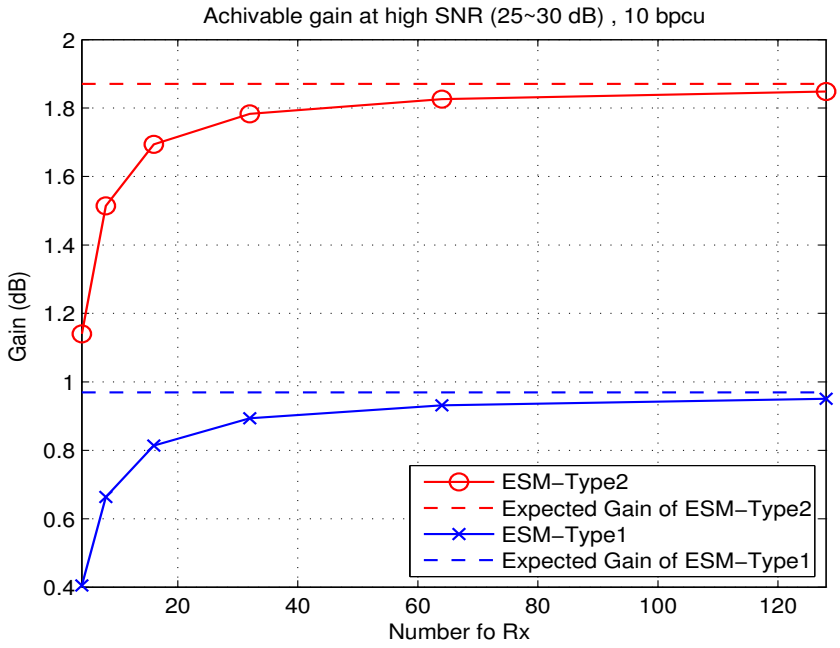

Fig. 6.23 Impact of the number of RX antennas on achievable gain.

In the second part of the chapter, extending the ESM scheme, we further introduced three other types of ESM schemes in which two transmit antennas remain systematically active. In addition to a primary constellation, these schemes use one or more constellations of reduced size and energy. The reduced size is compensated using a higher number of antenna/modulation combinations with respect to MSM. The new combinations are included in such a way as to preserve the Euclidean distance in the signal space while reducing the average total transmit energy. Using Monte Carlo simulations on Rayleigh fading channels, it was found that the proposed schemes achieve up to 2.2 dB gain compared to MSM in a 10-bpcu transmission and up to 2.9 dB gain in a 14-bpcu transmission with two active TX antennas.

Chapter 7

General conclusions and perspectives

In this chapter, we first revisit the motivation behind our work and the contributions we made, and then present some perspectives about possible future work.

7.1 General comments and conclusions

In this thesis, we investigated three fundamental components of a MIMO-OFDM system: signal design, channel estimation, and symbol detection, focusing on the issues of antenna correlation, imperfect CSI, multiple-user interference, computational complexity, and energy efficiency.

7.1.1 Channel modeling and estimation

In the first part of the thesis (in Chapter 3), we investigated a channel estimator for MIMO-OFDM systems where the wideband wireless channel has the spatial, time and frequency correlations. For this correlated channel, we derived a novel channel estimator that exploits the spatial, time and frequency correlations of the channel taps, and reduces the dimension of the parameter estimation space by retaining only the dominant terms. Our analysis showed that the proposed scheme can significantly suppress the impact of AWGN and therefore provide an improvement of the system performance. The same conclusion can also be found in our simulations with different channel models.

This channel estimator is useful for many post-channel-estimation applications. The example we presented is a codeword selection scheme where a user sends CSI to its serving

base station by sending an index from a codebook. This codeword selection process can be dramatically simplified using a quantization operation instead of exhaustive search, by reusing the resulting output of estimated AoD information from our proposed channel estimator. Furthermore, we showed that the proposed codeword selection can be applied to arbitrary codebook structure when a linear transform (calibration) is used to compensate the mismatch between the desired codebook and the DFT-based codebook. Our simulations showed that the proposed scheme can achieve the system performance close to the optimal one with very low computational complexity. This result is especially useful when we have a very large codebook or a very large number of TX antennas.

7.1.2 Robust symbol detection

The second part of the thesis, including Chapter 4 and Chapter 5, focused on understanding the robustness of symbol detection against to imperfect CSI and multiple-user interference. For this purpose, we first derived the optimal symbol detection under imperfect CSI based on the ML criterion. Considering the complexity, we then derived the linear symbol detection scheme with both imperfect CSI and multiple-user interference based on the MMSE criterion. Also, our study in this part included sections with practical considerations such as imperfect CDI, the timing delay of interference, the impact of the time/frequency selective interfering channel, and scalability in the number of TX antennas for interference suppression.

The first of these methods is the optimal ML detection that decodes the transmitted signal by jointly processing the received signal and the given pilot signal. This scheme decodes signal directly without the channel estimation process and guarantees the statically optimal result of symbol detection. In our numerical results, the largest performance gains can be found when the OSTBC is applied in the MIMO-OFDM systems. We also found that the CDI estimation is not really sensitive to the system performance and therefore it can simply be done by using BMS with only few predetermined CDIs.

The second method referred to as the LMMSE detection for the mixture types of interference, including both pilot and data types of signals. This scheme develops different strategies for the interfering data symbols and interfering pilot symbols, and the imperfect CSI in both the serving channel and the interfering channel are taken into account. In our simulations, the most significant performance gain was found when the interference is strong, the SNR is high and there is no timing delay. This is because the interfering pilot signal can be canceled accurately. Moreover, this scheme provides an impressive

performance gain when the interfering eNB only sends the pilot signal without sending any data signal.

For selective interfering channels, we developed an adaptive scheme that uses a sliding window for tracking the variation of interference. We focused on how to adapt the window size to deal with different types of interference. Based on our simulations, this scheme only depends on the SIR and SNR values and shows good robustness to power delay profiles of the channel. On the issue of scalability, we showed two simple schemes to apply additional TX antennas in order to improve the interference mitigation with slight complexity increase.

7.1.3 Spatial modulation design

In the third part of the thesis (Chapter 6), we focused on improving the spectral efficiency for SM systems. We introduced a new SM technique using one or two active antennas and multiple signal constellations. The proposed technique, which we refer to as ESM, conveys information bits not only by the index(es) of the active antenna(s), but also by the constellations transmitted from each of them. In addition to a primary constellation, these schemes use one or more constellations of reduced size and energy. The reduced size is compensated using a higher number of antenna/modulation combinations with respect to MSM. The new combinations are included in such a way as to preserve the Euclidean distance in the signal space while reducing the average total transmit energy. In our simulations, it was found that the proposed schemes achieve different levels of performance gains based on the reduction of the transmit energy. Also, an upper bound on the performance gain was derived, and it was shown that the bound can be approached when the number of RX antennas increases.

7.2 Discussion and future work

A Ph.D. thesis is carried out during a finite period of time and, as in any work with a time constraint, several possible research paths remain unexplored. We shall address some of them in this section.

7.2.1 Channel modeling and estimation

The most challenging and compelling extension to this work is the development of finding the optimal modeling order for the proposed channel estimator.

Different modeling orders make a huge impact on the system performance, which is shown in Fig. 3.1. In this figure, there is an optimal modeling order for any given SNR; increasing the modeling order does not necessarily improve the performance. In fact, our analysis reveals that a small modeling order can reduce the thermal noise. However, if the modeling order is too small to span the signal subspace, there will be an under-modeling error that degrades the performance. Therefore, a new technique for a good trade-off between the thermal noise and the under-modeling error is needed for the current design.

7.2.2 Robust symbol detection

A possible extension to the second part of the thesis is the generalization of the two-user interference channel to the case where K users interfere with each other. Multiple interferences, e.g. the K-user interference channel, are more challenging and compelling for future generation cellular networks. In this model, our schemes can still work, but might provide less gains as K increases. We show next how to apply our schemes for this issue.

The idea we have is to focus on suppressing the strongest interference and treating the rest of interference as AWGN. This procedure turns the K-user interference channel into the case of two-user interference, and that makes our schemes feasible. A preliminary result can be shown here for a 3-user interference channel case (see Fig. 7.1), where the number of RX antennas is given by four; the SINR of the first interference is given as 0 dB, the second interference has SINR as 6 dB; and assume that serving pilots and interfering pilots are not overlapped. Although some performance gains can be found in this figure, we believe that there exists a strategy that can further improve the suppression capability and, hence, achieve better performance in an efficient way.

7.2.3 Spatial modulation design

There are some attractive problems related to this work, for example, the optimal constellation design and its criterion to achieve the targeted throughput with an arbitrary number of TX antennas. This issue would fall into the category of high dimensional

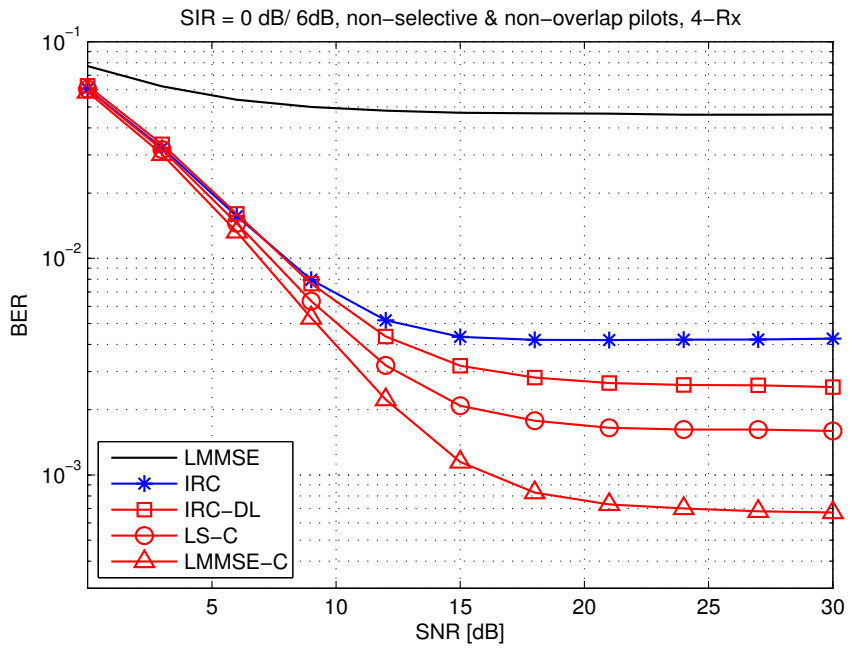

Fig. 7.1 BER vs SNR for the 3-user interference channel

optimization problems, where the constellation would include a signal modulation (i.e„ amplitude-phase modulation), an antenna domain modulation (i.e., space shift keying), and a constellation type modulation (i.e., the main concept of ESM). A key question is how to model a feasible optimization problem (i.e., linear or convex types of optimization) that provides a good balance between the constellation sizes in each domain to maximize the spectral efficiency.

Another interesting future work is the development of the optimal constellation labeling. Similar to the optimal constellation design, this issue is also a high dimensional problem, and apparently its results would be more attractive when the constellation and its labeling can be jointly optimized. However, achieving these two goals together might be a colossal task given the complexity each one of them separately has.

Appendix A

Chapter 5

A.1 Covariance estimates in (5.16)

We compare two different ways to estimate the covariance of $\mathbf{Y}_{d1}$: 1) using the residual matrix $\hat{\mathbf{V}}$ and 2) using the received signal $\mathbf{Y}_{d1}$. Assume that $\mathbf{Y}_{d1}$ and $\hat{\mathbf{V}}$ have the same symbol length, i.e., $N_p = N_d - N_p \triangleq N_o$, and the columns of $\mathbf{Y}_{d1}$ and $\hat{\mathbf{V}}$ are i.i.d. complex Gaussian vectors. Ignoring channel estimation errors, we conclude that

$$\hat{\mathbf{V}}\hat{\mathbf{V}}^H \sim \mathcal{W}_{N_R}(\Sigma_{\mathbf{V}}, N_o)$$
$$\mathbf{Y}_{d1}\mathbf{Y}_{d1}^H \sim \mathcal{W}_{N_R}(\Sigma_{\mathbf{Y}_{d1}}, N_o),$$

where $\mathcal{W}_{N_R}$ denotes the complex Wishart matrix [62] with N_R degrees of freedom, $\Sigma_{\mathbf{V}} = \bar{\mathbf{h}}\bar{\mathbf{h}}^H + N_0\mathbf{I}$ and $\Sigma_{\mathbf{Y}_{d1}} = \mathbf{h}\mathbf{h}^H + \Sigma_{\mathbf{V}}$ are the true covariance matrices. The variances of their diagonal entries are then given by

$$\mathrm{var}([\hat{\mathbf{V}}\hat{\mathbf{V}}^H]_{mm}) = \frac{2}{N_o^2}[\Sigma_{\mathbf{V}}]_{mm}^2$$
$$\mathrm{var}([\mathbf{Y}_{d1}\mathbf{Y}_{d1}^H]_{mm}) = \frac{2}{N_o^2}[\Sigma_{\mathbf{Y}_{d1}}]_{mm}^2$$

which are proportional to the covariance estimation errors. Since $[\Sigma_{\mathbf{V}}]_{mm}$ is always smaller than $[\Sigma_{\mathbf{Y}_{d1}}]_{mm}$, the estimation errors of $\hat{\mathbf{V}}$ is smaller than that $\mathbf{Y}_{d1}$ in general.

A.2 Derivation of LS-C in (5.22)

For notational brevity, we ignore the conditional part of a conditional expectation operator, e.g., $\mathbb{E}[\mathbf{X} \mid \mathbf{h}] = \mathbb{E}[\mathbf{X}]$. The weighting vector of the LS-C is given by

$$\begin{aligned}\mathbf{w}_{ls}^H &\overset{(a)}{=} \mathbb{E}\left[\mathbf{X}_{d1}\hat{\mathbf{V}}_b^H\right]\mathbb{E}\left[\hat{\mathbf{V}}_b\hat{\mathbf{V}}_b^H\right]^{-1} \\ &\overset{(b)}{=} \mathbb{E}\left[\mathbf{h}^H\right]\left(\mathbb{E}\left[\mathbf{h}\mathbf{h}^H\right] + N_0\mathbf{I}\right)^{-1} \\ &= \hat{\mathbf{h}}^H\left(\frac{N_p^2(\hat{\mathbf{h}}\hat{\mathbf{h}}^H)}{N_p^2-1} + \frac{N_p(\hat{\mathbf{h}}_b\hat{\mathbf{h}}_b^H)}{N_p^2-1} + N_0\mathbf{I}\right)^{-1}.\end{aligned}$$

In (a), the two conditional expectations on the RHS are

$$\begin{aligned}\mathbb{E}\left[\mathbf{X}_{d1}\hat{\mathbf{V}}_b^H\right] &= \mathbb{E}\left[\mathbf{X}_{d1}\left(\mathbf{h}\mathbf{X}_{d1} - \bar{\mathbf{E}}\bar{\mathbf{X}}_p + \mathbf{Z}'_p\right)^H\right] \\ &= N_p \cdot \mathbb{E}[\mathbf{h}^H] - \mathbb{E}\left[\mathbf{X}_{d1}\bar{\mathbf{X}}_p^H\bar{\mathbf{E}}^H\right] \\ &= N_p \cdot \mathbb{E}[\mathbf{h}^H] - \mathbb{E}\left[\mathbf{X}_{d1}\bar{\mathbf{X}}_p^H\left(\frac{1}{N_p}\bar{\mathbf{X}}_p\mathbf{X}_{d1}^H\mathbf{h}^H\right)\right] \\ &= \left(N_p - \frac{1}{N_p}\mathrm{Tr}\left(\bar{\mathbf{X}}_p^H\bar{\mathbf{X}}_p\mathbb{E}[\mathbf{X}_{d1}^H\mathbf{X}_{d1}]\right)\right)\mathbb{E}[\mathbf{h}^H] \\ &= (N_p - 2)\cdot\mathbb{E}[\mathbf{h}^H] \\ \mathrm{var}\left[\hat{\mathbf{V}}_b\right] &= \mathbb{E}\left[N_p\mathbf{h}\mathbf{h}^H + \bar{\mathbf{E}}\bar{\mathbf{X}}_p\bar{\mathbf{X}}_p^H\bar{\mathbf{E}}^H\right] + N_0N_p\mathbf{I} \\ &\quad - 2\cdot\mathbb{E}\left[\bar{\mathbf{E}}\bar{\mathbf{X}}_p\mathbf{X}_{d1}^H\mathbf{h}^H + \bar{\mathbf{E}}\bar{\mathbf{X}}_p\mathbf{Z}_p'^H\right] \\ &= (N_p-2)\cdot\left(\mathbb{E}[\mathbf{h}\mathbf{h}^H] + N_0\mathbf{I}\right),\end{aligned}$$

where we have used the following identities,

$$\begin{aligned}\mathbb{E}[\bar{\mathbf{E}}\bar{\mathbf{X}}_p\bar{\mathbf{X}}_p^H\bar{\mathbf{E}}^H] &= \frac{\mathrm{var}(\mathbf{h}\mathbf{X}_{d1}\bar{\mathbf{X}}_p^H\bar{\mathbf{X}}_p) + \mathrm{var}(\mathbf{Z}'_p\bar{\mathbf{X}}_p^H\bar{\mathbf{X}}_p)}{N_p^2} \\ &= 2\left(\mathbb{E}[\mathbf{h}\mathbf{h}^H] + N_0\mathbf{I}\right) \\ \mathbb{E}[\bar{\mathbf{E}}\bar{\mathbf{X}}_p\mathbf{X}_{d1}^H\mathbf{h}^H] &= \frac{1}{N_p}\mathbb{E}[\mathbf{h}\mathbf{X}_{d1}\bar{\mathbf{X}}_p^H\bar{\mathbf{X}}_p\mathbf{X}_{d1}^H\mathbf{h}^H] \\ &= \frac{1}{N_p}\mathrm{Tr}\left(\bar{\mathbf{X}}_p^H\bar{\mathbf{X}}_p\cdot\mathrm{var}(\mathbf{X}_{d1}^H)\right)\mathrm{var}(\mathbf{h}^H) \\ &= 2\cdot\mathbb{E}[\mathbf{h}\mathbf{h}^H] \\ \mathbb{E}[\bar{\mathbf{E}}\bar{\mathbf{X}}_p\mathbf{Z}_p'^H] &= \frac{1}{N_p}\mathrm{var}(\mathbf{Z}'_p\bar{\mathbf{X}}_p^H) = 2N_0\mathbf{I}.\end{aligned}$$

In (b), since the entries of the channel estimation error matrix are zero mean, we have $\mathbb{E}[\mathbf{h}] = \hat{\mathbf{h}}$. Invoking the relations

$$\begin{aligned}
\operatorname{var}\left(\mathbf{Ep}\right) &= \frac{\operatorname{var}(\mathbf{h}_b\bar{\mathbf{X}}_{d1}\mathbf{X}_p^H\mathbf{p}) + \operatorname{var}(\mathbf{Z}_p\mathbf{X}_p^H\mathbf{p})}{N_p^2} \\
&= \frac{\operatorname{Tr}(\mathbf{X}_p^H\mathbf{p}\mathbf{p}^H\mathbf{X}_p)\cdot\operatorname{Cov}(\bar{\mathbf{h}}) + N_pN_0\mathbf{I}}{N_p^2} \\
&= \frac{1}{N_p}\left(\mathbb{E}[\bar{\mathbf{h}}\bar{\mathbf{h}}^H] + N_0\mathbf{I}\right) \\
\mathbb{E}\left[\bar{\mathbf{h}}\bar{\mathbf{h}}^H\right] &= \hat{\mathbf{h}}_b\hat{\mathbf{h}}_b^H + \operatorname{var}\left(\bar{\mathbf{E}}\bar{\mathbf{p}}^H\right) \\
&= \hat{\mathbf{h}}_b\hat{\mathbf{h}}_b^H + \frac{1}{N_p}\left(\mathbb{E}\left[\mathbf{h}\mathbf{h}^H\right] + N_0\mathbf{I}_{N_R}\right),
\end{aligned}$$

We immediately obtain

$$\begin{aligned}
\mathbb{E}[\mathbf{h}\mathbf{h}^H] &= \hat{\mathbf{h}}\hat{\mathbf{h}}^H + \operatorname{var}\left(\mathbf{E}\mathbf{p}^H\right) \\
&= \hat{\mathbf{h}}\hat{\mathbf{h}}^H + \frac{1}{N_p}\left(\mathbb{E}\left[\bar{\mathbf{h}}\bar{\mathbf{h}}^H\right] + N_0\mathbf{I}\right) \\
&= \hat{\mathbf{h}}\hat{\mathbf{h}}^{\mathbf{H}} + \frac{N_0}{N_p}\mathbf{I} \\
&\quad + \frac{1}{N_p}\left(\hat{\mathbf{h}}_{\mathbf{b}}\hat{\mathbf{h}}_{\mathbf{b}}^{\mathbf{H}} + \frac{1}{N_p}\left(E\left[\mathbf{h}\mathbf{h}^H\right] + N_0\mathbf{I}_{N_R}\right)\right) \\
&= \left(1 + \frac{1}{N_p^2} + \cdots\right)\hat{\mathbf{h}}_1\hat{\mathbf{h}}_1^H \\
&\quad + \left(\frac{1}{N_p} + \frac{1}{N_p^3} + \cdots\right)\hat{\mathbf{h}}_2\hat{\mathbf{h}}_2^H \\
&\quad + \left(\frac{1}{N_p} + \frac{1}{N_p^2} + \cdots\right)N_0\mathbf{I}_{N_R} \\
&= \frac{N_p^2}{N_p^2-1}\hat{\mathbf{h}}_1\hat{\mathbf{h}}_1^H + \frac{N_p}{N_p^2-1}\hat{\mathbf{h}}_{\mathbf{2}}\hat{\mathbf{h}}_{\mathbf{2}}^{\mathbf{H}} + \frac{1}{N_p-1}N_0\mathbf{I}_{N_R}.
\end{aligned}$$

Similarly, we can show that the conditional expectations related to the interfering channel and the residual matrix are given by

$$\mathbb{E}\left[\mathbf{h}_b\mathbf{h}_b^H\right] = \frac{N_p^2}{N_p^2-1}\hat{\mathbf{h}}_b\hat{\mathbf{h}}_b^H + \frac{\hat{\mathbf{h}}\hat{\mathbf{h}}^H}{N_p-1} + \frac{N_0\mathbf{I}}{N_p-1}$$

$$\mathbb{E}\left[\hat{\mathbf{V}}\hat{\mathbf{V}}^H\right] = \frac{N_p^2(\hat{\mathbf{h}}_b\hat{\mathbf{h}}_b^H)}{N_p^2-1} + \frac{N_p(\hat{\mathbf{h}}\hat{\mathbf{h}}^H)}{N_p^2-1} + N_0\mathbf{I}.$$

A.3 Derivation of OPT in (5.28)

We first rewrite the system model into a compact form. The received symbol matrices are given by

$$\begin{cases} \mathbf{Y}_p &= \mathbf{H}\mathbf{X}_p + \alpha\bar{\mathbf{H}}\bar{\mathbf{p}}\bar{\mathbf{X}}_{d1} + \mathbf{Z}_p \\ \mathbf{Y}'_p &= \mathbf{H}\mathbf{p}\mathbf{X}_{d1} + \alpha\bar{\mathbf{H}}\bar{\mathbf{p}}\bar{\mathbf{X}}_p + \mathbf{Z}'_p \\ \mathbf{y} &= \mathbf{H}\mathbf{p}x + \alpha\bar{\mathbf{H}}\bar{\mathbf{p}}\bar{x} + \mathbf{z}_{d1} \end{cases},$$

where $\mathbf{y} \in \mathscr{C}^{N_R}$ is the vector of $\mathbf{Y}_{d1}$, x is the signal of interest from the data matrix $\mathbf{X}_1$ and $\mathbf{z}_{d1}$ is the AWGN vector. We further define $\mathscr{Y} \triangleq (\mathbf{Y}_p, \mathbf{Y}'_p, \mathbf{y})$, $\mathscr{Z} = (\mathbf{Z}_p, \mathbf{Z}'_p, \mathbf{z}_{d1})$, $\mathscr{H} = (\mathbf{H}, \alpha\bar{\mathbf{H}})$ and

$$\mathscr{X} \triangleq \begin{bmatrix} \mathbf{X}_p & \mathbf{X}_{d1} & \mathbf{p}x \\ \mathbf{p}\bar{\mathbf{X}}_{d1} & \bar{\mathbf{p}}\bar{\mathbf{X}}_p & \bar{\mathbf{p}}\bar{x} \end{bmatrix}.$$

Then we can rewrite the received matrices as:

$$\mathscr{Y} = \mathscr{H}\mathscr{X} + \mathscr{Z}.$$

Since $\mathscr{Z}$ is still the circularly symmetric complex Gaussian, we have the conditional probability $P(\mathscr{Y}|\mathscr{X},\mathscr{H})$ as follows:

$$P(\mathscr{Y}|\mathscr{X},\mathscr{H}) = \frac{\exp(-\|\mathscr{Y} - \mathscr{H}\mathscr{X}\|^2/N_0)}{(\pi N_0)^{N_R(2N_p+1)}}.$$

We define $\mathrm{vec}(\mathscr{H}) \sim \mathscr{N}_c(\mathbf{0}, \Sigma)$ because both channel matrices $\mathbf{H}$ and $\bar{\mathbf{H}}$ are complex Gaussian matrices. Then taking the average of $\mathscr{H}$ by using the Gaussian integral [23], we have

$$\begin{aligned} P(\mathscr{Y}|\mathscr{X}) &= \mathbb{E}_{\mathscr{H}}\left[P(\mathscr{Y}|\mathscr{X},\mathscr{H})\right] \\ &= \frac{\exp(\mathbf{b}^H\Sigma^{-1}\mathbf{A}^{-1}\mathbf{b} - \|\mathbf{Y}\|^2/N_0)]}{(\pi N_0)^{(2N_p+1)N_R}\det(\mathbf{A})}, \end{aligned}$$

where

$$\begin{aligned}\mathbf{A} &= \mathbf{I}_{2N_TN_R} + \Sigma\left(\left(\mathscr{X}\mathscr{X}^H/N_0\right)^T \otimes \mathbf{I}_{N_R}\right)\\ \mathbf{b} &= \Sigma\mathrm{vec}(\mathscr{Y}\mathscr{X}^H/N_0)\\ \Sigma &= \begin{bmatrix} 1 & 0\\ 0 & \alpha^2\end{bmatrix} \otimes \mathbf{I}_{N_TN_R}.\end{aligned}$$

Based on this fact, the OPT metric can be expressed as follows:

$$\begin{aligned}\hat{x} &= \arg\max_x \log P(x|\mathbf{y},\mathbf{Y}_p,\mathbf{Y}'_p,\mathbf{X}_p,\bar{\mathbf{X}}_p,\alpha,\mathbf{p},\bar{\mathbf{p}})\\ &= \arg\max_x \log \mathbb{E}_{\mathbf{X}_{d1},\bar{\mathbf{X}}_{d1},\bar{x}}[P(\mathscr{Y}|\mathscr{X})]\\ &= \arg\max_x \log \sum_{\mathbf{X}_{d1}}\sum_{\bar{\mathbf{X}}_{d1}}\sum_{\bar{x}} \frac{\exp(\mathbf{b}^H\Sigma^{-1}\mathbf{A}^{-1}\mathbf{b})}{\det(\mathbf{A})}\end{aligned}$$

where we apply the law of iterated expectations to add the lacking random variables in the conditional set.

A.4 SINR analysis of (5.36)

Assuming that perfect channel estimation and perfect covariance estimation are given, we derive three SINRs, one for each of the transmitted data matrices $\mathbf{X}_1$, $\mathbf{X}_2$, and $\mathbf{X}_3$. First of all, the resulting output of the conventional IRC on $\mathbf{X}_1$ is

$$\begin{aligned}\hat{x}_{1,irc} &= \mathbf{w}_{irc}^H\mathbf{y}_{d1}\\ &= \mathbf{w}_{irc}^H\mathbf{h}x_1 + \mathbf{w}_{irc}^H\bar{\mathbf{h}}\bar{x}_{d2} + \mathbf{w}_{irc}^H\mathbf{z}_{d1}\\ &\triangleq \beta x_1 + \omega_1\end{aligned}$$

where $\hat{x}_{1,irc}$, $\mathbf{y}_{d1}$, x_1, $\bar{x}_{d1}$, and $\mathbf{z}_p$ are the column elements of $\hat{\mathbf{X}}_{1,irc}$, $\mathbf{Y}_{d1}$, $\mathbf{X}_1$, $\bar{\mathbf{X}}_{d2}$, and $\mathbf{Z}_{d1}$, respectively. Next, we derive the average power of βx_1 and ω_1 by their variances,

$$\begin{aligned}\mathrm{var}(\beta x_1) &= \beta^2\mathscr{E}_d\\ \mathrm{var}(\omega_1) &= (\beta-\beta^2)\mathscr{E}_d.\end{aligned}$$

Therefore, the SINR of $\mathbf{X}_1$ is obtained as:

$$\mathrm{SINR}_{x_1} = \frac{\mathrm{var}(\beta x_1)}{\mathrm{var}(\omega_1)} = \frac{\beta^2}{\beta(1-\beta)}.$$

Following the same process, we derive the SINR of $\mathbf{X}_2$

$$\hat{x}_{2,irc} = \mathbf{w}_{irc}^H \mathbf{y}_{d2} \triangleq \beta x_2 + \omega_2$$

and their variances are

$$\begin{aligned}
\mathrm{var}(\beta x_2) &= \beta^2 \mathscr{E}_d \\
\mathrm{var}(\omega_2) &= \mathbf{w}_{irc}^H (\alpha^2 \mathscr{E}_p \bar{\Psi}_{p1} + N_0 \mathbf{I}) \mathbf{w}_{irc} \\
&= (\beta - \beta^2)\mathscr{E}_d + \alpha^2 \mathscr{E}_p \mathbf{w}_{irc}^H \bar{\Psi}_{p1} \mathbf{w}_{irc} \\
&\quad - \mathscr{E}_d \mathbf{w}_{irc}^H \bar{\mathbf{h}} \bar{\mathbf{h}}^H \mathbf{w}_{irc} \\
&\triangleq (\beta - \beta^2)\mathscr{E}_d + \mathscr{E}_p \phi_1 - \mathscr{E}_d \phi_2,
\end{aligned}$$

where $\mathbf{y}_{d2}$ and $\hat{x}_{2,irc}$ are the column of $\mathbf{Y}_{d2}$ and the column of the estimate of $\mathbf{X}_2$. Thus, the SINR of $\mathbf{X}_2$ is obtained by

$$\mathrm{SINR}_{x_2} = \frac{\beta^2}{\beta(1-\beta) + \frac{\mathscr{E}_p}{\mathscr{E}_d}\phi_1 - \phi_2}$$

The residual interference $(\mathscr{E}_p/\mathscr{E}_d)\phi_1 - \phi_2$ is due to the covariance mismatch between the weighting vector $\mathbf{w}_{irc}$ and the covariance matrix of $\mathbf{y}_{d2}$. To get more insight, we first define $\mathbf{R}^{-1} = \bar{\mathbf{h}}\bar{\mathbf{h}}^H + (N_0/\mathscr{E}_d)\mathbf{I}$ and then rewrite $\mathbf{w}_{irc}^H$ as:

$$\mathbf{w}_{irc}^H = \mathbf{h}^H \left(\mathbf{R} - \frac{\mathbf{R}\mathbf{h}\mathbf{h}^H\mathbf{R}}{1 + \mathbf{h}^H\mathbf{R}\mathbf{h}}\right).$$

Substituting this form into ϕ_1 and ϕ_2, we have

$$\begin{aligned}
\phi_1 &= \frac{\mathbf{h}^H \mathbf{R} \Psi_{p1} \mathbf{R}\mathbf{h}}{|1 + \mathbf{h}^H \mathbf{R}\mathbf{h}|^2} = \frac{|\mathbf{h}^H \mathbf{R} \bar{\mathbf{h}}_{p1}|^2}{|1 + \mathbf{h}^H \mathbf{R}\mathbf{h}|^2} \\
&= \xi^2 \cdot \left| \mathbf{h}^H \left[\left(\frac{N_0}{\mathscr{E}_d} + \bar{\mathbf{h}}^H \bar{\mathbf{h}} \right) \mathbf{I} - \bar{\mathbf{h}}\bar{\mathbf{h}}^H \right] \bar{\mathbf{h}}_{p1} \right|^2 \\
&= \xi^2 \cdot \left| \mathbf{h}^H \bar{\mathbf{h}}_{p1} \frac{N_0}{\mathscr{E}_d} + \bar{\mathbf{h}}^H \bar{\mathbf{h}} \mathbf{h}^H \bar{\mathbf{h}}_{p1} - \mathbf{h}^H \bar{\mathbf{h}} \bar{\mathbf{h}}^H \bar{\mathbf{h}}_{p1} \right|^2,
\end{aligned}$$

and

$$\begin{aligned}\phi_2 &= \frac{|\mathbf{h}^H\mathbf{R}\bar{\mathbf{h}}|^2}{|1+\mathbf{h}^H\mathbf{R}\mathbf{h}|^2} \\ &= \xi^2 \cdot \left|\mathbf{h}^H\left[\left(\frac{N_0}{\mathscr{E}_d}+\bar{\mathbf{h}}^H\bar{\mathbf{h}}\right)\mathbf{I}-\bar{\mathbf{h}}\bar{\mathbf{h}}^H\right]\bar{\mathbf{h}}\right|^2 \\ &= \xi^2 \cdot \left|\frac{N_0}{\mathscr{E}_d}\mathbf{h}^H\bar{\mathbf{h}}\right|^2,\end{aligned}$$

where $\bar{\Psi}_{p1} = \bar{\mathbf{h}}_{p1}\bar{\mathbf{h}}_{p1}^H$ by the Cholesky decomposition and

$$\begin{aligned}\xi &= \left|1+\mathbf{h}^H\mathbf{R}\mathbf{h}\right|^{-1}\left|\frac{N_0^2}{\mathscr{E}_d^2}+\frac{N_0}{\mathscr{E}_d}\cdot\bar{\mathbf{h}}^H\bar{\mathbf{h}}\right|^{-1} \\ &= \left|\left(\frac{N_0}{\mathscr{E}_d}\right)^2+\left(\frac{N_0}{\mathscr{E}_d}\right)\left(\bar{\mathbf{h}}^H\bar{\mathbf{h}}+\mathbf{h}^H\mathbf{h}\right)\right|^{-1}.\end{aligned}$$

To obtain above results, we need to rewrite $\mathbf{R}$ by the Sherman-Morrison formula, that is

$$\begin{aligned}\mathbf{R} &= \left(\bar{\mathbf{h}}\bar{\mathbf{h}}^H+\frac{N_0}{\mathscr{E}_d}\mathbf{I}\right)^{-1} = \frac{\mathscr{E}_d}{N_0}\mathbf{I}-\frac{\frac{\mathscr{E}_d}{N_0}\bar{\mathbf{h}}\bar{\mathbf{h}}^H\frac{\mathscr{E}_d}{N_0}}{1+\bar{\mathbf{h}}^H(\frac{\mathscr{E}_d}{N_0})\bar{\mathbf{h}}} \\ &= \left(\frac{N_0^2}{\mathscr{E}_d^2}+\frac{N_0}{\mathscr{E}_d}\bar{\mathbf{h}}^H\bar{\mathbf{h}}\right)^{-1}\left[\left(\frac{N_0}{\mathscr{E}_d}+\bar{\mathbf{h}}^H\bar{\mathbf{h}}\right)\mathbf{I}-\bar{\mathbf{h}}\bar{\mathbf{h}}^H\right].\end{aligned}$$

Therefore, the residual interference due to the covariance mismatch is obtained as follows:

$$\begin{aligned}\psi_1 &\triangleq \frac{\mathscr{E}_p}{\mathscr{E}_d}\phi_1-\phi_2 \\ &= \frac{\frac{\mathscr{E}_p}{\mathscr{E}_d}|\mathbf{h}^H\bar{\mathbf{h}}_{p1}|^2-|\bar{\mathbf{h}}^H\bar{\mathbf{h}}|^2}{1+|\bar{\mathbf{h}}^H\bar{\mathbf{h}}+\mathbf{h}^H\mathbf{h}|^2+2\frac{N_0}{\mathscr{E}_d}(\bar{\mathbf{h}}^H\bar{\mathbf{h}}+\mathbf{h}^H\mathbf{h})} \\ &\quad+\frac{\mathscr{E}_p\mathscr{E}_d}{\mathscr{E}_d N_0}\left(\frac{2\Re\left[\bar{\mathbf{h}}_{p1}^H\mathbf{h}(\bar{\mathbf{h}}^H\bar{\mathbf{h}}\mathbf{h}^H\bar{\mathbf{h}}_{p1}-\mathbf{h}^H\bar{\mathbf{h}}\bar{\mathbf{h}}^H\bar{\mathbf{h}}_{p1})\right]}{1+|\bar{\mathbf{h}}^H\bar{\mathbf{h}}+\mathbf{h}^H\mathbf{h}|^2+2\frac{N_0}{\mathscr{E}_d}(\bar{\mathbf{h}}^H\bar{\mathbf{h}}+\mathbf{h}^H\mathbf{h})}\right) \\ &\quad+\frac{\mathscr{E}_p\mathscr{E}_d^2}{\mathscr{E}_d N_0^2}\left(\frac{|\bar{\mathbf{h}}^H\bar{\mathbf{h}}\mathbf{h}^H\bar{\mathbf{h}}_{p1}-\mathbf{h}^H\bar{\mathbf{h}}\bar{\mathbf{h}}^H\bar{\mathbf{h}}_{p1}|^2}{1+|\bar{\mathbf{h}}^H\bar{\mathbf{h}}+\mathbf{h}^H\mathbf{h}|^2+2\frac{N_0}{\mathscr{E}_d}(\bar{\mathbf{h}}^H\bar{\mathbf{h}}+\mathbf{h}^H\mathbf{h})}\right).\end{aligned}$$

Suppose $\mathscr{E}_d \gg N_0$, then we can simplify further,

$$\psi_1 \approx \frac{\mathscr{E}_p\mathscr{E}_d^2}{\mathscr{E}_d N_0^2}\left(\frac{\left|\bar{\mathbf{h}}^H\bar{\mathbf{h}}\mathbf{h}^H\bar{\mathbf{h}}_{p1}-\mathbf{h}^H\bar{\mathbf{h}}\bar{\mathbf{h}}^H\bar{\mathbf{h}}_{p1}\right|^2}{1+|\bar{\mathbf{h}}^H\bar{\mathbf{h}}+\mathbf{h}^H\mathbf{h}|^2}\right)$$

$$= \frac{\mathscr{E}_p}{\mathscr{E}_d} \cdot \left(\frac{\mathscr{E}_d}{N_0}\right)^2 \cdot \frac{\alpha^6 \zeta_1}{\alpha^4 \zeta_2 + \alpha^4 \zeta_3 + \zeta_4} \geq 0$$
$$\propto \frac{\mathscr{E}_p}{\mathscr{E}_d} \cdot \mathrm{SNR}^2 \cdot \alpha^2$$

where we have the variable α from the interfering channel vectors $\bar{\mathbf{h}}$ and $\bar{\mathbf{h}}_{p1}$, and $\{\zeta_1, \zeta_2, \zeta_3, \zeta_4\}$ are defined for the rest terms we are not interested in. Finally, The SINR of $\mathbf{X}_3$ is obtained as follows:

$$\mathrm{SINR}_{x_3} = \frac{\beta^2}{\beta(1-\beta) + \psi_2}$$

where ψ_2 can be obtained by using $\bar{\mathbf{h}}_{p2}$ from $\bar{\Psi}_{p2} = \bar{\mathbf{h}}_{p2}\bar{\mathbf{h}}_{p2}^H$. Following the same process of SINR_{x_2}, we can have the same result that $\psi_2 \propto (\mathscr{E}_p/\mathscr{E}_d) \cdot \mathrm{SNR}^2 \cdot \alpha^2$.

A.5 Proof of Lemma 5.2.1

The details of the covariance estimation errors are given by

$$\Delta_k = \mathbf{R}_k - \frac{1}{N} \sum_{m \in \mathscr{P}} \left(\hat{\mathbf{v}}_m \hat{\mathbf{v}}^H\right) \triangleq \Delta_1 + \Delta_2 - \Delta_3,$$

Where we separate the whole term into three parts

$$\Delta_1 \triangleq \bar{\mathbf{h}}_k \bar{\mathbf{h}}_k^H - \frac{1}{N} \sum_{m \in \mathscr{P}} \bar{\mathbf{h}}_m \bar{\mathbf{x}}_m \bar{\mathbf{x}}_m^H \bar{\mathbf{h}}_m^H$$
$$\Delta_2 \triangleq N_0 \mathbf{I} - \frac{1}{N} \sum_{m \in \mathscr{P}} \mathbf{z}_m \mathbf{z}_m^H$$
$$\Delta_3 \triangleq \frac{1}{N} \sum_{m \in \mathscr{P}} \bar{\mathbf{h}}_m \bar{x}_m \mathbf{z}_m^H + \mathbf{z}_m \bar{x}_m^H \bar{\mathbf{h}}_m^H$$

Take an expectation of the estimation error matrix Δ_k

$$\mathbb{E}[(\Delta_k)_{pq}] = \left(\bar{\mathbf{h}}_k \bar{\mathbf{h}}_k^H - \frac{1}{N} \sum_{m \in \mathscr{P}} \left(\bar{\mathbf{h}}_m \bar{\mathbf{h}}_m^H\right)\right)_{pq}$$

The entry-wise variance of Δ_k can be obtained by ignoring some cross terms as follows.

$$var((\Delta_k)_{pq}) \approx var((\Delta_1)_{pq}) + var((\Delta_2)_{pq}) + var((\Delta_3)_{pq})$$

The first term is related to the true covariance matrix of interference:

$$
\begin{aligned}
&var((\Delta_1)_{pq}) \\
&= \frac{1}{N^2} \sum_{m \in \mathscr{P}} |(\bar{\mathbf{h}}_m \bar{\mathbf{h}}_m^H)_{pq}|^2 \times \begin{cases} 0 & \text{, PSK} \\ 0.32 & \text{, 16 QAM} \\ 0.3810 & \text{, 64 QAM} \end{cases}
\end{aligned}
$$

The second term is related to AWGN:

$$
\begin{aligned}
&var((\Delta_2)_{pq}) \\
&= \frac{1}{N} \begin{cases} var(|(\mathscr{R}((\mathbf{z}_m)_p) + \mathscr{I}((\mathbf{z}_m)_p)|^2) & p = q \\ var((\mathbf{z}_m)_p) var((\mathbf{z}_m)_q^H) & p \neq q \end{cases} \\
&= N_0^2 / N
\end{aligned}
$$

The last term is the mixture of interference and AWGN:

$$
var((\Delta_3)_{pq}) = \frac{N_0}{N^2} \sum_{m \in \mathscr{P}} \left(|(\bar{\mathbf{h}}_m)_p|^2 + |(\bar{\mathbf{h}}_m)_q|^2 \right),
$$

where we have to assume $\mathbb{E}[\bar{x}_m \bar{x}_m] = 0$. This equity holds if $\bar{x}$ is modulated with M-QAM or M-PSK modulation ($M \neq 2$).

A.6 Proof of Lemma 5.2.2

Based on the definition of the Frobenius norm, the MSE of Δ_k is obtained by the sum of entry-wise means' squares and entry-wise variances

$$
\mathbb{E}[\|\Delta_k\|_F^2] = \sum_{pq} \left(var((\Delta_k)_{pq}) + |\mathbb{E}[(\Delta_k)_{pq}]|^2 \right)
$$

Taking an average of the time-domain channel impulse response, we have the results as follows:

$$
\begin{aligned}
&\mathbb{E}\left[|\mathbb{E}[(\Delta_k)_{pq}] |^2 \right] \\
&= \Upsilon \cdot \mathbb{E}\left[\text{vec}(\bar{\mathbf{a}}_p \bar{\mathbf{a}}_q) \text{vec}(\bar{\mathbf{a}}_p \bar{\mathbf{a}}_q)^H \right] \cdot \Upsilon^H = \frac{\alpha^4}{L^2} \Upsilon \Upsilon^H
\end{aligned}
$$

and

$$\begin{aligned}&\mathbb{E}\left[var((\Delta_k)_{pq})\right]\\&\approx\begin{cases}\left(2\cdot\alpha^4\Psi+2\cdot\alpha^2N_0+N_0^2\right)/N, & p=q\\\left(\alpha^4\Psi+2\cdot\alpha^2N_0+N_0^2\right)/N, & p\neq q\end{cases}\end{aligned}$$

where we define

$$\Upsilon\triangleq\left((\mathbf{F}_k^H)^T\otimes\mathbf{F}_k\right)-\frac{1}{N}\sum_{m\in\mathscr{P}}\left((\mathbf{F}_m^H)^T\otimes\mathbf{F}_m\right)$$

A.7 Proof of Lemma 5.2.3

The original SINR maximization is equivalent to the form with $\mathbf{h}_k\mathbf{h}_k^H+\mathbf{R}_k$ instead of $\mathbf{R}_k$

$$\max\text{SINR}_k=\max\frac{|\mathbf{w}_k^H\mathbf{h}_k|^2}{\mathbf{w}_k^H(\mathbf{h}_k\mathbf{h}_k^H+\mathbf{R}_k)\mathbf{w}_k},$$

where the equality holds because it is an increasing function of the SINR. We reform the problem by substituting the covariance estimation and its estimation errors $\mathbf{R}_k=\hat{\mathbf{R}}_k+\Delta_k$

$$\begin{aligned}&\arg\min_{\mathbf{w}_k}\max_{\Delta_k}\mathbf{w}_k^H(\mathbf{h}_k\mathbf{h}_k^H+\hat{\mathbf{R}}_k+\Delta_k)\mathbf{w}_k\\&\text{s.t. }\mathbf{w}_k^H\mathbf{h}_k=1,\|\Delta_k\|\leq\epsilon_k.\end{aligned}$$

Since Δ_k is a Hermitian matrix, we have the simplified form

$$\max_{\|\Delta_k\|\leq\epsilon_k}\mathbf{w}_k^H\Delta_k\mathbf{w}_k=\epsilon_k\mathbf{w}_k^H\mathbf{w}_k.$$

Thus, by defining $\mathbf{R}_k^*=\mathbf{h}_k\mathbf{h}_k^H+\hat{\mathbf{R}}_k+\epsilon_k\mathbf{I}$, we have the optimal solution of $\mathbf{w}_k$ as:

$$\begin{aligned}\mathbf{w}_k^*&=\mathbf{R}_k^{*-1}\mathbf{h}_k\cdot(\mathbf{h}_k^H\mathbf{R}_k^{*-1}\mathbf{h}_k)^{-1}\approx\mathbf{R}_\mathbf{k}^{*-1}\mathbf{h}_\mathbf{k}\\&=\left(\mathbf{h}_k\mathbf{h}_k^H+\hat{\mathbf{R}}_k+\epsilon_k\mathbf{I}\right)^{-1}\mathbf{h}_k\end{aligned}$$

Here we omit the immaterial constant.

A.8 Derivation of SINR in (5.59)

Suppose the perfect CSI and the perfect covariance estimation are given. The signal power of serving and interfering symbols is defined by $\mathbb{E}[x_i^H x_i] = 1$ for $i = 1,2,3$. We write the resulting output of IRC($\mathbf{u}_1$) as follows:

$$\hat{x}_1 \triangleq \text{IRC}(\mathbf{u}_1) \tag{A.1}$$

$$= \underbrace{\tilde{\mathbf{g}}_1^H \tilde{\mathbf{h}}_1 x_1}_{\triangleq \beta_1 x_1} + \underbrace{\tilde{\mathbf{g}}_1^H \tilde{\mathbf{h}}_2 x_2 + \tilde{\mathbf{g}}_1^H \tilde{\mathbf{h}}_3 x_3 + \tilde{\mathbf{g}}^H \tilde{\mathbf{z}}}_{\triangleq \omega_1}, \tag{A.2}$$

where $\tilde{\mathbf{h}}_1 \triangleq \mathbf{W}^H \mathbf{H}_1 \mathbf{p}_1$, $\tilde{\mathbf{h}}_i \triangleq \mathbf{W}^H \alpha_i \mathbf{H}_i \mathbf{p}_i$, for $i = 2,3$ denote the equivalent channel matrices after preprocessing of $\mathbf{W}$, $\tilde{\mathbf{g}}_1^H = \tilde{\mathbf{h}}_1^H (\tilde{\mathbf{h}}_1 \tilde{\mathbf{h}}_1^H + \tilde{\mathbf{h}}_2 \tilde{\mathbf{h}}_2^H + \tilde{\mathbf{h}}_3 \tilde{\mathbf{h}}_3^H + N_0 \mathbf{W}^H \mathbf{W})^{-1}$, and $\tilde{\mathbf{z}} = \mathbf{W}^H \mathbf{z}$. Next, we derive the variance of the interference-plus-noise term ω_1

$$\begin{aligned} \sigma_{\omega_1}^2 &= \tilde{\mathbf{g}}_1^H (\tilde{\mathbf{h}}_1 \tilde{\mathbf{h}}_1^H + \tilde{\mathbf{h}}_2 \tilde{\mathbf{h}}_2^H + \tilde{\mathbf{h}}_3 \tilde{\mathbf{h}}_3^H + N_0 \mathbf{W}^H \mathbf{W}) \tilde{\mathbf{g}}_1 \\ &\quad - \tilde{\mathbf{g}}_1^H (\tilde{\mathbf{h}}_1 \tilde{\mathbf{h}}_1^H) \tilde{\mathbf{g}}_1 = \beta_1 (1 - \beta_1). \end{aligned}$$

Using the Sherman-Morrison formula and $\mathbf{R} = (\tilde{\mathbf{h}}_2 \tilde{\mathbf{h}}_2^H + \tilde{\mathbf{h}}_3 \tilde{\mathbf{h}}_3^H + N_0 \mathbf{W}^H \mathbf{W})^{-1}$, we have

$$\begin{aligned} \beta_1 &= \tilde{\mathbf{h}}_1^H (\mathbf{R}^{-1} + \tilde{\mathbf{h}}_1 \tilde{\mathbf{h}}_1^H) \tilde{\mathbf{h}}_1 \\ &= \tilde{\mathbf{h}}_1^H \left(\mathbf{R} - \frac{\mathbf{R} \tilde{\mathbf{h}}_1 \tilde{\mathbf{h}}_1^{\mathbf{H}} \mathbf{R}}{\mathbf{1} + \tilde{\mathbf{h}}_1^{\mathbf{H}} \mathbf{R} \tilde{\mathbf{h}}_1} \right) \tilde{\mathbf{h}}_1 = \frac{\tilde{\mathbf{h}}_1^H \mathbf{R} \tilde{\mathbf{h}}_1}{1 + \tilde{\mathbf{h}}_1^H \mathbf{R} \tilde{\mathbf{h}}_1}. \end{aligned}$$

Finally, the SINR can be shown to be:

$$\text{SINR}(\text{IRC}(\mathbf{u}_1)) = \mathbf{h}_1^H \mathbf{W} (\mathbf{W}^H \Sigma_v \mathbf{W})^{-1} \mathbf{W}^H \mathbf{h}_1, \tag{A.3}$$

where $\Sigma_v = \mathbf{h}_2 \mathbf{h}_2^H + \mathbf{h}_3 \mathbf{h}_3^H + N_0 \mathbf{I}$.

A.9 The optimal pre-processing matrix of (5.62)

The matrix inverse can be derived as:

$$(\mathbf{W}^H \Sigma_v \mathbf{W})^{-1} = \begin{bmatrix} \mathbf{w}_1^H \Sigma_v \mathbf{w}_1 & \mathbf{w}_1^H \Sigma_v \mathbf{w}_2 \\ \mathbf{w}_2^H \Sigma_v \mathbf{w}_1 & \mathbf{w}_2^H \Sigma_v \mathbf{w}_2 \end{bmatrix}^{-1} \tag{A.4}$$

$$\approx \begin{bmatrix} 1/\mathbf{w}_1^H \Sigma_v \mathbf{w}_1 & 0 \\ 0 & 1/\mathbf{w}_2^H \Sigma_v \mathbf{w}_2 \end{bmatrix}, \tag{A.5}$$

where $\mathbf{w}_k \in \mathscr{C}^{N_r+N_a}$ is the kth column of $\mathbf{W}$ and we ignore the cross terms between $\mathbf{w}_1$ and $\mathbf{w}_2$. Applying the approximation, i.e., $\mathbf{w}_1^H \Sigma_v \mathbf{w}_2 \approx 0$, we can rewrite the original problem as follows:

$$\max_{\mathbf{W}\neq\mathbf{0}} \mathbf{h}_1^H \mathbf{W} (\mathbf{W}^H \Sigma_v \mathbf{W})^{-1} \mathbf{W}^H \mathbf{h}_1 \tag{A.6}$$

$$\approx \max_{\mathbf{w}_k\neq\mathbf{0}} \frac{|\mathbf{h}_1^H \mathbf{w}_k|^2}{\mathbf{w}_k^H \Sigma_v \mathbf{w}_k}, \text{ for } k = 1,2 \tag{A.7}$$

$$= \max_{\mathbf{w}_k\neq\mathbf{0}} \frac{|\mathbf{h}_1^H \mathbf{w}_k|^2}{\mathbf{w}_k^H \Sigma_y \mathbf{w}_k}, \text{ for } k = 1,2 \tag{A.8}$$

where $\Sigma_y = \mathbf{h}_1 \mathbf{h}_1^H + \Sigma_v$ and the equality holds because it is an increasing function of the SINR. In order to find two meaningful pre-processing $\mathbf{w}_1$ and $\mathbf{w}_2$, we drop the precoding vector $\mathbf{p}_1$ and find $\mathbf{w}_k$ with respect to the kth column of $\mathbf{H}_1$

$$\max_{\mathbf{w}_k\neq\mathbf{0}} \frac{|(\mathbf{H}_1)_k^H \mathbf{w}_k|^2}{\mathbf{w}_k^H \Sigma_y \mathbf{w}_k}, \text{ for } k = 1,2 \tag{A.9}$$

The problem is equivalent to the following form

$$\arg\min_{\mathbf{w}_k} \mathbf{w}_k^H \Sigma_y \mathbf{w}_k \tag{A.10}$$

$$\text{s.t. } \mathbf{w}_k^H (\mathbf{H}_1)_k = 1 \tag{A.11}$$

The $Lagrangian\, L : \mathscr{C}^{N_r+N_a} \times \mathscr{C} \rightarrow \mathscr{R}$ is defined as

$$L(\mathbf{w}_k, \lambda) = \mathbf{w}_k^H \Sigma_y \mathbf{w}_k + \frac{\lambda^H}{2}(\mathbf{w}_k^H (\mathbf{H}_1)_k - 1) + \frac{\lambda}{2}((\mathbf{H}_1)_k^H \mathbf{w}_k - 1)$$

We differentiate $L(\mathbf{w}_k, \lambda)$ with respect to $\mathbf{w}_k^H$ and λ; setting these partial derivatives equal to zero, we have

$$\frac{\partial L}{\partial \mathbf{w}_k^H} = \Sigma_y \mathbf{w}_k + \frac{\lambda}{2}(\mathbf{H}_1)_k \rightarrow 0$$

$$\hat{\mathbf{w}}_k = -\Sigma_y^{-1} (\mathbf{H}_1)_k \frac{\lambda}{2}.$$

Imposing the constraint $(\mathbf{H}_1)_k^H \hat{\mathbf{w}}_k = 1$, then

$$\lambda^* = -2((\mathbf{H}_1)_k^H \Sigma_v^{-1} (\mathbf{H}_1)_k)^{-1}.$$

Therefore, the optimal solution of $\mathbf{w}_k$ is given by

$$\hat{\mathbf{w}}_k = \Sigma_y^{-1}(\mathbf{H}_1)_k \cdot ((\mathbf{H}_1)_k^H \Sigma_y^{-1}(\mathbf{H}_1)_k)^{-1} \tag{A.12}$$

$$\approx \Sigma_y^{-1}(\mathbf{H}_1)_k \tag{A.13}$$

Here we omit the immaterial constant.

A.10 Optimal codebook of (5.68)

We evaluate the average loss of the quantized solutions by

$$\mathscr{W} = \arg\min_{\mathscr{W}'} \mathbb{E}_B \left[\lambda_{min}^2(\mathbf{W}_{un}\mathbf{B}) - \min_{\mathbf{W}_j \in \mathscr{W}'} \lambda_{min}^2(\mathbf{W}_j\mathbf{B}) \right].$$

This formulation means finding the subset $\mathscr{W}$ in order to minimize the average loss between the unquantized solution $\mathbf{W}_{un}$ and the best quantized solution $\mathbf{W}_j$ in the set $\mathscr{W}$. The argument of the average loss can be further derived as follows:

$$\begin{aligned}
&\mathbb{E}\left[\lambda_{min}^2(\bar{\mathbf{U}}_b^H\mathbf{B})\right] - \mathbb{E}\left[\min_{\mathbf{W}_j} \lambda_{min}^2(\mathbf{W}_j\mathbf{B})\right] \\
&\overset{(a)}{\leq} \mathbb{E}\left[\lambda_{min}^2(\mathbf{B})\right] - \mathbb{E}\left[\min_{\mathbf{W}_j} \lambda_{min}^2(\mathbf{W}_j\bar{\mathbf{U}}_b\bar{\Sigma}_b)\right] \\
&\overset{(b)}{\leq} \mathbb{E}\left[\lambda_{min}^2(\mathbf{B})\right] - \mathbb{E}\left[\lambda_{min}^2(\mathbf{B})\right]\mathbb{E}\left[\min_{\mathbf{W}_j} \lambda_{min}^2(\mathbf{W}_j\bar{\mathbf{U}}_b)\right] \\
&\triangleq \mathbb{E}\left[\lambda_{min}^2(\mathbf{B})\right]\mathbb{E}\left[\min_{\mathbf{W}_j} \mathrm{d}_{proj}^2(\mathbf{W}_j^H, \bar{\mathbf{U}}_b)\right],
\end{aligned}$$

where (a) follows from zeroing the two largest singular values of $\mathbf{B}$, and $\bar{\Sigma}_b$ denotes the singular values corresponding to $\bar{\mathbf{U}}_b$. In (b), it follows by substituting λ_{min} for the other nonzero singular values in (a) and follows from the fact that singular values and singular vectors of complex normal matrices are independent. The projection distance between the matrices $\mathbf{F}_1$ and $\mathbf{F}_2$ is denoted by $\mathrm{d}_{proj}(\mathbf{F}_1, \mathbf{F}_2)$. As a result, the optimal codebook can be obtained by

$$\mathscr{W} = \arg\min_{\mathscr{W}'} \mathbb{E}\left[\min_{\mathbf{W}_j \in \mathscr{W}'} \mathrm{d}_{proj}^2(\mathbf{W}_j^H, \bar{\mathbf{U}}_b)\right]. \tag{A.14}$$

Note that we now have an equivalent problem to that treated in [38], that is finding a quantized codebook which minimizes the subspace distance between the best codeword and a random matrix.

References

[1] H. Bölcskei, "MIMO-OFDM wireless systems: basics, perspectives, and challenges," *IEEE Trans. Wireless Commun.*, vol. 13, no. 4, pp. 31–37, 2006.

[2] D. Tse and P. Viswanath, *Fundamentals of Wireless Communication*. Cambridge University Press, 2005.

[3] D.-S. Shiu, G. J. Foschini, M. J. Gans, and J. M. Kahn, "Fading correlation and its effect on the capacity of multielement antenna systems," *IEEE Trans. Commun.*, vol. 48, no. 3, pp. 502–513, 2000.

[4] G. Foschini and M. Gans, "On limits of wireless communications in a fading environment when using multiple antennas," *Wireless Personal Communications*, vol. 6, pp. 311–335, 1998.

[5] W. Weichselberger, M. Herdin, H. Ozcelik, and E. Bonek, "A stochastic MIMO channel model with joint correlation of both link ends," *IEEE Trans. Wireless Commun.*, vol. 5, no. 1, pp. 90–100, 2006.

[6] A. M. Sayeed, "Deconstructing multiantenna fading channels," *IEEE Trans. Signal Processing*, vol. 50, no. 10, pp. 2563–2579, 2002.

[7] V. V. Veeravalli, Y. Liang, and A. M. Sayeed, "Correlated MIMO wireless channels: capacity, optimal signaling, and asymptotics," *IEEE Trans. Inform. Theory*, vol. 51, no. 6, pp. 2058–2072, 2005.

[8] X. Gao, B. Jiang, X. Li, A. B. Gershman, and M. R. McKay, "Statistical eigenmode transmission over jointly correlated MIMO channels," *IEEE Trans. Inform. Theory*, vol. 55, no. 8, pp. 3735–3750, 2009.

[9] Y.-C. Chen and Y. T. Su, "MIMO channel estimation in correlated fading environments," *IEEE Trans. Wireless Commun.*, vol. 9, no. 3, pp. 1108–1119, 2010.

[10] D. Yang, L.-L. Yang, and L. Hanzo, "DFT-based beamforming weight-vector codebook design for spatially correlated channels in the unitary precoding aided multiuser downlink," in *Proc. IEEE Int. Conf. on Communications (ICC)*, 2010.

[11] B. M. Hochwald, T. L. Marzetta, T. J. Richardson, W. Sweldens, and R. Urbanke, "Systematic design of unitary space-time constellations," *IEEE Trans. Inform. Theory*, vol. 46, no. 6, pp. 1962–1973, 2000.

[12] D. J. Love and R. W. Heath, "Limited feedback unitary precoding for spatial multiplexing systems," *IEEE Trans. Inform. Theory*, vol. 51, no. 8, pp. 2967–2976, 2005.

[13] R. A. Horn and C. R. Johnson, *Topics in matrix analysis*. Cambridge University Press New York, NY, USA, June 1994.

[14] J. Heath, R. W. and A. Paulraj, "Antenna selection for spatial multiplexing systems based on minimum error rate," in *Proc. IEEE Int. Conf. on Communications (ICC)*, 2001.

[15] G. Taricco and E. Biglieri, "Space-time decoding with imperfect channel estimation," *IEEE Trans. Wireless Commun.*, vol. 4, no. 4, pp. 1874–1888, 2005.

[16] G. Coluccia, E. Riegler, C. Mecklenbrauker, and G. Taricco, "Optimum MIMO-OFDM detection with pilot-aided channel state information," *IEEE Journal of Selected Topics in Signal Processing*, vol. 3, no. 6, pp. 1053–1065, 2009.

[17] S. Sadough, P. Piantanida, and P. Duhamel, "MIMO-OFDM optimal decoding and achievable information rates under imperfect channel estimation," in *Proc. IEEE Signal Processing Advances in Wireless Communications (SPAWC)*, 2007.

[18] B. S. Thian and A. Goldsmith, "Decoding for MIMO systems with correlated channel estimation errors," in *Proc. Allerton Conf. on Communication, Control, and Computing (Allerton)*, 2011.

[19] J. Park and J. Chun, "Improved lattice reduction-aided MIMO successive interference cancellation under imperfect channel estimation," *IEEE Trans. Signal Processing*, vol. 60, no. 6, pp. 3346–3351, 2012.

[20] C. Xiao, J. Wu, S.-Y. Leong, Y. R. Zheng, and K. B. Letaief, "A discrete-time model for triply selective MIMO Rayleigh fading channels," *IEEE Trans. Wireless Commun.*, vol. 3, no. 5, pp. 1678–1688, 2004.

[21] *Physical Channels and Modulation*, 3GPP TS 36.211 Std. V8.6.0, Mar. 2009.

[22] M. Clyde and E. I. George, "Model uncertainty," *Statistical Science*, vol. 19, no. 1, pp. pp. 81–94, 2004.

[23] G. Taricco, "Optimum receiver design and performance analysis of arbitrarily correlated Rician fading MIMO channels with imperfect channel state information," *IEEE Trans. Inform. Theory*, vol. 56, no. 3, pp. 1114–1134, 2010.

[24] D. Lopez-Perez, I. Guvenc, G. De la Roche, M. Kountouris, T. Quek, and J. Zhang, "Enhanced intercell interference coordination challenges in heterogeneous networks," *IEEE Trans. Wireless Commun.*, vol. 18, no. 3, pp. 22–30, 2011.

[25] D. Asztély and B. Ottersten, "MLSE and spatio-temporal interference rejection combining with antenna arrays," in *Proc. IEEE European Signal Processing Conference (Eusipco)*, 1998.

[26] J. Karlsson and J. Heinegard, "Interference rejection combining for GSM," in *Proc. Universal Personal Communications Conf.*, 1996.

[27] B. Bandemer, M. Haardt, and S. Visuri, "Linear MMSE multi-user MIMO downlink precoding for users with multiple antennas," in *Proc. IEEE Personal, Indoor and Mobile Radio Communications (PIMRC)*, 2006.

[28] M. Lampinen, F. Del Carpio, T. Kuosmanen, T. Koivisto, and M. Enescu, "System-level modeling and evaluation of interference suppression receivers in LTE system," in *Proc. IEEE Vehicular Technology Conf. (VTC)*, 2012.

[29] R. Narasimhan and S. Cheng, "Channel estimation and co-channel interference rejection for LTE-advanced MIMO uplink," in *Proc. IEEE Wireless Communications and Networking Conference (WCNC)*, 2012.

[30] N.-D. Dao, J. Soler-Garrido, R. Cepeda, Y. Sun, and W. H. Chin, "Design and evaluation of antenna selection methods for interference rejection combining," *IEEE Trans. Wireless Commun.*, vol. 11, pp. 2751–2759, 2012.

[31] X. Mestre and M.-A. Lagunas, "Finite sample size effect on minimum variance beamformers: optimum diagonal loading factor for large arrays," *IEEE Trans. Signal Processing*, vol. 54, no. 1, pp. 69–82, 2006.

[32] N. Ma and J. T. Goh, "Efficient method to determine diagonal loading value," in *Porc. IEEE International Conference on Acoustics, Speech, and Signal Processing (ICASSP)*, 2003.

[33] K. P. Murphy, "Naive Bayes classifiers," 2006.

[34] M. Escartin and P. Ranta, "Interference rejection with a small antenna array at the mobile scattering environment," in *Proc. Signal Processing Advances in Wireless Communications (SPAWC)*, april 1997.

[35] H. Minn, V. Bhargava, and K. Letaief, "A robust timing and frequency synchronization for OFDM systems," *IEEE Trans. Wireless Commun.*, vol. 2, no. 4, pp. 822–839, 2003.

[36] M. Speth, S. Fechtel, G. Fock, and H. Meyr, "Optimum receiver design for wireless broad-band systems using OFDM. I," *IEEE Trans. Commun.*, vol. 47, no. 11, pp. 1668–1677, 1999.

[37] D. Love, "Grassmannian subspace packing." [Online]. Available: https://engineering.purdue.edu/~djlove/grass.html

[38] D. Love and R. Heath, "Limited feedback unitary precoding for orthogonal space-time block codes," *IEEE Trans. Signal Processing*, vol. 53, pp. 64–73, 2005.

[39] C. Xiao, J. Wu, S.-Y. Leong, Y. Zheng, and K. Letaief, "A discrete-time model for triply selective MIMO rayleigh fading channels," *IEEE Trans. Wireless Commun.*, vol. 3, no. 5, pp. 1678–1688, 2004.

[40] A. Goldsmith, *Wireless communications*. Cambridge University Press, 2005.

[41] R. Mesleh, H. Haas, S. Sinanovic, C. W. Ahn, and S. Yun, "Spatial modulation," *IEEE Trans. Veh. Technol.*, vol. 57, no. 4, pp. 2228–2241, 2008.

[42] M. Di Renzo, H. Haas, and P. M. Grant, "Spatial modulation for multiple-antenna wireless systems: a survey," *IEEE Commun. Mag.*, vol. 49, no. 12, pp. 182–191, 2011.

[43] A. Mohammadi and F. Ghannouchi, "Single RF front-end MIMO transceivers," *IEEE Commun. Mag.*, vol. 49, no. 12, pp. 104–109, 2011.

[44] J. Jeganathan, A. Ghrayeb, L. Szczecinski, and A. Ceron, "Space shift keying modulation for MIMO channels," *IEEE Trans. Wireless Commun.*, vol. 8, no. 7, pp. 3692–3703, 2009.

[45] A. Younis, N. Serafimovski, R. Mesleh, and H. Haas, "Generalised spatial modulation," in *Proc. Asilomar Conference on Signals, Systems and Computers (ASILOMAR)*, 2010.

[46] J. Fu, C. Hou, W. Xiang, L. Yan, and Y. Hou, "Generalised spatial modulation with multiple active transmit antennas," in *Proc. IEEE Global Telecommunications Conference Workshops (GC Wkshps)*, 2010.

[47] J. Wang, S. Jia, and J. Song, "Generalised spatial modulation system with multiple active transmit antennas and low complexity detection scheme," *IEEE Trans. Wireless Commun.*, vol. 11, no. 4, pp. 1605–1615, 2012.

[48] M. Di Renzo, H. Haas, A. Ghrayeb, S. Sugiura, and L. Hanzo, "Spatial modulation for generalized MIMO: Challenges, opportunities, and implementation," *Proceedings of the IEEE*, vol. 102, no. 1, pp. 56–103, 2014.

[49] J. Jeganathan, A. Ghrayeb, and L. Szczecinski, "Generalized space shift keying modulation for MIMO channels," in *Proc. IEEE Personal, Indoor and Mobile Radio Communications (PIMRC)*, 2008.

[50] J. Jeganathan, A. Ghrayeb, L. Szczecinski, and A. Ceron, "Space shift keying modulation for MIMO channels," *IEEE Trans. Wireless Commun.*, vol. 8, no. 7, pp. 3692–3703, July 2009.

[51] R. Chang, S.-J. Lin, and W.-H. Chung, "New space shift keying modulation with Hamming code-aided constellation design," *IEEE Wireless Commun. Lett.*, vol. 1, no. 1, pp. 2–5, February 2012.

[52] E. Basar, U. Aygolu, E. Panayirci, and H. Poor, "Space-time block coded spatial modulation," *IEEE Trans. Commun.*, vol. 59, no. 3, pp. 823–832, 2011.

[53] S. Sugiura, S. Chen, and L. Hanzo, "Generalized space-time shift keying designed for flexible diversity-, multiplexing- and complexity-tradeoffs," *IEEE Trans. Wireless Commun.*, vol. 10, no. 4, pp. 1144–1153, 2011.

[54] M.-T. Le, V.-D. Ngo, H.-A. Mai, X. N. Tran, and M. Di Renzo, "Spatially modulated orthogonal space-time block codes with non-vanishing determinants," *IEEE Trans. Commun.*, vol. 62, no. 1, pp. 85–99, 2014.

[55] M. Di Renzo and H. Haas, "Bit error probability of SM-MIMO over generalized fading channels," *IEEE Trans. Veh. Commun.*, vol. 61, no. 3, pp. 1124–1144, March 2012.

[56] R. Mesleh, S. Ikki, and H. Aggoune, "Quadrature spatial modulation," *IEEE Trans. Veh. Technol.*, 2014.

[57] K. Ntontin, M. Di Renzo, A. Perez Neira, and C. Verikoukis, "Performance analysis of multistream spatial modulation with maximum-likelihood detection," in *Proc. IEEE Global Communications Conference (GLOBECOM)*, 2013.

[58] H. Jafarkhani, *Space-time coding: theory and practice*. Cambridge University Press, 2005.

[59] A. Younis, S. Sinanovic, M. Di Renzo, R. Mesleh, and H. Haas, "Generalised sphere decoding for spatial modulation," *IEEE Trans. Commun.*, vol. 61, no. 7, pp. 2805–2815, July 2013.

[60] K. Ishibashi and S. Sugiura, "Effects of antenna switching on band-limited spatial modulation," *IEEE Wireless Commun. Lett.*, vol. 3, no. 4, pp. 345–348, Aug 2014.

[61] N. Serafimovski, A. Younis, R. Mesleh, P. Chambers, M. Di Renzo, C.-X. Wang, P. Grant, M. Beach, and H. Haas, "Practical implementation of spatial modulation," *IEEE Trans. Veh. Commun.*, vol. 62, no. 9, pp. 4511–4523, Nov 2013.

[62] S. W. Nydick, "The Wishart and inverse Wishart distributions," 2012.